DISSERTATION

ENGINEERING BACTERIOPHAGE NANOCARRIERS FOR TARGETED DELIVERY OF PROTEIN REAGENTS TO PROSTATE CANCER CELLS

Submitted by

Sandra M. DePorter

Department of Chemistry

In partial fulfillment of the requirements

For the Degree of Doctor of Philosophy

Colorado State University

Fort Collins, Colorado

Fall 2014

Doctoral Committee:

Advisor: Brian McNaughton

Alan Kennan
Debbie Crans
Melissa Reynolds
Santiago Di Pietro

ABSTRACT

ENGINEERING BACTERIOPHAGE NANOCARRIERS FOR TARGETED DELIVERY OF PROTEIN REAGENTS TO PROSTATE CANCER CELLS

Proteinaceous reagents, including antibodies and synthetic proteins, have become some of the most effective reagents for targeted treatment and diagnosis of disease. The unique catalytic activity of some proteins and ability to bind disease-relevant receptors that can evade small molecule discovery, make these reagents well suited for use as therapeutic and bioimaging reagents. However, the large size and charge distribution of most proteins greatly inhibits their intracellular delivery to diseased cells, limiting targets to those displayed on the cell surface. In response to this challenge, we have developed a bacteriophage nanocarrier to deliver large payloads of proteinaceous cargo to the interior of prostate cancer cells. This reagent employs two distinct components: a genetically defined prostate cancer cell-selective protein transduction domain, and a biotinylation site on an orthogonal coat protein, which allows for complexation with streptavidin fusion proteins. Collectively, this approach permits targeted intracellular delivery of ~20 exogenous proteins per phage to human prostate cancer cells. This multifunctional technology offers a cell-selective solution to the challenges associated with delivering protein cargo to the interior of diseased cells and may lead to an expansion in the use of protein reagents.

ACKNOWLEDGMENTS

Foremost, I would like to thank my advisor, Professor Brian McNaughton, for his guidance and encouragement. I could not have asked for a better mentor. His dedication and passion for research transformed me into a scientist with the drive to take on difficult projects and the skills to succeed. I would also like to acknowledge my family, in particular my mother, who always said I could accomplish anything that I put my mind to. Finally, I would like to express my deepest gratitude to my husband, Tim Rhorer. His continued support and patience has strengthened my determination to succeed through the challenges of graduate school.

TABLE OF CONTENTS

LIST OF TABLES

Chapter 1

Chapter 2

Chapter 5

LIST OF FIGURES

Chapter 1

Chapter 2

Chapter 3

Chapter 4

Chapter 5

ABBREVIATIONS

ABT	antibody-binding terminus
ADCC	antibody-dependent cellular cytotoxicity
Ad-Pb	adenovirus penton base
Antp	antennapedia-homeodomain-derived peptide
APP	amyloid precursor protein
APS	ammonium persulfate
ARM	antibody-recruiting molecule
CCMV	cowpea chlorotic mottle virus
CLT	cytotoxic T-cell lymphocytes
DEAE	diethylaminoethanol
DNA	deoxyribonucleic acid
DNP	dinitrophenyl
DOX	doxycycline
CBT	cell-binding terminus
CDC	complement-dependent cytotoxicity
CMV	cytomegalovirus
CPP	cell-penetrating peptide
DAPI	4′,6-diamidino-2-phenylindole
EDC	1-ethyl-3-(3-dimethylaminopropyl)carbodiimide

EGF	epidermal growth factor
EGFR	epidermal growth factor receptor
Erb2	receptor tyrosine-protein kinase (also called HER2)
FITC	fluorescein isothiocyanate
GFP	green fluorescent protein
HBsAg	hepatitis B virus surface antigen
HER2	human epidermal growth factor receptor 2
HIV	human immunodeficiency virus
HRP	horseradish peroxidase
HSV	herpes simplex virus
IAA	indole-3-acetic acid
IgG	immunoglobulin G
mAbs	monoclonal antibodies
MAP	model amphipathic peptide
MLV	murine leukemia virus
MNP	magnetic nanoparticle
MTT	3-(4,5-dimethylthiazol-2-yl)-2,5-diphenyltetrazolium bromide
NHS	*N*-hydroxysuccinimide
NIR	near-infared
nLuc	nano luciferase

PCL-P2VP	poly(caprolactone-*b*-2-vinylpyridine)
PDMS	Poly(dimethyl siloxane)
PEG	polyethylene glycol
Pen	penetratin
PET	positron emission tomography
PmpD	polymorphic membrane protein D
PSMA	prostate specific membrane antigen
PTD	protein transduction domain
PVX	potato virus X
QD	quantum dot
RGD	arginylglycylaspartic acid (integrin binding peptide)
RNA	ribonucleic acid
SAV	streptavidin
SBP	SPARC binding peptide
SEM	scanning electron microscope
sfGFP	superfolder green fluorescent protein
siRNA	small interfering ribonucleic acid
SAMs	self-assembled monolayers
SAMIM	solvent-assisted micromolding
SPARC	secreted protein, acidic and rich in cysteine

ssDNA	single-stranded deoxyribonucleic acid
SDS	sodium dodecyl sulfate
SV40	Simian virus 40
SWNT	single-walled carbon nanotube
TEMED	tetramethylethylene-diamine
TMB	3,3′,5,5′-tetramethylbenzidine
TMV	tobacco mosaic virus
TVCV	turnip vein clearing virus
VLP	virus-like particle

CHAPTER ONE

GENETICALLY-DEFINED NANOCARRIERS FOR TARGETED INTRACELLULAR DELIVERY

1.1 Introduction

Perhaps foremost among the challenges faced by researchers focused on expanding the utility of proteinaceous imaging and therapeutic reagents is their targeted intracellular delivery. While many protein reagents have the unique ability to target and alter disease-relevant macromolecules that evade traditional approaches, they are largely limited to cell surface targets, by virtue of their general inability to cross the cellular membrane of mammalian cells. A number of technologies have been developed for the intracellular delivery of proteins, including encapsulation or conjugation to protein transduction domains (cell-penetrating peptides), which facilitate cell-penetration. However, targeted intracellular delivery of relatively large payloads of protein cargo remains a significant challenge. As part of a larger effort to overcome challenges to the targeted intracellular delivery of proteinaceous reagents to diseased cells, I have employed genetic and enzymatic manipulation to engineer spatially-defined M13 bacteriophage nanorods that potently and selectively deliver functional exogenous enzymes to human prostate cancer cells. The modularity of this method, coupled with the ability to evolve phage that potently recognize and penetrate virtually

any target cell, allows for a possible general solution to the problem of targeted protein transduction, and thus, may lead to an expansion in the use of protein reagents in various applications, including enzyme replacement therapy and bioimaging.

1.2 Proteinaceous Reagents in Basic Research and Medicine

Recently, proteinaceous therapeutics (commonly referred to as biologics), including antibody, antibody-fragment, natural and synthetic proteins have become an important sector within the global pharmaceutical industry.[1] Protein-based reagents are particularly useful in basic research and therapeutic applications, by virtue of their unique ability to recognize receptors that evade small molecule-dependent recognition and control. In contrast to small molecules, the size, relatively high folding energies and well-defined structure of proteins enables selective recognition and binding to large surfaces of disease-relevant macromolecules. Moreover, some proteins with bioimaging or therapeutic utility have robust enzymatic activities, which allow researchers to image or alter cell function and fate with a relatively small amount of enzyme, compared to many small molecule reagents and drugs. Medically-relevant features unique to protein biologics have not escaped the global pharmaceutical and biotechnology spheres. The total sales for biologics in the United States reached an all-time high in 2012 at ~$63.6 billion, an 18.2% increase over 2011 sales.[2] Foremost among these are monoclonal

antibodies (mAbs); five new mAbs were approved in 2012-2013 and mAbs represent the highest selling class of biologic drugs.[2] The development of new classes of small stable proteins that are easy to express in large quantities in *E. coli*, such as nanobodies[3], and the new stream of proteins with evolved and desirable biomedical applications[4] will provide researchers with a large set of reagents for the perturbation of disease-relevant cell function and fate.

However, the most significant barrier to the broader use of proteins in basic research and medical applications is their delivery to the cytoplasm of diseased cells. Unlike most traditional small molecule drugs, the majority of natural and synthetic proteins are not able to penetrate the lipid bilayer membrane of mammalian cells. This largely limits the potential applications of protein drugs to those that target cell surface receptors, which make up a relatively small fraction of therapeutically relevant targets.[5] In response to this limitation, researchers have devoted significant effort and resources to the development of technologies for intracellular delivery of exogenous proteins. *General* intracellular delivery across the cell membrane, such as the utilization of a highly charged cell-penetrating peptide[6], can mediate unbiased uptake of the cargo to the interior of cells. However, internalization by healthy cells can increase adverse side effects. Alternatively, *selective* intracellular delivery methods can target a diseased cell by binding a specific cell-surface receptor, which then mediates cellular uptake.

Selective delivery limits internalization by healthy cells, therefore reducing overall toxicity, dosage and cost.

1.3 Methods for the Delivery of Exogenous Protein Reagents to the Interior of Mammalian Cells, and Challenges Therein

There are a number of methods for *general* intracellular delivery of functional protein reagents, which include: microinjection[7], liposomes[8], lipid-linked proteins[9], nanoparticles[10], fusions to receptor ligands[11], polyarginine and arginine grafting[12,13], supercharged proteins[14–17], and protein transduction domains[18] (also referred to as cell-penetrating peptides). *Selective* intracellular delivery of functional exogenous proteins is often mediated by antibody fusions and conjugates. However, antibodies generally target a cell-surface receptor and do not actively deliver protein cargo to the interior of the cell. Few examples of a cell-penetrating antibodies have been reported, however.[19,20]

The most common method for intracellular delivery is fusion of the protein of interest to a cell-penetrating peptide (CPP) or protein transduction domain (PTD).[21] Protein transduction domains are typically short peptides (~8 - 20 amino acids) that facilitate active translocation of various small molecule[22–24], protein[25–27], small interfering RNA (siRNA)[28,29], and nanomaterial[30–32] cargo across the cell membrane. PTD-dependent translocation across the cell membrane is typically achieved as a result of high

theoretical net charge, which has been shown to be important for the uptake of the PTDs.[33]

Some of the most well-studied PTDs include polyarginine (RRRRRRRRR)[12], the Tat peptide from the transactivating protein Tat of HIV-1 (GRKKRRQRRRPPQ)[34,35], the third helix of the homeodomain of *antennapedia* called penetratin (RQIKIWFQNRRMKWKK)[36], transportan (GWTLNSAGYLLGKINLKALAALAKKIL)[37] and VP22 (DAATATRGRSAASRPTERPRAPARSASRPRRPVD)[38]. A more comprehensive review of PTDs can be found in Chapter 2.1. The mechanism of internalization for many PTDs has been extensively studied and, is often highly dependent on the sequence of the PTD and its cargo. For example, mechanisms spanning direct translocation[39] and energy-dependent macropinocytosis[40] have been suggested for Tat. The mechanisms of uptake for various PTDs are discussed at length in Chapter 2.8.

While PTDs facilitate intracellular delivery of exogenous reagents to mammalian cells, including proteins, PTDs are often unable to selectively target diseased cells. Moreover, traditional PTD-dependent delivery can result in sequestration within endosomes and late-stage lysosomes, limiting the functional utility of the fused exogenous reagent. Finally, a major challenge with PTD fusions to protein cargo is efficiency. For example, a simple genetic fusion or chemical conjugation between a

protein and PTD means that each cell penetration event results in the delivery of a single exogenous protein reagent. Thus, methods for the *selective* delivery of *large payloads* of exogenous protein cargo to diseased cells remains a primary focus.

1.4 Benefits and Challenges of Synthetic Nanomaterials as Chaperones for Intracellular Delivery of Exogenous Protein to Mammalian Cells

Nanomaterials overcome some of the challenges associated with delivering large payloads of exogenous proteins to the interior of mammalian cells. For example, nanomaterials can be loaded with protein cargo via direct conjugation with a genetic fusion, chemical conjugation, physical adsorption, or covalent/noncovalent encapsulation (**Table 1.1**).[41–51] Nanocarriers such as polymeric nanoparticles offer

Table 1.1 Synthetic nanomaterials for protein delivery

Nanoparticle	Composition	Size (nm)	Protein delivered	References
Lipid-based nanoparticles				
Liposome	lipids from spinach thylakoids; TFA-DODAPL, DOPE	-	Bak; caspase-3, caspase-8, granzyme B	**42, 43**
Solid-lipid nanoparticle	Witepsol E 85, monosteol, superpolystate	550-650	lysozyme	**44**
Inorganic nanoparticles				
Carbon nanotubes	SWNT	1-5	streptavidin	**45**
Quantum dots (QDs)	CdSe QDs	20	cTnC/NLS peptide	**46**
Gold nanoparticles (AuNP)	Peptide-coated AuNP	2.5	β-galactosidase	**47**
Silica nanoparticles	mesoporous silica	5.4	cytochrome c	**48**
Magnetic nanoparticles	Iron oxide NPs	300	catalase and superoxide dimutase	**49**
Polymeric nanoparticles				
Polymeric beads	6-*O*-glucosyl methacrylate, acrylic acid, styrene	150	EGFP	**50**
Microgels	acrylamide, hydrophilic triglyme	200-500	Ovalbumin (OVA)	**51**

several advantages over PTD-fusions. First, they can be engineered to protect the protein cargo from degradation and denaturing interactions *in vivo*.[52–54] Encapsulation can also shield immunogenic ligands from immune recognition.[55] The large size of the nanocarriers also aids in biodistribution and reduces renal filtration.[54,56] Finally, nanocarriers can be functionalized with ligands that enhance cellular uptake, endosomolytic escape, cell targeting, or evading immune recognition.[57] Precise chemical and physical control over the synthesis, assembly and conjugation of nanocarriers permits researchers to define all properties of the nanocarriers such as size, shape, hydrophilicity, rigidity, and surface charge.

However, the need to control particle assembly and presentation, largely through chemical means, presents a series of challenges to their development. Chemical conjugation of protein reagents can change protein structure and impede protein function. The process of coupling cell-targeting and/or cell-penetration components and immune-compatible reagents may require multiple synthetic and purification steps. Additionally, small changes in the chemical composition of polymeric nanoparticles can often result in dramatically different properties such as biodistribution, biocompatibility, stability, and function.

1.5 Genetically-Defined Nanomaterials Overcome Challenges to Controlled Assembly

An alternative approach to chemical methods for controlled nanomaterial assembly and functionalization is genetically-defined architectures. These include virus-

Table 1.2 Genetically-defined nanocarriers for protein delivery

Nanocarrier Type	Shape	Subunits	Size (nm)	Protein delivered	References
Protein nanocages					
Ferritin	Isosahedral	24	12	AP-1 peptide	**60**
Virus-like Particles (VLPs)					
Cowpea chlorotic mottle virus (CCMV)	Icosahedral	180	30	PalB	**61**
Bacteriophage Qβ	Icosahedral	180	25	N-propargyl transferrin; N-terminal aspartate dipeptidase	**62, 63**
P22	Icosahedral	420	64	EGFP/mCherry	**64**
MS2	Icosahedral	180	27.5	Ricin toxin A	**65**
Bacteriophages					
M13	Filamentous	>2700	800 × 7	Sfp phosphopantetheinyl transferase	**66**
T7	Spherical head and tail	72	55	celA; α-amylase and xylanase A	**67, 68**
Plant viruses					
Potato Virus X (PVX)	Filamentous	1270	500 × 13	CalB; GFP	**69, 70**
Turnip Vein Clearing Virus (TVCV)	Rod	>2100	200 × 18	fragment of protein A	**71**
Tobacco mosaic virus (TMV)	Rod	2130	300 × 18	GFP-streptavidin	**72**
Animal viruses					
Murine leukemia virus (MLV)	Icosahedral nucleocapsid and capsid	-	100	Human tPA	**73**

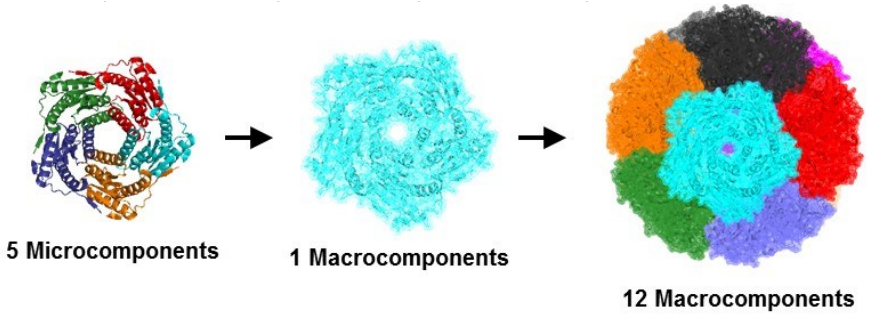

Figure 1.1. Engineered lumazine synthase protein nanocage. The cage is composed of five subunits that form one pentamer. Twelve macrocomponents assemble to form protein nanocages.

like particles (VLPs), protein nanocages, bacteriophage, plant and animal viruses (**Table 1.2**).[58–73] An example of a particularly well-studied and representative protein nanoparticle is shown in **Figure 1.1**. The engineered lumazine synthase nanocage is composed of a mixture of 12 pentamers.[74] Upon assembly, the lumazine synthase nanocage forms a stable nanoparticle for protein encapsulation.

VLPs and protein nanocages are composed of protein subunits that are expressed *in vivo* and self-assembled under *in vitro* conditions. In contrast to the fabrication of nanoparticles via chemical manipulation, the genetic sequence of each component permits their precise assembly into a single well-defined nanostructure with spatially-defined patches, largely through protein-protein interactions. Thus, precise and controlled assembly is built into the system and doesn't need to be manipulated or refined by laborious and costly chemical means. Additionally, relatively elaborate decoration of the well-defined nanostructure can be achieved via molecular biology-based "rewiring" of the genetic information, further circumventing the need for chemical approaches. For example, incorporation of exogenous peptides or proteins can be easily genetically encoded at the N- or C- terminus or within loop regions of the protein subunits.[60,75,76] These materials can be further elaborated to encapsulate or display particular proteinaceous cargo, including those with potent cell-penetrating capability.[77] VPLs and protein nanocages offer the ability to functionalize and genetically engineer nanocarriers for intracellular delivery without the challenges

associated with chemical synthesis of nanoparticles. This emerging field has gained momentum in the last 10 years and will certainly continue to develop as a technology for protein delivery.

A conceptually-related platform for nanoparticle-directed intracellular protein delivery that is particularly well-studied is bacteriophage. Bacteriophage (referred to as phage herein) are bacteria viruses composed of a protein coat encapsulating a DNA or RNA genome. The phage genome encodes for the coat proteins, along with the proteins that facilitate phage assembly and amplification. Phage are an incredibly well-studied nanomaterial and the coat proteins can be genetically or enzymatically manipulated for conjugation to protein cargo. The genetically distinct nature of the coat proteins allows for spatial segregation of incorporated cargo and controlled manipulation of the coat proteins. We chose to focus our efforts toward phage nanorods to act as nanocarriers for exogenous proteins and enzymes to mammalian cells.

1.6 Phage as a Reagent in Basic Biomedical Research and Human Health

Bacteriophage, or bacterial viruses, were first discovered independently by Frederick Twort in 1915 and Felix d'Herelle in 1917.[78,79] Phage were commercially sold by US pharmaceutical companies in the 1930s as treatment for gastrointestinal and skin infections; however, the introduction of antibiotics such as penicillin in the 1940s

quickly replaced phage as antibacterial reagents in the United States. In Eastern Europe and the former Soviet Union, phage continued to be produced for therapeutic use and numerous studies were performed to determine phage therapy efficacy on various bacterial strains[80]. To date phage products are still sold in Tbilisi, Republic of Georgia for the treatment of bacterial infections. Over the past 15 years, a renewed interest in

Table 1.3 Bacteriophage classification

Phage family	Virus	Life cycle	Shape
ssDNA genome			
Microviridae	∅x174	lytic	Isosahedral
Inoviridae	M13, fd	lysogenic	Filamentous
dsDNA genome			
Podoviridae	T7, P22, ∅29	lytic	Icosahedral (with tail)
Myoviridae	T4, P2/P4	lytic	Icosahedral (with tail)
Siphoviridae	Lambda, HK97	lytic	Icosahedral (with tail)
Corticoviridae	PM2	lytic	Icosahedral (lipid layer inside)
Tectiviridae	PRD1	lytic	Icosahedral (lipid layer inside)
Fuselloviridae	SSV1	lysogenic	Spindlelike (lipid outer envelope)
Plasmaviridae	L2	lysogenic	Pleomorphic (lipid outer envelope)
Lipothrixviridae	TTV-1, SIFV	lysogenic	Filamentous
Rudiviridae	SIRV1	lysogenic	Filamentous
ssRNA genome			
Leviviridae	MS2, Qβ	lytic	Icosahedral
dsRNA genome			
Cystoviridae	∅6	lytic	Icosahedral

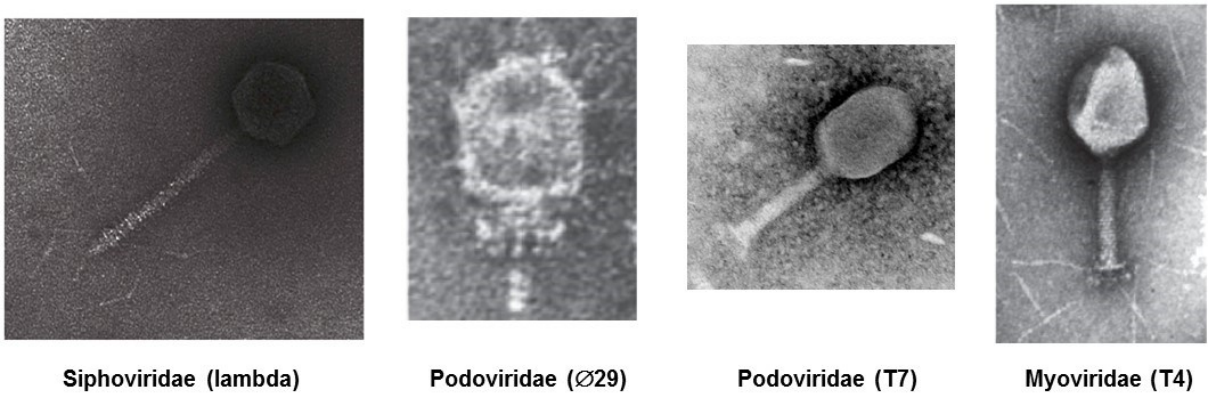

Figure 1.2. Electron microscopy images of bacteriophage particles. Phage from left to right: lambda[147], ∅29, T7 and T4[148].

phage therapy in the United States has been largely driven by the evolution of antibiotic resistant bacteria and an improved knowledge of phage biology.

There are 3 different classes of bacteriophage, lytic, lysogenic, and temperate (**Table 1.3**). Lytic phage are replicated in the bacterial host and released by lysing open the host cell to release the phage progeny. Lysogenic phage release progeny without lysing the host bacterial cell and replicate either by integrating their genomes into the host chromosome or exclusively as episomes. Temperate phage can replicate using either cycle. The majority of bacteriophage that have been utilized for antibacterial therapy have been lytic phage.

Bacteriophage therapy as a treatment for bacterial infections is gaining momentum as there is a growing need for treatment of antibiotic resistant bacterial strains. A comparison of phage therapy to antibiotic treatment is described in **Table 1.4**.[81] One of the greatest advantages to phage therapy for bacterial infections is the ability to quickly evolve phage to target a new bacterial host or a bacterial strain that has developed resistance to treatment.

Animal studies have been performed to access the safety and therapeutic utility of bacteriophage against bacteria strains such as *Pseudomonas aeruginosa*[82,83], *Staphylococcus aureus*[84], vancomycin-resistant *Enterococcus faecium*[85], *Clostridium difficile*[86], and *Klebsiella pneumoniae*[87]. In total these animal trials demonstrated the efficacy and

Table 1.4 Comparison of bacteriophage and antibiotics to treat bacterial infections

Bacteriophages	Antibiotics	Comments
Target specific bacterial species	Target pathogenic and normal bacteria	For phage therapy to be effective, the bacterial species must be identified. Phage specificity does not affect normal microflora.
Amplify at site of infection	Metabolized and eliminated from the body	Replication of phage at the infection site may require less frequent and lower dosage of phage to treat the infection.
No serious side effects have been reported	Side effects: intestinal disorders, allergies, secondary infections, antibiotic resistance	Minor side effects of phage therapy were reported from endotoxins released from bacteria lysed *in vivo* by phage. These side effects have also been reported with antibiotics.
Phage resistant bacteria are not resistant to other phage with similar targets	Antibiotic resistance is not limited to targeted bacteria	Phage specificity limits the resistance developed by other bacterial species, thus limiting overall phage resistance.
Evolving new phage for a bacterial host is a quick process that can be accomplished in days or weeks	New antibiotics take many years of development	New phage can be rapidly selected against a bacterial strain that may have developed antibiotic resistance or phage resistance.

safety of phage-based therapeutics against bacteria pathogens in animal models. As mentioned previously, the majority of human phage therapeutic research was performed in Eastern Europe and the former Soviet Union (reviews 81, 88, 89), many of the studies were controversial in the rest of the world because of the lack of rigorous controls. However, the western world has taken a renewed interest in phage therapy to treat bacterial infections and has performed a number of trials in humans. Human safety trials have evaluated Staphylococcal phage lysate and phage mixtures against *P. aeruginosa, S. aureus,* and *E. coli*.[88,90] In fact, a recent phase I safety trial in Texas that utilized the phage cocktail against *P. aeruginosa, S. aureus,* and *E. coli* for venous leg ulcers showed no increase in adverse reactions with phage treatment.[91] Moreover, a phase I/II clinical trial for phage therapy against antibiotic-resistant *P. aeruginosa* in

chronic otitis demonstrated that topical application of phage decreased bacterial loads.[92] This study showed that with an initial determination of pathogen composition of the bacterial infection and proper choice of phage strain to target the bacteria is an effective therapy for antibiotic resistant infections. Taken together phage therapy has been shown to be a safe and effective treatment of bacterial infections and may be one of the greatest weapons in the war against antibiotic resistant bacteria.

1.7 Phage as a Nanocarrier for Targeted Delivery of Bioimaging Reagents and Therapeutics

In addition to the utility of phage as cell-selective antibacterial reagents, phage have also been developed as a drug delivery systems that have the potential to treat human disease. The majority of Section 1.7 will focus on lysogenic filamentous bacteriophage, f1, M13, fd, that replicate exclusively episomally. As shown in **Figure 1.3**, filamentous phage are composed of 5 coat proteins, 4 minor coat proteins—p3, p6, p7, p9 and the major coat protein p8. The coat proteins encapsulate a single-stranded deoxyribonucleic acid (ssDNA) genome that is replicated by a rolling circle mechanism. Interestingly, filamentous phage are a unique member of the bacterial virus family because their assembly is membrane-embedded, and therefore a live host is required to release their progeny.[93] Overall, filamentous phage have been extensively studied and

used in a diverse range of applications including drug delivery, vaccine development and materials design. This section with focus on phage as a targeted therapeutic delivery reagent and bioimaging platform.

Table 1.5 Filamentous phage proteins and properties

Protein	Size (aa)	Function	Location	Display?
p1	348	Assembly	Inner membrane	-
p11	108	Assembly	Inner membrane	-
p2	409	Replication (nickase)	Cytoplasm	-
p10	111	Replication	Cytoplasm	-
p4	405	Assembly (exit channel)	Outer membrane	-
p5	87	Replication (ssDNA bp)	Cytoplasm	-
p3	406	Virion component	Virion tip (end)	N-term
p6	112	Virion component	Virion tip (end)	C-term
p7	33	Virion component	Virion tip (start)	N-term
p8	50	Virion component	Virion filament	N- and C-term
p9	32	Virion component	Virion tip (start)	N-term

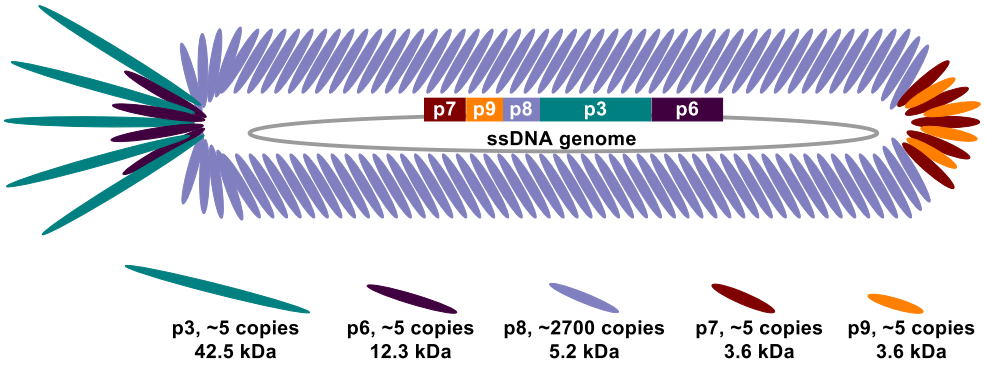

Figure 1.3. The structure of M13 filamentous phage.

1.7.1 Phage-Dependent Small Molecule Delivery

There have been a number of studies using phage conjugated to small molecules for imaging and drug delivery applications. Phage offer several advantages over traditional drug delivery methods. Multiple copies of each of the coat proteins

facilitates conjugation of a high payload of drug, particularly conjugation to the ~2700 copies of p8. Additionally, phage nanocarriers can be modified to display a targeting moiety to direct the drug to the target cells. Phage have been used extensively to bind to a target cell for small molecule delivery, but this section will focus on phage-mediated delivery of reagents to the interior of the cells.

Lytic phage have been used extensively as a treatment for bacterial infections, but filamentous phage have also been modified to target and destroy bacteria with the selective delivery of antibiotics. Itai Benhar and colleagues at Tel-Aviv University have published a number of studies on the conjugation of phage to antibiotics and their delivery to bacterial cells.[94–96] They utilized a filamentous phage displaying an immunoglobulin G (IgG) antibodies linked to the p3 of the phage by an IgG-binding ZZ domain displayed on p3. They then conjugated the hemolytic antibiotic chloramphenicol with an aminoglycoside linker, neomycin, to improve solubility and enhance the drug-loading capacity of the phage.[95] They observed that the phage-based antibiotic delivery system completely inhibited bacterial growth in *Staphylococcus aureus, Streptococcus pyogenes,* and *Escherichia coli* and increased the potency of the antibiotics by ~20,000 fold. This work demonstrates that conjugation to phage enables a large payload of antibiotic to be delivered to the bacteria and selective delivery to the bacteria of interest, by either displaying a targeted ligand or by utilizing phage that have already been evolved by nature to infect a particular bacteria.

Bacteriophage have also been used for imaging applications, such as the delivery of fluorescent dyes to cells.[97,98] Weissleder *et al*. labeled phage with a number of fluorophores including fluorescein isothiocyanate, tetramethyl rhodamine isothiocyanate, Cy3.5, Cy5.5, VT680, and AF750.[97] The filamentous phage were then targeted with a p3 displayed peptide to target Secreted Protein Acidic and Rich in Cysteine (SPARC), which is overexpressed in many invasive cancers.[99] In order to perform *in vivo* optical imaging, they employed phage labeled with the far-red fluorophores and tested the tumor targeting ability of their in vitro selected peptides against SPARC. They showed that SPARC peptide phage were able to preferentially target the Lewis lung carcinoma cell tumors and directly image mice for tumor targeting verification. In addition to the obvious therapeutic relevance of targeted bioimaging reagent delivery to diseased cells, this technology could also be utilized for *in vivo* phage display to quickly eliminate off target *in vitro* clones, which holds much promise for the identification of selective reagents using *in vivo* phage display.

Phage have also been used to deliver cytotoxic drugs to diseased mammalian cells.[100,101] One study in particular presented an innovative phage-polymer nanoassembly for drug delivery.[101] Filamentous M13 phage were conjugated to folate to act as a targeting moiety for cells expressing the folate receptor. The folate-M13 phage forms an outer shell around the copolymer poly(caprolactone-*b*-2-vinylpyridine) (PCL-P2VP), which encapsulates an antitumor drug, doxorubicin (DOX). The copolymer

serves as the release system for the drug as it is comprised of a biodegradable hydrophobic block (PCL) and a pH-sensitive block (P2VP). The DOX-loaded folate-M13-PCL-P2VP showed selective uptake into tumor cells expressing the folate receptor and minimal uptake into the cells without folate receptors. Additionally, the nanoassemblies displayed increased tumor selectivity when compared to free DOX. This work demonstrates the utility of phage to assemble nanoparticles that have the ability to control drug release and therefore control the selectivity of the drug delivery.

Finally, phage have been used to selectively conjugate both a small molecule imaging reagent and a cytotoxic drug as described in 2012 by Belcher.[102] They used several conjugation methods to guide the conjugation of the small molecules onto the p3, p8, and p9 coat proteins of M13 phage. They incorporated a SPARC binding peptide on p3 to direct the phage to DU145 prostate cancer cells. DOX was conjugated onto p8 with an NHS/EDC chemical coupling reaction to provide cytotoxic drug delivery to the cancer cells. Finally, they fused a streptavidin-AlexaFluor 488 fluorophore onto p9 with the display of a biotin acceptor peptide, which was subsequently biotinylated by BirA biotin ligase. The streptavidin-fluorophore fusion protein was then complexed to the biotinylated p9. The functionalized phage were able to target the tumor cells and provide simultaneous imaging and drug delivery. This study demonstrated that phage can be selectively spatially coupled with a number of

reagents to enable multifunctional delivery of small molecule therapeutics and imaging reagents.

1.7.2 Phage-Dependent Nanoparticle Delivery

Many nanoparticles have inherent properties that make them attractive reagents for bioimaging applications. For example, CdSe-ZnS quantum dots are fluorescent, iron-oxide nanoparticles have been utilized as MRI contrast agents, and radioactive ^{64}Cu, ^{62}Cu, ^{82}Rb, and ^{68}Ca nanoparticles have been utilized in positron emission tomography (PET) imaging. Nanoparticles themselves can be functionalized for delivery to target cells; however, conjugation to a carrier would enable a higher payload of nanoparticles to be delivered to the target cells.

Bacteriophage networks of nanoparticles hold several delivery advantages over targeted nanoparticles alone. Phage are highly biocompatible and can mediate the organization of nanoparticles while still maintaining a targeting moiety with a displayed peptide. Souza *et al* were able to show that the use of phage to create gold nanoparticle (AuNP) networks could be a powerful imaging tool.[103] AuNPs are an attractive tool for bioimaging because their optical properties can be manipulated simply by changing assembly conditions to enable imaging by fluorescence, dark-field microscopy, or near-infrared surface-enhanced Raman scattering (NIR SERS)

spectroscopy. The authors used filamentous phage to assemble networks of AuNPs without the use of complex conjugation techniques. They then targeted the AuNP-phage networks to cells by displaying an RGD peptide on p3 to target the cell surface receptor α_v integrins. They confirmed that AuNP-phage networks were able to bind to the target cells with confocal fluorescence microscopy, dark-field microscopy and SERS. Additionally, they demonstrated that networks with a smaller fractal dimension were able to penetrate the cells. This work shows that phage can be utilized to spontaneously assemble AuNPs and target those networks to cells of interest with a displayed peptide.

Kelly and colleagues took a different approach to the delivery of nanoparticles with phage, by assembling the nanoparticles onto the major coat protein of the phage.[104] They used an engineered phage that displayed a tri-glutamate moiety on p8 of the M13 filamentous phage.[105] The negatively charged M13 p8 can then be assembled electrostatically with positively charged magnetic iron oxide nanoparticles (MNPs). The M13-MNP were targeted to prostate cancer cells by a peptide that targets SPARC, termed SPARC binding peptide (SBP). They then compared the M13-MNP-SBP to nanoparticles that display the SBP (MNP-SBP). Interestingly, they able to show that the phage complex had improved magnetic resonance contrast potential over several clinically relevant superparamagnetic iron oxide particles. Moreover, when incubated with the target cell line, the M13-MNP-SBP amplified the signal in comparison to MNP-SBP because of the increased number of nanoparticles conjugated per phage. This work

demonstrates that conjugation to filamentous phage can be an attractive approach for intensifying a signal with a low amount of targeting ligand presented on the cell surface.

An alternative conjugation technique is to specifically incorporate a peptide binder onto the surface of the phage. Belcher and coworkers at MIT were able to accomplish this with single-walled carbon nanotubes (SWNTs).[106] They conjugated SWNTs onto M13 filamentous phage with a peptide displayed on the p8 coat protein (DSPHTELP), which was previously selected for binding SWNTs.[107] They used an anti-PSMA antibody and SBP conjugated to p3 to target prostate tumors. They were able to show that the phage-SWNT could be used *in vivo* for second NIR window fluorescence of prostate tumors. Additionally, they demonstrated that phage-SWNTs were detected in deep tissue samples at concentrations as low as 2 μg/mL. This shows that phage provide a targeted scaffold for the delivery of stable SWNT to the tissue of interest without the common issues such as limited biocompatibility and bundle formation, which can affect fluorescence. Overall, these studies demonstrate the effectiveness of phage as a nanoparticle carrier to not only enhance the signal, but also improve the biocompatibility and delivery of these reagents.

1.7.3 Phage-Dependent DNA Delivery

The ability to deliver protected DNA to the interior of a target cell is a powerful tool in the field of gene therapy. There are a number of methods for gene delivery to mammalian cells, including the use of retroviruses, adenoviruses, adeno-associated viruses, and liposome complexes.[108] While each method has its own benefits, there are some inherent limitations to these technologies. One of the biggest challenges is that animal viral vectors must be produced to be completely free of replication competent virus to ensure that they do not recover their ability to infect cells. Bacteriophage delivery has been of particular interest because they are not an animal viral vector and they are easily modified and amplified. Additionally, phage can be evolved to induce uptake by the target cells with relative ease compared to other gene delivery methods.

The earliest studies of phage-mediated transfection was performed with the aid of transfection reagents like diethylaminoethanol (DEAE)-dextran or lipopolyamine.[109] However, the technology quickly adapted as phage were modified to display peptides that interact with the mammalian cell surface, as was demonstrated by Dunn in 1996.[110] They were able to employ an Arg-Gly-Asp (RGD)-modified λ phage to interact with β1-expressing mammalian cells. They then encoded the double stranded phage genome with a simian virus 40 (SV40) promoter and a β-galactosidase reporter gene. Although the transfection efficiency of the modified λ phage was lower than with the aid of

transfection reagents, they were able to show that phage are able to mediate the transfection and delivery of a gene.

Larocca and colleagues greatly expanded the scope of this delivery technique with a number of studies utilizing filamentous phage.[111–114] One study in particular used a receptor targeted approach to deliver the gene of interest to the mammalian cells.[112] They designed a phagemid vector, pUCMG4, with a cytomegalovirus (CMV)-promoter regulated green fluorescent protein (GFP) expression cassette and an epidermal growth factor (EGF)-p3 fusion to target the epidermal growth factor receptor (EGFR). The multivalent display resulted in 100 to 1000 times more potent phage transduction into PC-3 human prostate cancer cells when compared to monovalent displayed phage. This was the first phage study to demonstrate the role of avidity in the transfection efficiency of the phage.

A different approach to targeting mammalian cell internalization utilizes an antibody to target a cell surface receptor displayed on the desired mammalian cell. Marks *et al.* first used phage display to isolate an antibody to facilitate phage internalization by ErbB2 (HER2 receptor) expressing mammalian cells.[115] They then evaluated the cellular delivery of the anti-ErbB2 antibody (fused to p3) phage by using a GFP reporter gene (cloned into the phagemid), under the control of the CMV promoter to mediate gene transfer. They were able to show that mammalian cell GFP

fluorescence was phage concentration dependent. Furthermore, they observed GFP gene expression with as little as 2.0×10^7 pfu of phage. This technique of direct fusion of the targeting moiety to the p3 is much more efficient than indirect conjugation techniques.

The delivery of genes with phage has also been utilized in an effort to combat bacterial resistance.[116–118] Westwater and coworkers used a non-lytic phage to deliver DNA encoding bactericidal proteins to *E. coli*.[116] They chose 2 conditionally lethal genes, *gef* and *chpBK*, that only when translated caused bacterial cell death. They showed that the phage were lethal to the target bacterial cell line. Additionally, phage delivery of the pGef and pChpBK phagemids reduced bacterial load in infected mice. Five hours after treatment with the lethal-agent phage, the mice showed a 94-98% reduction in blood bacterial titers, when compared to the control group mice. Therefore demonstrating that lethal gene delivery can be used to selectively target bacteria.

In an alternative method to target bacteria for cell death, Collins *et al.* constructed phage to deliver genes for proteins that would target gene networks to enhance antibiotic effectiveness against bacteria.[117] They targeted the SOS DNA repair system to prevent the bacteria from overcoming the damage caused by bactericidal antibiotics. They engineered the M13mp18 filamentous phage to overexpress lexA3, a known repressor of the SOS system. The repression of the SOS system thus blocks the repair of

DNA damaged after the addition of antibiotics and increasing bacteria cell death. The addition of phage with the *lexA3* gene improved antibiotic efficacy against cells that persisted in the population after antibiotic treatment and increased potency for bacteria in biofilms. Moreover, they were able to show that mice that were infected with bacteria had increased survival when treated with the *lexA3* engineering phage and antibiotic (ofloxacin). These results confirmed that their engineered phage could be used to target and regulate other gene networks, such as S*oxR* or *CsrA* or to manipulate sensitivity to antibiotics with genes such as *OmpF*. This dual antimicrobial strategy of weakening the repair mechanism while also treating cells with a bactericidal antibiotic represents an important strategy for reducing antibiotic resistance.

1.7.4 Phage-Dependent Vaccine Delivery

Two types of vaccines have been of wide interest in the field of phage delivery, peptide display to elicit a T-cell response and nucleic acid immunization. Peptide vaccines are composed of parts of the antigenic proteins and are usually coupled to carrier protein for immunization. However, peptide vaccines suffer from some drawbacks including short life span in serum and limited targeting. Phage display has been widely used to identify and screen immunogenic peptides and that may be the reason phage have been developed as a vaccine carrier. A significant amount of

research has been conducted to utilize phage as a carrier of a protective epitope to induce an immune response to a pathogenic target, such as hepatitis virus[119], herpes simplex virus (HSV)[120], HIV[121–123], anthrax[124,125] and other pathogens[126–131]. Although peptide displayed phage vaccines do not deliver the peptide reagents to the interior of the cells, they are acting as a targeted therapeutic reagent to elicit an immune response.

Phage have been used as a vaccine against Alzheimer's disease[132]. Solomon *et al.* devised an immunization technique designed to induce auto-immune antibodies in amyloid precursor proteins to reduce aggregation of β-amyloid plaques. They achieved this by utilizing a filamentous phage displaying an epitope to evoke anti-aggregating antibodies. They are able to conjugate ~300 copies of the epitope onto p8 of the filamentous phage to elicit high titers of antibody to respond to the epitope and disaggregate the β-amyloid plaques. They also showed a reduction of plaques in the brain of transgenic mice. This study suggests that phage can be utilized as a carrier for an epitope that activates antibodies to disassemble the amyloid aggregates and prevent further amyloid plaque formation.

Epitope display on filamentous phage has also been used to stimulate anti-tumor immunity as well.[133–136] There are a number of tumor expressing antigens that are targets for cytotoxic T lymphocyte (CTL) effectors, which can induce cytolysis and produce cytokines. In a 2002 study, researchers were able to show that phage displaying

a tumor antigen on p8 was able to elicit both a protective and anti-tumor CTL response.[133] They evaluated the recombinant phage displaying the anti-tumor epitope for immunogenicity and protective potential in DBA/2 mice. They were able to show that mice that were treated with the phage construct had a survival advantage over control mice when challenged with tumor cells. They also assessed the survival of mice with an established tumor and they again found an increased survival with those mice treated with the epitope-displaying phage (50% survived after 60 days, in contrast to phage not displaying the epitope, only 10% survived after 60 days).

Another type of vaccine that phage have been developed to deliver, is nucleic acid immunisation. Nucleic acid immunisation is the delivery of genes that encode antigens to host eukaryotic cells where they are expressed. Nucleic acid vaccines can be directly taken up by the target cells, but it is a relatively ineffective process and the nucleic acids may be degraded before uptake. Bacteriophage have been utilized for nucleic acid immunisation because the phage can encode and protect the DNA for delivery to the cells, while offering an additional advantage of display of a targeting reagent for selective delivery.[137–140]

Some of the first research efforts in nucleic acid immunisation employing bacteriophage as the delivery method was done by Clark and March.[137,138] They utilized bacteriophage λ because they can be taken up by antigen-presenting cells (APCs),

mainly targeted to the spleen and liver Kupffer cells. The phage vectors contain a hepatitis B surface antigen (HBsAg) under the control of the cytomegalovirus promoter (CMV) for antigen expression in target cells. They immunized BALB/c mice with HBsAg protein, HBsAg DNA, and phage λ containing HBsAg DNA (λ-HBsAg). They found that mice vaccinated with 10^{11} pfu of (λ-HBsAg) showed significant anti-HBsAg responses. In total they found that the phage delivery of DNA was 10 times more efficient than plasmid vectors for DNA immunisation. Taken together, these data demonstrate the utility of phage nanocarriers for vaccine development and administration.

1.7.5 Phage-Dependent Delivery of Proteins, Peptides, and Antibodies

There has been only a limited number of studies on the delivery of functional therapeutic proteins and antibodies using bacteriophage, despite the great amount of research using phage display systems to screen protein and antibody libraries.[141,142] One study that does utilize a protein to induce phage internalization has been demonstrated.[143] In 2000, a group reported using filamentous phage to conjugate an adenovirus penton base (Ad-Pb) protein to p3, which would allow for binding and internalization via the integrin receptors. The adenovirus penton base protein also promotes endosomal release of the virus particle following endocytosis, which makes

this protein advantageous as a targeting and delivery moiety. The authors show that the phage were able to internalize into cells displaying a variety of integrin receptors. Despite the targeting and internalization of the phage, they were not able to show high expression of their delivered mammalian expression cassette. This may be due to a number of causes including intracellular degradation of phage, limited nuclear localization of DNA, or issues with the transduction of the ssDNA of the phage encoding the gene. Even so, the authors did demonstrate selective binding and internalization with the integrin receptors.

A large number of peptide antigens and peptides to direct receptor binding and internalization have been delivered to cells; however, the delivery of functional peptide therapeutics by phage have been largely limited. Phage have been used to deliver a therapeutic peptide to inhibit bacterial infection.[144] Dean *et al.* utilized M13 filamentous phage displaying an integrin binding peptide (RGD) to bind and induce integrin mediated endocytosis. Additionally, they displayed polymorphic membrane protein D (PmpD) peptide, which interferes with *Chlamydia trachomatic* (*Ct*) propagation, to reduce the infection in mammalian cells. They demonstrated that the PmpD peptide is responsible for reducing the *Ct* infection in HeLa and primary endocervical cells. Moreover, they performed additional experiments in an endocervical milieu, which mimics the *in vivo* mucosal cellular environment, and were able to show that phage-mediated display overcomes the delivery limitations of vector approaches and may be

effective in preventing other sexually transmitted pathogens. Additionally, this approach eliminates need for antibiotic administration, which may generate antibiotic resistance, an ever increasing problem in bacterial infection treatments.

Antibodies have been widely used to target phage for the delivery of small molecules, nucleic acids or to target antigen; however, studies on the delivery of therapeutically relevant antibodies with a phage nanocarriers are more limited.[145,146] One particularly interesting study proposes the eventual use of phage to display anti-β amyloid antibodies to detect amyloid plaque formation in living patients.[146] The current methods for detecting amyloid plaques *in vivo* are limited in specificity and detection resolution. Display on filamentous phage could provide a non-toxic carrier, while maintaining the biological function of the displayed antibodies. To test their theory, the researchers evaluated filamentous phage display of an anti-β amyloid antibody on p3 and treated Alzheimer's amyloid precursor protein (APP) transgenic mice. The anti-β amyloid-phage were able to target amyloid plaque formation with high specificity *in vivo* This study is the first example utilizing phage to penetrate the central nervous system, without degradation of the phage particle or the conjugated cargo.

1.8 Conclusions

Intracellular delivery of proteinaceous imaging and therapeutic reagents remains a challenge to the broader utility of protein reagents. Genetically-defined nanocarriers, such as bacteriophage, offer a promising approach to the delivery of these reagents. Bacteriophages are particularly well-studied and have been utilized as targeted antibacterial therapeutics. Additionally, phage have been engineered to act as nanocarriers for small-molecules, DNA, nanoparticles, vaccines, peptides and antibodies. However, the potential of phage for the delivery of protein reagents has yet to be fully realized. The unique structure of the phage virion allows for incorporation of genetically and spatially defined features for controlled display of the desired cargo. The ability to engineer phage nanocarriers that potently and selectively deliver protein reagents to mammalian cells offers a solution to the problem of intracellular protein delivery and could potentially lead to an expansion in the utility of protein reagents for the treatment and diagnosis of disease.

1.9 Thesis Overview

Bacteriophage have been used to deliver a variety of constructs to mammalian and bacterial cells; however, the delivery of fully functional proteins remains largely unexplored. My research has focused on the development of phage nanocarriers for

selective delivery of exogenous proteins and enzymes to prostate cancer cells. Chapters 2 and 3 focuses on the evolution and optimization of a cell-selective protein transduction domain to facilitate selective delivery of phage nanocarriers to prostate cancer cells. Chapter 4 discusses the development of phage nanocarriers for the delivery of exogenous proteins and enzymes to prostate cancer cell. Chapter 5 focuses on additional research in the McNaughton lab, including the development of cell-imprinted polyacrylamide hydrogels for programmed cell adhesion and engineering protein-based antibody recruiting molecules.

REFERENCES

(1) Ho, R. J. Y., and Chien, J. Y. (2012) Drug delivery trends in clinical trials and translational medicine: growth in biologic molecule development and impact on rheumatoid arthritis, Crohn's disease, and colitis. *J. Pharm. Sci. 101*, 2668–74.

(2) Aggarwal, R. S. (2014) What's fueling the biotech engine-2012 to 2013. *Nat. Biotechnol. 32*, 32–9.

(3) Muyldermans, S. (2013) Nanobodies: natural single-domain antibodies. *Annu. Rev. Biochem. 82*, 775–97.

(4) Skerra, A. (2000) Engineered protein scaffolds for molecular recognition. *J. Mol. Recognit. 13*, 167–87.

(5) Overington, J. P., Al-Lazikani, B., and Hopkins, A. L. (2006) How many drug targets are there? *Nat. Rev. Drug Discov. 5*, 993–6.

(6) Stanzl, E. G., Trantow, B. M., Vargas, J. R., and Wender, P. A. (2013) Fifteen years of cell-penetrating, guanidinium-rich molecular transporters: basic science, research tools, and clinical applications. *Acc. Chem. Res. 46*, 2944–54.

(7) Feramisco, J. R., Gross, M., Kamata, T., Rosenberg, M., and Sweet, R. W. (1984) Microinjection of the oncogene form of the human H-ras (t-24) protein results in rapid proliferation of quiescent cells. *Cell 38*, 109–117.

(8) Gregoriadis, G. (1995) Engineering liposomes for drug delivery: progress and problems. *Trends Biotechnol. 13*, 527–37.

(9) Zelphati, O., Wang, Y., Kitada, S., Reed, J. C., Felgner, P. L., and Corbeil, J. (2001) Intracellular delivery of proteins with a new lipid-mediated delivery system. *J. Biol. Chem. 276*, 35103–10.

(10) Utama, R. H., Guo, Y., Zetterlund, P. B., and Stenzel, M. H. (2012) Synthesis of hollow polymeric nanoparticles for protein delivery via inverse miniemulsion periphery RAFT polymerization. *Chem. Commun. (Camb). 48*, 11103–5.

(11) Gabel, C. A. (1986) Mannose 6-phosphate receptor-mediated endocytosis of acid hydrolases: internalization of beta-glucuronidase is accompanied by a limited dephosphorylation. *J. Cell Biol. 103*, 1817–1827.

(12) Fuchs, S. M., and Raines, R. T. (2005) Polyarginine as a multifunctional fusion tag. *Protein Sci. 14*, 1538–44.

(13) Fuchs, S. M., and Raines, R. T. (2007) Arginine grafting to endow cell permeability. *ACS Chem. Biol. 2*, 167–70.

(14) Cronican, J. J., Beier, K. T., Davis, T. N., Tseng, J.-C., Li, W., Thompson, D. B., Shih, A. F., May, E. M., Cepko, C. L., Kung, A. L., Zhou, Q., and Liu, D. R. (2011) A class of human proteins that deliver functional proteins into mammalian cells in vitro and in vivo. *Chem. Biol. 18*, 833–8.

(15) Cronican, J. J., Thompson, D. B., Beier, K. T., McNaughton, B. R., Cepko, C. L., and Liu, D. R. (2010) Potent delivery of functional proteins into Mammalian cells in vitro and in vivo using a supercharged protein. *ACS Chem. Biol. 5*, 747–52.

(16) McNaughton, B. R., Cronican, J. J., Thompson, D. B., and Liu, D. R. (2009) Mammalian cell penetration, siRNA transfection, and DNA transfection by supercharged proteins. *Proc. Natl. Acad. Sci. U. S. A. 106*, 6111–6.

(17) Thompson, D. B., Cronican, J. J., and Liu, D. R. (2012) Engineering and identifying supercharged proteins for macromolecule delivery into mammalian cells. *Methods Enzymol. 503*, 293–319.

(18) Deshayes, S., Morris, M. C., Divita, G., and Heitz, F. (2005) Cell-penetrating peptides: tools for intracellular delivery of therapeutics. *Cell. Mol. Life Sci. 62*, 1839–49.

(19) Favoreel, H. W., Nauwynck, H. J., Halewyck, H. M., Van Oostveldt, P., Mettenleiter, T. C., and Pensaert, M. B. (1999) Antibody-induced endocytosis of viral glycoproteins and major histocompatibility complex class I on pseudorabies virus-infected monocytes. *J. Gen. Virol. 80 (Pt 5)*, 1283–91.

(20) Sarmiento, R. E., Tirado, R. G., Valverde, L. E., and Gómez-Garcia, B. (2007) Kinetics of antibody-induced modulation of respiratory syncytial virus antigens in a human epithelial cell line. *Virol. J. 4*, 68.

(21) Torchilin, V. (2008) Intracellular delivery of protein and peptide therapeutics. *Drug Discov. Today Technol. 5*, e95–e103.

(22) Fritzer, M., Szekeres, T., Szüts, V., Jarayam, H. N., and Goldenberg, H. (1996) Cytotoxic effects of a doxorubicin-transferrin conjugate in multidrug-resistant KB cells. *Biochem. Pharmacol. 51*, 489–93.

(23) Rothbard, J. B., Garlington, S., Lin, Q., Kirschberg, T., Kreider, E., McGrane, P. L., Wender, P. a, and Khavari, P. a. (2000) Conjugation of arginine oligomers to cyclosporin A facilitates topical delivery and inhibition of inflammation. *Nat. Med. 6*, 1253–7.

(24) Mazel, M., Clair, P., Rousselle, C., Vidal, P., Scherrmann, J. M., Mathieu, D., and Temsamani, J. (2001) Doxorubicin-peptide conjugates overcome multidrug resistance. *Anticancer. Drugs 12*, 107–16.

(25) Kim, D. T., Mitchell, D. J., Brockstedt, D. G., Fong, L., Nolan, G. P., Fathman, C. G., Engleman, E. G., and Rothbard, J. B. (1997) Introduction of soluble proteins into the MHC class I pathway by conjugation to an HIV tat peptide. *J. Immunol. 159*, 1666–8.

(26) Fawell, S., Seery, J., Daikh, Y., Moore, C., Chen, L. L., Pepinsky, B., and Barsoum, J. (1994) Tat-mediated delivery of heterologous proteins into cells. *Proc. Natl. Acad. Sci. U. S. A. 91*, 664–8.

(27) Moy, P., Daikh, Y., Pepinsky, B., Thomas, D., Fawell, S., and Barsoum, J. (1996) Tat-mediated protein delivery can facilitate MHC class I presentation of antigens. *Mol. Biotechnol. 6*, 105–13.

(28) Veldhoen, S., Laufer, S. D., Trampe, A., and Restle, T. (2006) Cellular delivery of small interfering RNA by a non-covalently attached cell-penetrating peptide: quantitative analysis of uptake and biological effect. *Nucleic Acids Res. 34*, 6561–73.

(29) Meade, B. R., and Dowdy, S. F. (2007) Exogenous siRNA delivery using peptide transduction domains/cell penetrating peptides. *Adv. Drug Deliv. Rev. 59*, 134–40.

(30) Maus, L., Dick, O., Bading, H., Spatz, J. P., and Fiammengo, R. (2010) Conjugation of peptides to the passivation shell of gold nanoparticles for targeting of cell-surface receptors. *ACS Nano 4*, 6617–28.

(31) Smith, C.-A. M., de la Fuente, J., Pelaz, B., Furlani, E. P., Mullin, M., and Berry, C. C. (2010) The effect of static magnetic fields and tat peptides on cellular and nuclear uptake of magnetic nanoparticles. *Biomaterials 31*, 4392–400.

(32) Jabbari, E., Yang, X., Moeinzadeh, S., and He, X. (2013) Drug release kinetics, cell uptake, and tumor toxicity of hybrid VVVVVVKK peptide-assembled polylactide nanoparticles. *Eur. J. Pharm. Biopharm. 84*, 49–62.

(33) Mitchell, D. J., Steinman, L., Kim, D. T., Fathman, C. G., and Rothbard, J. B. (2000) Polyarginine enters cells more efficiently than other polycationic homopolymers. *J. Pept. Res. 56*, 318–325.

(34) Frankel, A. D., and Pabo, C. O. (1988) Cellular uptake of the tat protein from human immunodeficiency virus. *Cell 55*, 1189–1193.

(35) Green, M., and Loewenstein, P. M. (1988) Autonomous functional domains of chemically synthesized human immunodeficiency virus tat trans-activator protein. *Cell 55*, 1179–88.

(36) Derossi, D., Joliot, A. H., Chassaing, G., and Prochiantz, A. (1994) The third helix of the Antennapedia homeodomain translocates through biological membranes. *J. Biol. Chem. 269*, 10444–50.

(37) Pooga, M., Hällbrink, M., Zorko, M., and Langel, U. (1998) Cell penetration by transportan. *FASEB J. 12*, 67–77.

(38) Elliott, G., and O'Hare, P. (1997) Intercellular trafficking and protein delivery by a herpesvirus structural protein. *Cell 88*, 223–33.

(39) Vivès, E., Brodin, P., and Lebleu, B. (1997) A truncated HIV-1 Tat protein basic domain rapidly translocates through the plasma membrane and accumulates in the cell nucleus. *J. Biol. Chem. 272*, 16010–7.

(40) Console, S., Marty, C., García-Echeverría, C., Schwendener, R., and Ballmer-Hofer, K. (2003) Antennapedia and HIV transactivator of transcription (TAT) "protein transduction domains" promote endocytosis of high molecular weight cargo upon binding to cell surface glycosaminoglycans. *J. Biol. Chem. 278*, 35109–14.

(41) Gu, Z., Biswas, A., Zhao, M., and Tang, Y. (2011) Tailoring nanocarriers for intracellular protein delivery. *Chem. Soc. Rev. 40*, 3638–55.

(42) Liguori, L., Marques, B., Villegas-Mendez, A., Rothe, R., and Lenormand, J.-L. (2008) Liposomes-mediated delivery of pro-apoptotic therapeutic membrane proteins. *J. Control. Release 126*, 217–27.

(43) Zelphati, O., Wang, Y., Kitada, S., Reed, J. C., Felgner, P. L., and Corbeil, J. (2001) Intracellular delivery of proteins with a new lipid-mediated delivery system. *J. Biol. Chem. 276*, 35103–10.

(44) Almeida, A. J., Runge, S., and Müller, R. H. (1997) Peptide-loaded solid lipid nanoparticles (SLN): Influence of production parameters. *Int. J. Pharm. 149*, 255–265.

(45) Shi Kam, N. W., Jessop, T. C., Wender, P. A., and Dai, H. (2004) Nanotube molecular transporters: internalization of carbon nanotube-protein conjugates into Mammalian cells. *J. Am. Chem. Soc. 126*, 6850–1.

(46) Koshman, Y. E., Waters, S. B., Walker, L. A., Los, T., de Tombe, P., Goldspink, P. H., and Russell, B. (2008) Delivery and visualization of proteins conjugated to quantum dots in cardiac myocytes. *J. Mol. Cell. Cardiol. 45*, 853–6.

(47) Ghosh, P., Yang, X., Arvizo, R., Zhu, Z.-J., Agasti, S. S., Mo, Z., and Rotello, V. M. (2010) Intracellular delivery of a membrane-impermeable enzyme in active form using functionalized gold nanoparticles. *J. Am. Chem. Soc. 132*, 2642–5.

(48) Slowing, I. I., Trewyn, B. G., and Lin, V. S.-Y. (2007) Mesoporous silica nanoparticles for intracellular delivery of membrane-impermeable proteins. *J. Am. Chem. Soc. 129*, 8845–9.

(49) Chorny, M., Hood, E., Levy, R. J., and Muzykantov, V. R. (2010) Endothelial delivery of antioxidant enzymes loaded into non-polymeric magnetic nanoparticles. *J. Control. Release 146*, 144–51.

(50) Jung, S., Huh, S., Cheon, Y.-P., and Park, S. (2009) Intracellular protein delivery by glucose-coated polymeric beads. *Chem. Commun. (Camb).* 5003–5.

(51) Murthy, N., Xu, M., Schuck, S., Kunisawa, J., Shastri, N., and Fréchet, J. M. J. (2003) A macromolecular delivery vehicle for protein-based vaccines: acid-degradable protein-loaded microgels. *Proc. Natl. Acad. Sci. U. S. A. 100*, 4995–5000.

(52) Gao, J., and Xu, B. (2009) Applications of nanomaterials inside cells. *Nano Today 4*, 37–51.

(53) Faraji, A. H., and Wipf, P. (2009) Nanoparticles in cellular drug delivery. *Bioorg. Med. Chem. 17*, 2950–62.

(54) Peer, D., Karp, J. M., Hong, S., Farokhzad, O. C., Margalit, R., and Langer, R. (2007) Nanocarriers as an emerging platform for cancer therapy. *Nat. Nanotechnol. 2*, 751–60.

(55) Lee, K. Y., and Yuk, S. H. (2007) Polymeric protein delivery systems. *Prog. Polym. Sci. 32*, 669–697.

(56) Gaberc-Porekar, V., Zore, I., Podobnik, B., and Menart, V. (2008) Obstacles and pitfalls in the PEGylation of therapeutic proteins. *Curr. Opin. Drug Discov. Devel. 11*, 242–50.

(57) Solaro, R. (2008) Targeted delivery of proteins by nanosized carriers. *J. Polym. Sci. Part A Polym. Chem. 46*, 1–11.

(58) Molino, N. M., and Wang, S.-W. (2014) Caged protein nanoparticles for drug delivery. *Curr. Opin. Biotechnol. 28C*, 75–82.

(59) Uchida, M., Klem, M. T., Allen, M., Suci, P., Flenniken, M., Gillitzer, E., Varpness, Z., Liepold, L. O., Young, M., and Douglas, T. (2007) Biological Containers: Protein Cages as Multifunctional Nanoplatforms. *Adv. Mater. 19*, 1025–1042.

(60) Jeon, J. O., Kim, S., Choi, E., Shin, K., Cha, K., So, I.-S., Kim, S.-J., Jun, E., Kim, D., Ahn, H. J., Lee, B.-H., Lee, S.-H., and Kim, I.-S. (2013) Designed nanocage displaying ligand-specific Peptide bunches for high affinity and biological activity. *ACS Nano 7*, 7462–71.

(61) Minten, I. J., Claessen, V. I., Blank, K., Rowan, A. E., Nolte, R. J. M., and Cornelissen, J. J. L. M. (2011) Catalytic capsids: the art of confinement. *Chem. Sci. 2*, 358.

(62) Strable, E., Prasuhn, D. E., Udit, A. K., Brown, S., Link, A. J., Ngo, J. T., Lander, G., Quispe, J., Potter, C. S., Carragher, B., Tirrell, D. A., and Finn, M. G. (2008) Unnatural amino acid incorporation into virus-like particles. *Bioconjug. Chem. 19*, 866–75.

(63) Fiedler, J. D., Brown, S. D., Lau, J. L., and Finn, M. G. (2010) RNA-directed packaging of enzymes within virus-like particles. *Angew. Chem. Int. Ed. Engl. 49*, 9648–51.

(64) O'Neil, A., Reichhardt, C., Johnson, B., Prevelige, P. E., and Douglas, T. (2011) Genetically programmed in vivo packaging of protein cargo and its controlled release from bacteriophage P22. *Angew. Chem. Int. Ed. Engl. 50*, 7425–8.

(65) Ashley, C. E., Carnes, E. C., Phillips, G. K., Durfee, P. N., Buley, M. D., Lino, C. a, Padilla, D. P., Phillips, B., Carter, M. B., Willman, C. L., Brinker, C. J., Caldeira, J. D. C., Chackerian, B., Wharton, W., and Peabody, D. S. (2011) Cell-specific delivery of diverse cargos by bacteriophage MS2 virus-like particles. *ACS Nano 5*, 5729–45.

(66) Sunbul, M., Emerson, N., and Yin, J. (2011) Enzyme-catalyzed substrate attachment to phage surfaces for the selection of catalytic activities. *Chembiochem 12*, 380–6.

(67) Zachariou, M., Widdowson, C. A., and Straffon, M. J. (2006, April 7) Bacteriophages Displaying Functional Enzymes and Uses Thereof.

(68) Collins, James, J., Kobayashi, H., Kearn, M., Araki, M., Friedland, A., and Kuan-Ta Lu, T. (2006, December 29) Engineered Enzymatically Active Bacteriophages and Methods of Uses Thereof.

(69) Carette, N., Engelkamp, H., Akpa, E., Pierre, S. J., Cameron, N. R., Christianen, P. C. M., Maan, J. C., Thies, J. C., Weberskirch, R., Rowan, A. E., Nolte, R. J. M., Michon, T., and Van Hest, J. C. M. (2007) A virus-based biocatalyst. *Nat. Nanotechnol. 2*, 226–9.

(70) Cruz, S. S., Chapman, S., Roberts, A. G., Roberts, I. M., Prior, D. A., and Oparka, K. J. (1996) Assembly and movement of a plant virus carrying a green fluorescent protein overcoat. *Proc. Natl. Acad. Sci. 93*, 6286–6290.

(71) Werner, S., Marillonnet, S., Hause, G., Klimyuk, V., and Gleba, Y. (2006) Immunoabsorbent nanoparticles based on a tobamovirus displaying protein A. *Proc. Natl. Acad. Sci. U. S. A. 103*, 17678–83.

(72) Smith, M. L., Lindbo, J. A., Dillard-Telm, S., Brosio, P. M., Lasnik, A. B., McCormick, A. A., Nguyen, L. V, and Palmer, K. E. (2006) Modified tobacco mosaic virus particles as scaffolds for display of protein antigens for vaccine applications. *Virology 348*, 475–88.

(73) Granieri, L., Baret, J.-C., Griffiths, A. D., and Merten, C. A. (2010) High-throughput screening of enzymes by retroviral display using droplet-based microfluidics. *Chem. Biol. 17*, 229–35.

(74) Wörsdörfer, B., Pianowski, Z., and Hilvert, D. (2012) Efficient in vitro encapsulation of protein cargo by an engineered protein container. *J. Am. Chem. Soc. 134*, 909–11.

(75) Franco, D., Liu, W., Gardiner, D. F., Hahn, B. H., and Ho, D. D. (2011) CD40L-containing virus-like particle as a candidate HIV-1 vaccine targeting dendritic cells. *J. Acquir. Immune Defic. Syndr. 56*, 393–400.

(76) Kaczmarczyk, S. J., Sitaraman, K., Young, H. A., Hughes, S. H., and Chatterjee, D. K. (2011) Protein delivery using engineered virus-like particles. *Proc. Natl. Acad. Sci. U. S. A. 108*, 16998–17003.

(77) Wörsdörfer, B., Woycechowsky, K. J., and Hilvert, D. (2011) Directed evolution of a protein container. *Science 331*, 589–92.

(78) Twort, F. W. (1915) An Investigation On the Nature of Ultra-Microscopic Viruses. *Lancet 186*, 1241–1243.

(79) D'Herelle, F. (1917) Sur un microbe invisible antagoniste des bacilles dysentériques. *Acad. Sci. Paris 165*, 373–375.

(80) Housby, J. N., and Mann, N. H. (2009) Phage therapy. *Drug Discov. Today 14*, 536–40.

(81) Sulakvelidze, A. (2001) Bacteriophage therapy. *Antimicrob. agents … 45*.

(82) Soothill, J. S. (1994) Bacteriophage prevents destruction of skin grafts by Pseudomonas aeruginosa. *Burns 20*, 209–11.

(83) Hawkins, C., Harper, D., Burch, D., Anggård, E., and Soothill, J. (2010) Topical treatment of Pseudomonas aeruginosa otitis of dogs with a bacteriophage mixture: a before/after clinical trial. *Vet. Microbiol. 146*, 309–13.

(84) Matsuzaki, S., Yasuda, M., Nishikawa, H., Kuroda, M., Ujihara, T., Shuin, T., Shen, Y., Jin, Z., Fujimoto, S., Nasimuzzaman, M. D., Wakiguchi, H., Sugihara, S., Sugiura, T., Koda, S., Muraoka, A., and Imai, S. (2003) Experimental protection of mice against lethal Staphylococcus aureus infection by novel bacteriophage phi MR11. *J. Infect. Dis. 187*, 613–24.

(85) Biswas, B., Adhya, S., Washart, P., Paul, B., Trostel, A. N., Powell, B., Carlton, R., and Merril, C. R. (2002) Bacteriophage therapy rescues mice bacteremic from a clinical isolate of vancomycin-resistant Enterococcus faecium. *Infect. Immun. 70*, 204–10.

(86) Ramesh, V., Fralick, J. A., and Rolfe, R. D. (1999) Prevention of Clostridium difficile -induced ileocecitis with Bacteriophage. *Anaerobe 5*, 69–78.

(87) Gu, J., Liu, X., Li, Y., Han, W., Lei, L., Yang, Y., Zhao, H., Gao, Y., Song, J., Lu, R., Sun, C., and Feng, X. (2012) A method for generation phage cocktail with great therapeutic potential. *PLoS One* (Spellberg, B., Ed.) *7*, e31698.

(88) Abedon, S. T., Kuhl, S. J., Blasdel, B. G., and Kutter, E. M. (2011) Phage treatment of human infections. *Bacteriophage 1*, 66–85.

(89) Summers, W. C. (2001) Bacteriophage therapy. *Annu. Rev. Microbiol. 55*, 437–51.

(90) Kutter, E., De Vos, D., Gvasalia, G., Alavidze, Z., Gogokhia, L., Kuhl, S., and Abedon, S. T. (2010) Phage therapy in clinical practice: treatment of human infections. *Curr. Pharm. Biotechnol. 11*, 69–86.

(91) Rhoads, D. D., Wolcott, R. D., Kuskowski, M. A., Wolcott, B. M., Ward, L. S., and Sulakvelidze, A. (2009) Bacteriophage therapy of venous leg ulcers in humans: results of a phase I safety trial. *J. Wound Care 18*, 237–8, 240–3.

(92) Wright, a, Hawkins, C. H., Anggård, E. E., and Harper, D. R. (2009) A controlled clinical trial of a therapeutic bacteriophage preparation in chronic otitis due to antibiotic-resistant Pseudomonas aeruginosa; a preliminary report of efficacy. *Clin. Otolaryngol. 34*, 349–57.

(93) Rakonjac, J. (2012) Filamentous Bacteriophages : Biology and Applications.

(94) Vaks, L., and Benhar, I. (2011) In vivo characteristics of targeted drug-carrying filamentous bacteriophage nanomedicines. *J. Nanobiotechnology 9*, 58.

(95) Yacoby, I., Bar, H., and Benhar, I. (2007) Targeted drug-carrying bacteriophages as antibacterial nanomedicines. *Antimicrob. Agents Chemother. 51*, 2156–63.

(96) Yacoby, I., Shamis, M., Bar, H., Shabat, D., and Benhar, I. (2006) Targeting antibacterial agents by using drug-carrying filamentous bacteriophages. *Antimicrob. Agents Chemother. 50*, 2087–97.

(97) Kelly, K. A., Waterman, P., and Weissleder, R. (2006) In vivo imaging of molecularly targeted phage. *Neoplasia 8*, 1011–8.

(98) Li, K., Chen, Y., Li, S., Nguyen, H. G., Niu, Z., You, S., Mello, C. M., Lu, X., and Wang, Q. (2010) Chemical modification of M13 bacteriophage and its application in cancer cell imaging. *Bioconjug. Chem. 21*, 1369–77.

(99) Clark, C. J., and Sage, E. H. (2008) A prototypic matricellular protein in the tumor microenvironment--where there's SPARC, there's fire. *J. Cell. Biochem. 104*, 721–32.

(100) Bar, H., Yacoby, I., and Benhar, I. (2008) Killing cancer cells by targeted drug-carrying phage nanomedicines. *BMC Biotechnol. 8*, 37.

(101) Suthiwangcharoen, N., Li, T., Li, K., Thompson, P., You, S., and Wang, Q. (2011) M13 bacteriophage-polymer nanoassemblies as drug delivery vehicles. *Nano Res. 4*, 483–493.

(102) Ghosh, D., Kohli, A. G., Moser, F., Endy, D., and Belcher, A. M. (2012) Refactored M13 bacteriophage as a platform for tumor cell imaging and drug delivery. *ACS Synth. Biol. 1*, 576–82.

(103) Souza, G. R., Christianson, D. R., Staquicini, F. I., Ozawa, M. G., Snyder, E. Y., Sidman, R. L., Miller, J. H., Arap, W., and Pasqualini, R. (2006) Networks of gold nanoparticles and bacteriophage as biological sensors and cell-targeting agents. *Proc. Natl. Acad. Sci. U. S. A. 103*, 1215–20.

(104) Ghosh, D., Lee, Y., Thomas, S., Kohli, A. G., Yun, D. S., Belcher, A. M., and Kelly, K. A. (2012) M13-templated magnetic nanoparticles for targeted in vivo imaging of prostate cancer. *Nat. Nanotechnol. 7*, 677–82.

(105) Yoo, P. J., Nam, K. T., Qi, J., Lee, S.-K., Park, J., Belcher, A. M., and Hammond, P. T. (2006) Spontaneous assembly of viruses on multilayered polymer surfaces. *Nat. Mater. 5*, 234–40.

(106) Yi, H., Ghosh, D., Ham, M.-H., Qi, J., Barone, P. W., Strano, M. S., and Belcher, A. M. (2012) M13 phage-functionalized single-walled carbon nanotubes as nanoprobes for second near-infrared window fluorescence imaging of targeted tumors. *Nano Lett. 12*, 1176–83.

(107) Dang, X., Yi, H., Ham, M.-H., Qi, J., Yun, D. S., Ladewski, R., Strano, M. S., Hammond, P. T., and Belcher, A. M. (2011) Virus-templated self-assembled single-walled carbon nanotubes for highly efficient electron collection in photovoltaic devices. *Nat. Nanotechnol. 6*, 377–84.

(108) Misra, S. (2013) Human gene therapy: a brief overview of the genetic revolution. *J. Assoc. Physicians India 61*, 127–33.

(109) Yokoyama-Kobayashi, M., and Kato, S. (1994) Recombinant f1 phage-mediated transfection of mammalian cells using lipopolyamine technique. *Anal. Biochem. 223*, 130–4.

(110) Dunn, I. S. (1996) Mammalian cell binding and transfection mediated by surface-modified bacteriophage lambda. *Biochimie 137*, 37.

(111) Larocca, D., and Witte, A. (1998) Targeting bacteriophage to mammalian cell surface receptors for gene delivery. *Hum. Gene Ther. 2399*, 2393–2399.

(112) Larocca, D., Jensen-Pergakes, K., Burg, M. A., and Baird, A. (2001) Receptor-targeted gene delivery using multivalent phagemid particles. *Mol. Ther. 3*, 476–84.

(113) Larocca, D., Burg, M. A., Jensen-Pergakes, K., Ravey, E. P., Gonzalez, A. M., and Baird, A. (2002) Evolving phage vectors for cell targeted gene delivery. *Curr. Pharm. Biotechnol. 3*, 45–57.

(114) Burg, M. A., Jensen-pergakes, K., Gonzalez, A. M., Cells, C., Ravey, P., Baird, A., and Larocca, D. (2002) Enhanced Phagemid Particle Gene Transfer in Camptothecin-treated Carcinoma Cells Advances in Brief Enhanced Phagemid Particle Gene Transfer in Camptothecin-treated. *Cancer Res. 62*, 977–981.

(115) Poul, M. a, and Marks, J. D. (1999) Targeted gene delivery to mammalian cells by filamentous bacteriophage. *J. Mol. Biol. 288*, 203–11.

(116) Westwater, C., and Kasman, L. (2003) Use of genetically engineered phage to deliver antimicrobial agents to bacteria: an alternative therapy for treatment of bacterial infections. *Antimicrob. agents … 47*, 1301–1307.

(117) Lu, T. K., and Collins, J. J. (2009) Engineered bacteriophage targeting gene networks as adjuvants for antibiotic therapy. *Proc. Natl. Acad. Sci. U. S. A. 106*, 4629–34.

(118) Edgar, R., Friedman, N., Molshanski-Mor, S., and Qimron, U. (2012) Reversing bacterial resistance to antibiotics by phage-mediated delivery of dominant sensitive genes. *Appl. Environ. Microbiol. 78*, 744–51.

(119) Wan, Y., Wu, Y., Bian, J., Wang, X. Z., Zhou, W., Jia, Z. C., Tan, Y., and Zhou, L. (2001) Induction of hepatitis B virus-specific cytotoxic T lymphocytes response in vivo by filamentous phage display vaccine. *Vaccine 19*, 2918–23.

(120) Grabowska, a M., Jennings, R., Laing, P., Darsley, M., Jameson, C. L., Swift, L., and Irving, W. L. (2000) Immunisation with phage displaying peptides representing single epitopes of the glycoprotein G can give rise to partial protective immunity to HSV-2. *Virology 269*, 47–53.

(121) Sathaliyawala, T., Rao, M., Maclean, D. M., Birx, D. L., Alving, C. R., and Rao, V. B. (2006) Assembly of human immunodeficiency virus (HIV) antigens on bacteriophage T4: a novel in vitro approach to construct multicomponent HIV vaccines. *J. Virol. 80*, 7688–98.

(122) De Berardinis, P., D'Apice, L., Prisco, a, Ombra, M. N., Barba, P., Del Pozzo, G., Petukhov, S., Malik, P., Perham, R. N., and Guardiola, J. (1999) Recognition of HIV-derived B and T cell epitopes displayed on filamentous phages. *Vaccine 17*, 1434–41.

(123) De Berardinis, P., Sartorius, R., Fanutti, C., Perham, R. N., Del Pozzo, G., and Guardiola, J. (2000) Phage display of peptide epitopes from HIV-1 elicits strong cytolytic responses. *Nat. Biotechnol. 18*, 873–6.

(124) Li, Q., Shivachandra, S. B., Zhang, Z., and Rao, V. B. (2007) Assembly of the small outer capsid protein, Soc, on bacteriophage T4: a novel system for high density display of multiple large anthrax toxins and foreign proteins on phage capsid. *J. Mol. Biol. 370*, 1006–19.

(125) Shivachandra, S. B., Li, Q., Peachman, K. K., Matyas, G. R., Leppla, S. H., Alving, C. R., Rao, M., and Rao, V. B. (2007) Multicomponent anthrax toxin display and delivery using bacteriophage T4. *Vaccine 25*, 1225–35.

(126) Hayes, S., Gamage, L. N. a, and Hayes, C. (2010) Dual expression system for assembling phage lambda display particle (LDP) vaccine to porcine Circovirus 2 (PCV2). *Vaccine 28*, 6789–99.

(127) Gamage, L. N. a, Ellis, J., and Hayes, S. (2009) Immunogenicity of bacteriophage lambda particles displaying porcine Circovirus 2 (PCV2) capsid protein epitopes. *Vaccine 27*, 6595–604.

(128) Ren, Z. J., Tian, C. J., Zhu, Q. S., Zhao, M. Y., Xin, a G., Nie, W. X., Ling, S. R., Zhu, M. W., Wu, J. Y., Lan, H. Y., Cao, Y. C., and Bi, Y. Z. (2008) Orally delivered foot-and-mouth disease virus capsid protomer vaccine displayed on T4 bacteriophage surface: 100% protection from potency challenge in mice. *Vaccine 26*, 1471–81.

(129) Wu, J., Tu, C., Yu, X., Zhang, M., Zhang, N., Zhao, M., Nie, W., and Ren, Z. (2007) Bacteriophage T4 nanoparticle capsid surface SOC and HOC bipartite display with enhanced classical swine fever virus immunogenicity: a powerful immunological approach. *J. Virol. Methods 139*, 50–60.

(130) Wang, G., Sun, M., Fang, J., Yang, Q., Tong, H., and Wang, L. (2006) Protective immune responses against systemic candidiasis mediated by phage-displayed specific epitope of Candida albicans heat shock protein 90 in C57BL/6J mice. *Vaccine 24*, 6065–73.

(131) Bastien, N., Trudel, M., and Simard, C. (1997) Protective immune responses induced by the immunization of mice with a recombinant bacteriophage displaying an epitope of the human respiratory syncytial virus. *Virology 234*, 118–22.

(132) Frenkel, D., Dewachter, I., Leuven, F. Van, and Solomon, B. (2003) Reduction of β-amyloid plaques in brain of transgenic mouse model of Alzheimer's disease by EFRH-phage immunization. *Vaccine 21*, 1060–1065.

(133) Wu, Y., Wan, Y., Bian, J., and Zhao, J. (2002) Phage display particles expressing tumor-specific antigens induce preventive and therapeutic anti-tumor immunity in murine p815 model. *Int. J. cancer 753*, 748–753.

(134) Eriksson, F., Culp, W. D., Massey, R., Egevad, L., Garland, D., Persson, M. a a, and Pisa, P. (2007) Tumor specific phage particles promote tumor regression in a mouse melanoma model. *Cancer Immunol. Immunother. 56*, 677–87.

(135) Eriksson, F., Tsagozis, P., Lundberg, K., Parsa, R., Mangsbo, S. M., Persson, M. a a, Harris, R. a, and Pisa, P. (2009) Tumor-specific bacteriophages induce tumor destruction through activation of tumor-associated macrophages. *J. Immunol. 182*, 3105–11.

(136) Sartorius, R., Pisu, P., D'Apice, L., Pizzella, L., Romano, C., Cortese, G., Giorgini, A., Santoni, A., Velotti, F., and De Berardinis, P. (2008) The use of filamentous bacteriophage fd to deliver MAGE-A10 or MAGE-A3 HLA-A2-restricted peptides and to induce strong antitumor CTL responses. *J. Immunol. 180*, 3719–28.

(137) Clark, J. R., and March, J. B. (2004) Bacteriophage-mediated nucleic acid immunisation. *FEMS Immunol. Med. Microbiol. 40*, 21–26.

(138) March, J. B., Clark, J. R., and Jepson, C. D. (2004) Genetic immunisation against hepatitis B using whole bacteriophage lambda particles. *Vaccine 22*, 1666–71.

(139) Jepson, C. D., and March, J. B. (2004) Bacteriophage lambda is a highly stable DNA vaccine delivery vehicle. *Vaccine 22*, 2413–9.

(140) Hashemi, H., Bamdad, T., Jamali, A., Pouyanfard, S., and Mohammadi, M. G. (2010) Evaluation of humoral and cellular immune responses against HSV-1 using genetic immunization by filamentous phage particles: a comparative approach to conventional DNA vaccine. *J. Virol. Methods 163*, 440–4.

(141) Barbas, C. F. I., Burton, D. R., Scott, J. K., and Silverman, G. J. (2004) Phage Display: A Laboratory Manual. CSHL Press.

(142) Clackson, T., and Lowman, H. B. (2004) Phage Display: A Practical Approach. Oxford University Press.

(143) Di Giovine, M., Salone, B., Martina, Y., Amati, V., Zambruno, G., Cundari, E., Failla, C. M., and Saggio, I. (2001) Binding properties, cell delivery, and gene transfer of adenoviral penton base displaying bacteriophage. *Virology 282*, 102–12.

(144) Bhattarai, S. R., Yoo, S. Y., Lee, S.-W., and Dean, D. (2012) Engineered phage-based therapeutic materials inhibit Chlamydia trachomatis intracellular infection. *Biomaterials 33*, 5166–74.

(145) Dickerson, T. J., Kaufmann, G. F., and Janda, K. D. (2005) Bacteriophage-mediated protein delivery into the central nervous system and its application in immunopharmacotherapy. *Expert Opin. Biol. Ther. 5*, 773–81.

(146) Frenkel, D., and Solomon, B. (2002) Filamentous phage as vector-mediated antibody delivery to the brain. *Proc. Natl. Acad. Sci. U. S. A. 99*, 5675–9.

(147) Casjens, S. R., Medical, U., and City, S. L. (2001) Bacteriophage Lambda and its Relatives. *Encycl. life Sci.*

(148) Cuervo, A., and Carrascosa, J. L. (2012) Bacteriophages : Structure. *Encycl. life Sci.*

CHAPTER TWO

A PROTEIN TRANSDUCTION DOMAIN WITH CELL UPTAKE AND SELECTIVITY PROFILES THAT ARE CONTROLLED BY MULTIVALENCY EFFECTS

2.1 Introduction

In Chapter 1 we discussed the challenge of delivering macromolecular biologics to the interior of diseased cells to target intracellular function. We aimed to develop a nanocarrier technology that selectively delivers exogenous protein cargo to the interior of human prostate cancer cells. In order to achieve targeted protein delivery with a phage nanocarrier, we first had to develop a reagent to enable selective phage internalization. Therefore, we evolved a cell-selective protein transduction domain to enable cell penetration. This chapter details our efforts to develop a cell-selective transduction reagent for targeted delivery to PC-3 prostate cancer cells.

2.2 Developing a Cell-Selective Protein Transduction Domain to Target PC-3 Prostate Cancer Cells

Antibodies have been widely employed to target diseased cells often by targeting cell-surface receptors. The most common method for selectively delivering cargo to a specific cell is through fusion to a monoclonal antibody or its fragment antigen-binding

region (Fab fragment), which binds a receptor present on the target cell. Although such immunoconjugate-targeted therapies are often cell-selective, they do not directly address the problem of cellular internalization. Some examples of cell-penetrating antibodies have been reported[1] and the development of new cell-penetrating antibodies, such as TransMabs[2], has greatly increased over the past decade. However, the production, distribution, and storage of these antibody reagents is very costly.[3,4]

The development of cell-penetrating peptides (CPPs) or protein transduction domains (PTDs) has offered a solution to many of the limitations of antibody-based delivery systems. The small size of PTDs (typically <20 amino acids) enables relatively facile production, purification and fusion to cargo for delivery.[5–7] PTDs are generally divided into three different categories, amphipathic helical peptides, arginine rich peptides, and signal sequence-based peptides (**Table 2.1**)[8–21]. Amphipathic helical peptides are rich in lysine residues and include the PTDs transportan and model amphipathic peptide (MAP). Arginine-rich peptides such as trans-activating

Table 2.1 Sequences of protein transduction domains

Name	Sequence	References
Amphipathic helical peptides		
transportan	GWTLNSAGYLLKINLKALAALAKKIL	**9**
MAP	KLALKLALKALKAALKLA	**10**
Arginine-rich peptides		
Tat_{49-60}	RKKRRQRRR	**11**
Arg_9	RRRRRRRRR	**12, 13**
VP22	DAATATRGRSAASRPTERPRAPARSASRPRRPVD	**14**
penetratin	RQIKIWFQNRRMKWKK	**15, 16**
Signal sequence peptides		
Kaposi FGF signal sequences	AAVALLPAVLLALLAP	**17, 18**
Human β3 integrin signal sequence	VTVLALGALAGVGVG	**19**
gp41 fusion sequence	GALFLGWLGAAGSTMGA	**20, 21**

transcriptional activator (Tat), the homeodomain of Antennapedia (Antp), and penetratin are among the most commonly used protein-derived peptides. Signal sequence-based peptides target specific surface-exposed receptors that facilitate internalization and many times do not contain a high charge. PTDs cross the lipid bilayer of the plasma membrane through a variety of mechanisms, covered in Section 2.8, but entry is often highly dependent not only on the PTD, but also the cargo and the cell-line.

As part of a research program focused on the diagnosis and treatment of prostate cancer, we aimed to develop a prostate cancer cell-selective PTD. Prostate-specific membrane antigen (PSMA) is a membrane-bound glycoprotein that is often found in prostate tissue and is a commonly targeted cancer biomarker. Previously, studies analyzing the expression of PSMA have found an upregulation in correlation with prostate cancer.[22,23] Unsurprisingly, targeted delivery of cargo to prostate cancer cells often relies on antibodies, Fab fragments[24–26], or other ligands such as aptamers that bind PSMA.[27] However, the expression level of PSMA varies dramatically among prostate cancer and many prostate cancer cells do not express PSMA.[28,29] Moreover, reports of elevated levels of PSMA in healthy males and females have indicated that PSMA is not a prostate-cancer specific biomarker.[30] Therefore, we did not target PSMA and focused on targeting the entire cell surface of a PSMA-negative prostate cancer cell line, PC-3 cells.

2.3 Phage Display *In Vitro* Evolution of a Cell-Specific Protein Transduction Domain

Phage display has been widely utilized to identify peptides, proteins and antibodies that bind to a particular protein or cell-surface marker.[31,32] Phage evolution has been used to identify PTDs not found in Nature.[33–37] Phage display is commonly performed on an immobilized target, the phage library is panned against the target and the bound phage are eluted after washing. However, our selection was not targeted to one particular cell-surface receptor, instead we were evaluating cell internalization; therefore, we chose to use whole cells as our target. As summarized in **Figure 2.1**, the

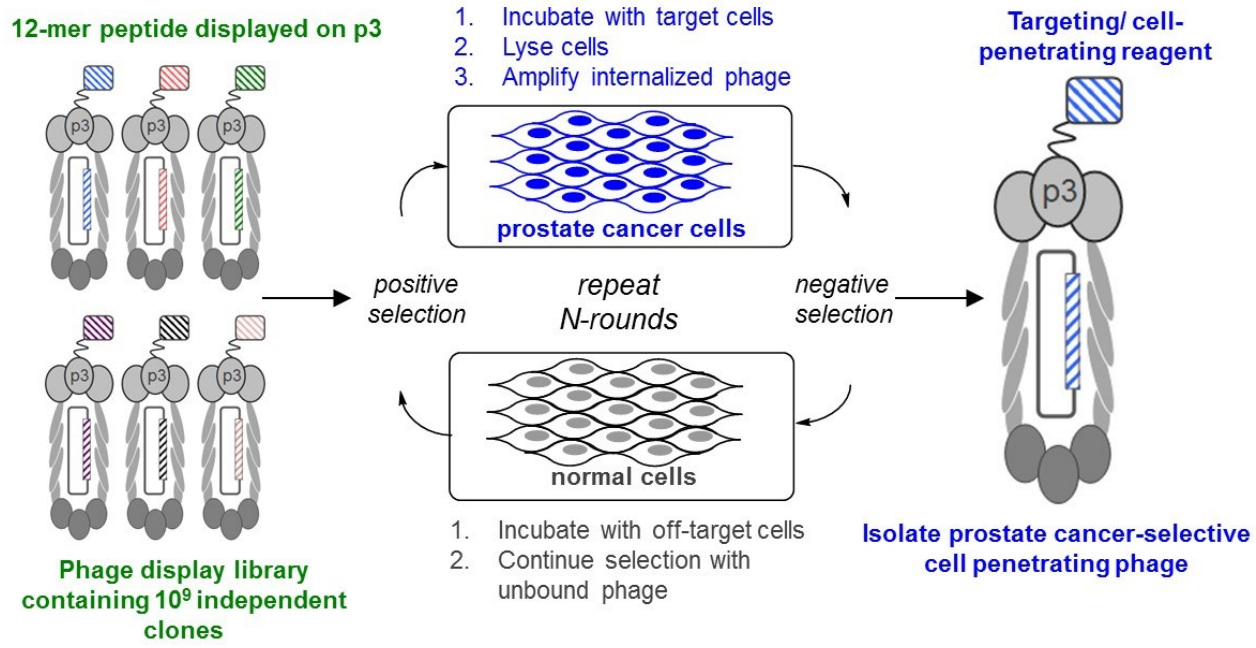

Figure 2.1 Phage panning for a PC-3 prostate cancer cell-selective protein transduction domain. Phage are incubated with PC-3 prostate cancer cells and enriched for cell-penetration. Cell-penetrating phage are then incubated with off-target cell lines, and phage that are not internalized by off-target cells are moved to another round of selection.

selection involved incubating the phage display library with a monolayer of PC-3 prostate cancer cells.

We began by performing alternating rounds of positive selections to enrich phage that penetrate PC-3 cells, a human prostate cancer cell line with high metastatic potential and low PSMA expression levels, and negative selection rounds against four off-target cell lines to remove non-selective PTDs. After three rounds of positive and negative selection, only phage with modest potency of uptake and poor cell-selectivity were enriched. Changing the order of the selection (positive to negative or negative to positive) did not resolve the problem. One possible reason for this undesired outcome is the selection strategy itself. In this scheme, "winners" may be phage with poor uptake efficiencies in both targeted and untargeted cells. This phage would be expected to barely survive both the positive and negative selection. Moreover, those phage may be preferentially amplified over other phage that are truly internalized.

Based on our initial results, we modified our selection strategy to include an initial depletion step, in which the phage library is first incubated with a tissue culture plate to remove polycationic library members that preferentially bind to the negatively charged surface. A vacuum-gas plasma-treated tissue culture plate contains a monolayer of carboxylic acids on the tissue culture plate surface and is therefore

negatively charged at physiological pH. Only library members not bound to the tissue culture plate surface were moved to the positive selection.

In order to assure that only internalized phage were selected and enriched, as opposed to phage that simply bind to the surface of PC-3 cells, an extensive washing protocol was developed from components of numerous literature reports.[34,35] Briefly, media containing phage without affinity for PC-3 cells was removed, and the cells were washed five times with PBS and then three times with Tris-buffered saline (TBS)/0.1 % Tween-20 solution. Cells were then treated with 3 mg/mL subtilisin in TBS for 40 minutes at 4 °C, which removed any remaining cell-surface-bound phage by proteolytic degradation of the p3 minor coat protein to render the phage non-infective. Following subtilisin treatment, cells were washed three times with PBS containing protease inhibitor cocktail and pelleted by centrifugation. Plaque forming assay of the final PBS wash solution after subtilisin treatment showed that no cell-surface-bound phage were present, indicating that the washing scheme removed all phage that did not penetrate the cells (**Figure 2.2**). Cells were then lysed with a solution previously shown to lyse human cells, but not disrupt the phage particle. Phage present in the cell lysate were amplified in *Escherichia coli* and moved on to the negative selection round. After the final round of selection, enriched phage were amplified in *E. coli* and grown as single plaques on an agar plate. Single plaques were isolated and grown in Luria Broth (LB), and the ssDNA sequenced using standard methods. The most abundant sequence

enriched from this selection was "Ypep" (N-YTFGLKTSFNVQ-C); little sequence homology was observed among the evolved peptide sequences. Among the enriched peptides displayed on the phage, Ypep was determined to be the most cell-selective and potent PTD.

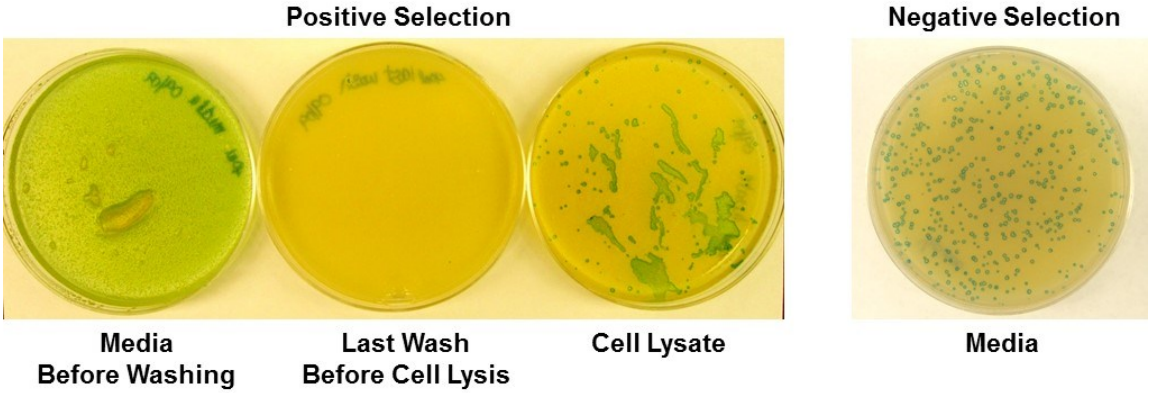

Figure 2.2 Phage titering results from positive and negative selections. Phage amplified from cell culture media before washing (positive selection, left), the last wash before cell lysis (positive selection, center), and cell lysate (positive selection, right). Phage remaining in media in the negative screen are shown as well.

2.4 Determining the Potency of Ypep-fusion Protein Uptake

We prepared a fusion protein consisting of an N-terminal Ypep sequence, a $(GGS)_4$ linker, and super-folder green fluorescent protein (sfGFP). This fusion protein is referred to as "Ypep-GFP" throughout. In many ways, GFP is an ideal protein to test the characteristics of a PTD. GFP is simple to express, is stable, and cellular uptake can be easily imaged on a fluorescence microscope.[38] Although not of human origin, the molecular weight (27 kDa) and net theoretical charge at physiological pH (-6) of GFP

are within the average range among human proteins expressed in *E. coli*.[39] Like most proteins, wild-type GFP does not penetrate human cells (**Figure 2.3C**). Finally, GFP and its variants, or proteins with similar biophysical characteristic, have been used for various *in vitro* and *in vivo* bioimaging applications.

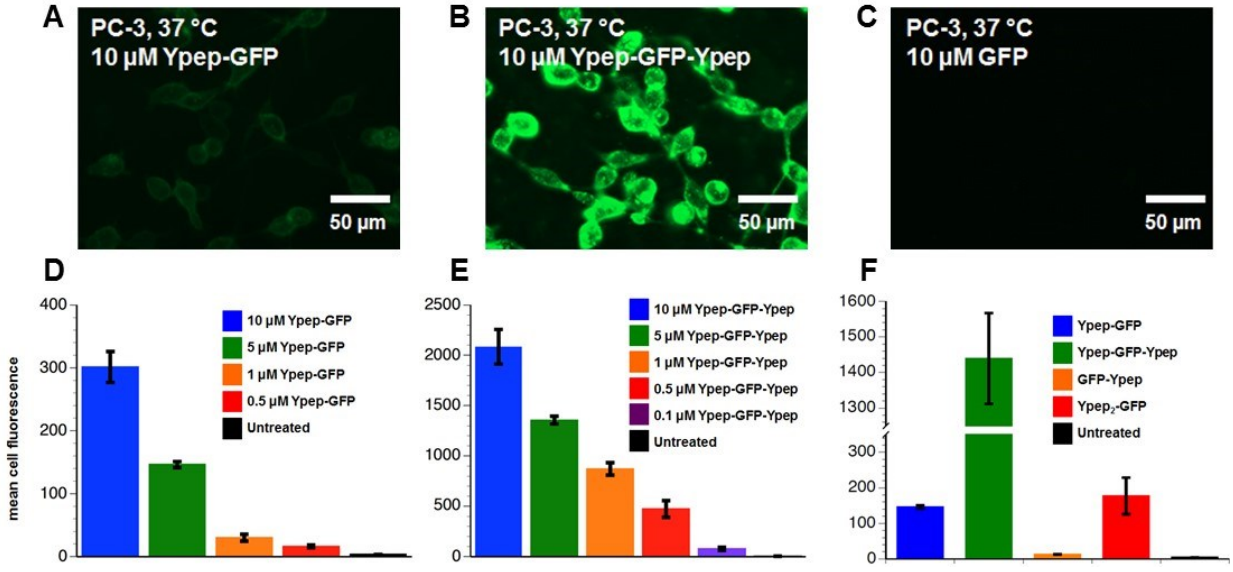

Figure 2.3 Comparing GFP uptake of Ypep fusion proteins in PC-3 cells. A-C) Fluorescence microscopy images of PC-3 cells after a 1 hour treatment with 10 μM Ypep-GFP, Ypep-GFP-Ypep, or GFP and subsequent washing with PBS containing 20 U/ml heparin sulfate. All images were taken using an EVOS fl fluorescence microscope at 20% lamp intensity, 500 ms exposure. D-E) Amounts of internalized GFP in PC-3 cells after treatment with 0.1, 0.5, 1, 5, or 10 μM Ypep-GFP or Ypep-GFP-Ypep. F) Direct comparison of GFP delivery to PC-3 cells treated with 5 μM Ypep-GFP, Ypep-GFP-Ypep, GFP-Ypep or $Ypep_2$-GFP after a 3 hour incubation. Values and error bars represent the mean and standard deviation of three independent experiments.

PC-3 cells were evaluated for protein uptake by treatment with 0.5, 1, 5, or 10 μM Ypep-GFP. Following treatment, this solution was removed, and the cells were washed three times with a PBS solution containing 20 U/mL heparin sulfate, which has been previously shown to remove surface-bound protein.[39–42] Cells were then trypsinized and

assayed for internalized Ypep-GFP by flow cytometry. As shown in **Figure 2.2 D**, we observed a concentration-dependent increase in Ypep-GFP levels in PC-3 prostate cancer cells. Flow cytometry data demonstrated a ~42- and ~86-fold increase in fluorescence in cells following treatment with 5 or 10 μM Ypep-GFP, respectively. Fluorescence microscopy images show internalized Ypep-GFP in PC-3 cells following treatment with 10 μM Ypep-GFP (**Figure 2.3A**). In contrast, no appreciable fluorescent was observed in cells treated with 10 μM GFP, then washed, and imaged using the same conditions (**Figure 2.3C**). Taken together, these data validate the PTD selection.

2.5 Multivalency Increases Cellular Uptake of Ypep-Fusion Proteins

Although we were pleased to observe that a single copy of Ypep delivers GFP to PC-3 prostate cancer cells, we were somewhat surprised by the modest potency of cellular uptake. We reasoned that because selections involve phage, which present 5 copies of Ypep on the N terminus of the minor coat protein 3 (p3), multivalent display may be needed to facilitate highly potent Ypep-dependent delivery.

Multivalency effects play critical roles in numerous biological processes[43] and has been shown to contribute to the mechanism of uptake for previously reported PTDs[44]. Multivalent display can increase the individual binding events from a low affinity interaction ($K_d^{affinity}$ ~mM-μM) to a high avidity interaction ($K_d^{avitity}$ ~nM).[43,45]

Thermodynamically, multivalent interactions may be favored because the enthalpy of binding is favorable and there is little unfavorable entropy of the additional binding interactions. If the first binding event does not inhibit the second binding event, the enthalpy of a multivalent interaction is additive.[43] Moreover, lower unfavorable entropy may be gained if the initial binding step increases the local concentration of the ligand present and the spacing between the ligands allows for unstrained binding to the receptors.[43]

In biological systems, there are a number of advantages to multivalent interactions. Ligands with a small surface area can achieve tight binding to a receptor through polyvalent interactions.[43] Alternatively, multivalency enables contact over a large surface area, such as contact between two cells for communication. Multivalency is also evolutionary efficient—by simply multiplying an existing low affinity monovalent interaction, Nature creates a high avidity polyvalent interaction instead of evolving a completely new ligand.[43] Interestingly, if the multivalent interaction involves one type of ligand interacting with different receptors, heteromeric polyvalency can be achieved. This type of interaction can increase the strength and specificity of the binding interaction.

To evaluate the role of multivalency in the uptake of Ypep protein fusions, we prepared a fusion protein with Ypep on the N- and C-termini of GFP (Ypep-GFP-Ypep).

PC-3 cells were then treated with solutions containing 0.1-10 μM Ypep-GFP-Ypep, washed to remove cell-surface-bound proteins, trypsinized from the tissue culture plate, and GFP uptake was measured by flow cytometry. As shown in **Figure 2.3E**, we observed a concentration-dependent increase in Ypep-GFP-Ypep delivery in PC-3 cells, with a dramatic increase in the potency of uptake. This increase in GFP uptake was further confirmed by comparing microscopy images of cells treated with 10 μM Ypep-GFP (**Figure 2.3A**) to cells treated with the same concentration of Ypep-GFP-Ypep (**Figure 2.3B**). GFP fluorescence increased by ~29-fold in PC-3 cells treated with 0.5 μM Ypep-GFP-Ypep when compared to PC-3 cells treated with the same concentration of Ypep-GFP. Moreover, PC-3 cells treated with 0.5 μM Ypep-GFP-Ypep exhibited ~3-fold higher GFP fluorescence than cells treated with 5 μM Ypep-GFP. Interestingly, we tested a GFP fusion with Ypep displayed on only the C-terminus (**Figure 2.3F**), GFP-Ypep, and we didn't not observe any GFP uptake, further suggesting that multivalency plays a key role in the potency of Ypep-dependent delivery.

2.6 Comparing the Effect Bivalent Display of Ypep, Tat, and Penetratin Has on the Potency of GFP Uptake

Intrigued by the dramatic increase in the potency of GFP uptake in PC-3 cells as a result of bivalent display of Ypep, we set out to measure if this observation is

universal among commonly used and commercially available PTDs. We prepared GFP fusion proteins that contain either a single N-terminal fusion with Tat or penetratin (referred to as Tat-GFP and Pen-GFP, respectively). In addition, we prepared GFP fusion proteins that contain N- and C-terminal Tat or penetratin (referred to as Tat-GFP-Tat and Pen-GFP-Pen, respectively). Like Ypep-GFP and Ypep-GFP-Ypep fusion proteins, Tat and penetratin are separated from GFP through a $(GGS)_4$ linker. Polyarginine is another commonly used PTD[12]; unfortunately, all attempts to express and purify $(Arg)_9$-GFP and $(Arg)_9$-GFP-$(Arg)_9$ were unsuccessful.

We began by testing GFP uptake with monovalent display of the fusion proteins. PC-3 cells were treated with solutions containing 5 μM Ypep-GFP, Tat-GFP, or Pen-GFP. This concentration was chosen because it was the lowest concentration that resulted in relatively high levels of Ypep-GFP delivery. Cells were washed to remove cell-surface-bound proteins, as previously described, and GFP fluorescence was measured by flow cytometry. As seen in **Figure 2.4A**, treatment with this concentration of fusion protein resulted in the delivery of comparatively high levels of Ypep-GFP and Pen-GFP to PC-3 cells. In contrast, appreciable levels of Tat-GFP did not penetrate PC-3 cells at the concentration tested.

Next we tested the bivalent constructs for GFP uptake. We incubated PC-3 cells with solutions containing 100 nM Ypep-GFP-Ypep, Tat-GFP-Tat, or Pen-GFP-Pen. This

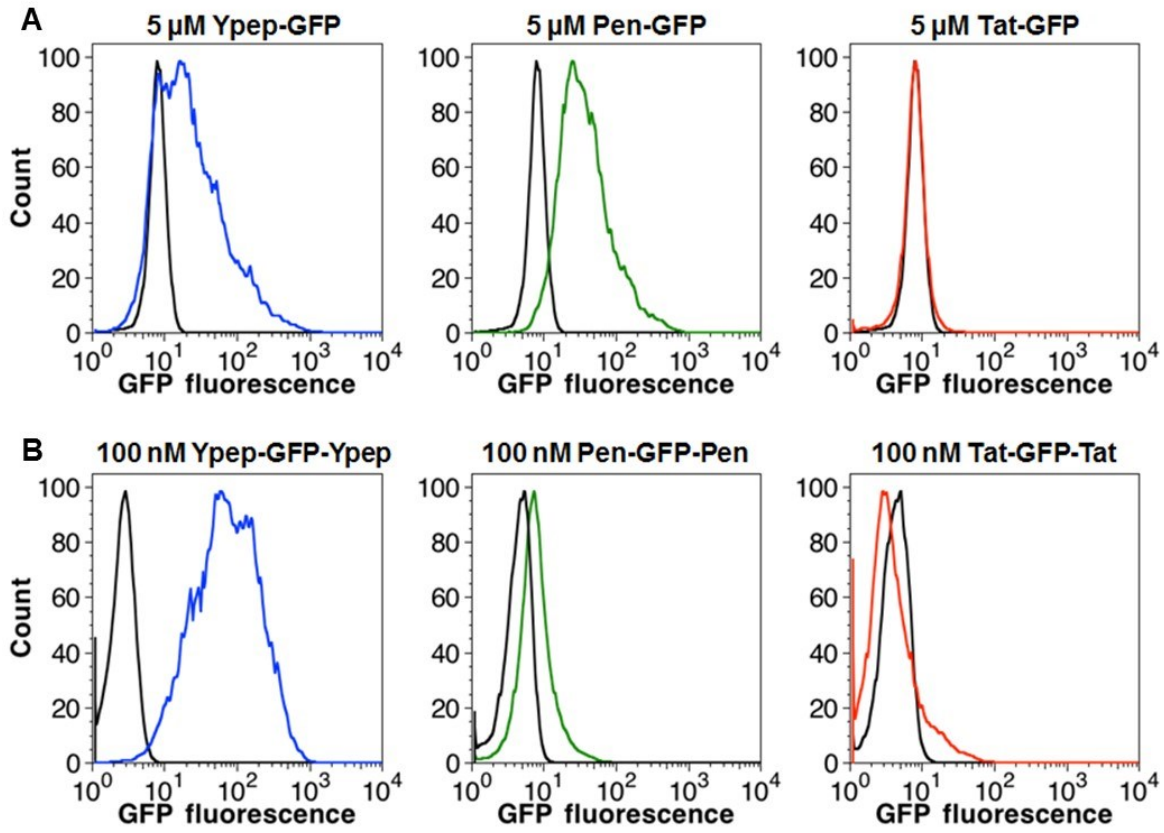

Figure 2.4 Comparing the effect bivalent display of Ypep, Tat, and penetratin has on GFP uptake in PC-3 cells. A) Flow cytometry data showing amounts of internalized GFP in PC-3 cells after treatment with 5 μM Ypep-GFP (blue), penetratin-GFP (green), or Tat-GFP (red). B) Flow cytometry data showing amounts of internalized GFP in PC-3 cells after treatment with 100 nM Ypep-GFP-Ypep (blue), penetratin-GFP-penetratin (green), or Tat-GFP-Tat (red). In each figure, untreated cells are represented in black, and colored lines represent treated cells.

concentration was chosen as it was the lowest concentration that resulted in relatively high levels of Ypep-GFP-Ypep delivery. As shown in **Figure 2.4B**, although bivalent display of Ypep resulted in a ~20-fold increase in GFP delivery the same effect was not observed for Pen-GFP-Pen and Tat-GFP-Tat fusions. Moreover, bivalent penetratin display does not increase uptake. Previous reports have shown that 4-5 copies of Tat and as many as 10-50 copies of penetratin are required for a significant increase in the potency of uptake, compared to the potency of delivery observed for a monomeric

fusion.[46] In addition, multivalent dendrimer-PTD conjugates have been reported to increase potency of uptake compared to a monovalent species.[47,48] However, these species typically contain >20 copies of the PTD per dendrimer. In contrast, we observe a dramatic increase in the potency of delivery for GFP fusions containing two copies of Ypep. Taken together, these data show the unique role multivalency plays on the potency of Ypep-dependent delivery of GFP.

2.7 Cell-Selectivity of Ypep-fusion Proteins

Given the role multivalency plays in the potency of Ypep-dependent delivery, we hypothesized that those same effects may contribute to cell-selectivity as well. We compared the delivery of Ypep-GFP, Ypep-GFP-Ypep, and $(Ypep)_5$-phage in PC-3 human prostate cancer cells (PSMA-neg), LNCaP human prostate cancer cells (PSMA-pos), HEK-293T human embryonic kidney cells, MRC-9 human lung fibroblast cells, and Hs 697.Sp human spleen fibroblast cells. The potency and cell-selectivity of Ypep-GFP and Ypep-GFP-Ypep delivery was measured by flow cytometry. Phage titering from cell lysate was used to compare the amount of internalized phage in each cell line.

As shown in **Figure 2.5A**, a single copy of Ypep endows appreciable selectivity of delivery. Following treatment with 5 μM Ypep-GFP, we observed ~4-, ~8-, and ~5-fold more internalized GFP in target PC-3 cells compared to off-target LNCaP, HEK-293T,

and Hs 687.Sp cells. However, high levels of GFP fluorescence was also present in off-target MRC-9 cells; only ~1.4-fold more fluorescence was observed in target PC-3 cells. These data suggest that monomeric Ypep is moderately selective for PC-3 cells.

We next compared the cell-selectivity of Ypep-GFP-Ypep in PC-3, LNCaP, HEK-293T, Hs 697.Sp, and MRC-9 cells. **Figure 2.5B** shows higher cell-selectivity of GFP

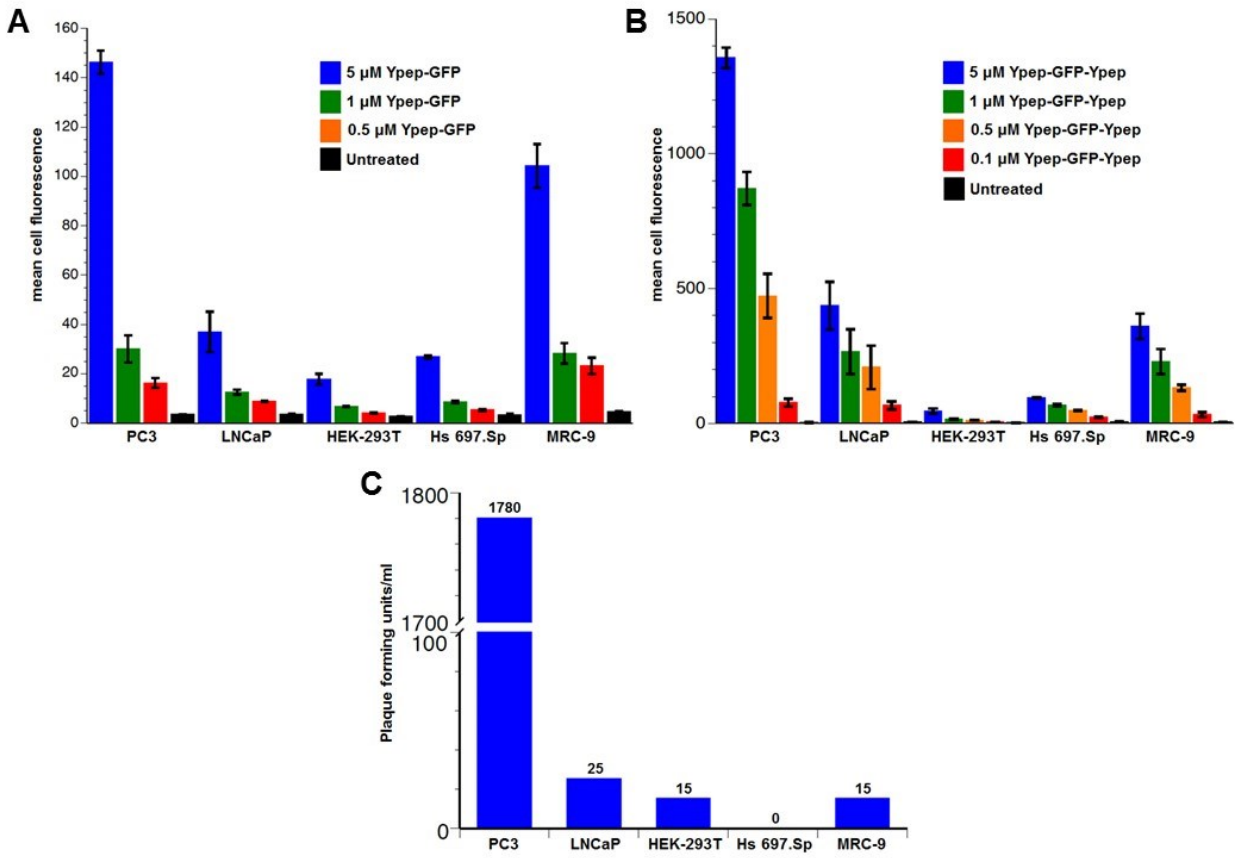

Figure 2.5 The cell-selectivity of Ypep fusion proteins and phage. A) Amounts of internalized GFP in PC-3, LNCaP, HEK293T, Hs 697.Sp, and MRC-9 after treatment with 0.5, 1, or 5 μM Ypep-GFP B) Amounts of internalized GFP in PC-3, LNCaP, HEK-293T, Hs 697.Sp, and MRC-9 after treatment with 0.1, 0.5, 1, or 5 μM. C) Representative phage plaque forming units per milliliter generated from the cell lysate of each cell line tested after treatment with 1×10^{9} pfu/ml $(Ypep)_5$-phage. Values and error bars in A & B represent the mean and standard deviation of three independent experiments.

uptake in PC-3 cells treated with bivalent Ypep-GFP-Ypep when compared to monomer Ypep-GFP. Like Ypep-GFP, Ypep-GFP-Ypep was taken up by targeted PC-3 cells, and much lower levels of internalized GFP was detected in off-target LNCaP, HEK-293T, and Hs 697.Sp cells. However, unlike Ypep-GFP, which was taken up well in both target PC-3 and off-target MRC-9 cells, Ypep-GFP-Ypep showed a ~4-fold preference for PC-3 cells over MRC-9 cells. Taken together, these data demonstrate an important role for multivalency in the cell-selectivity of delivery.

Finally, we tested the cell-selectivity of $(Ypep)_5$-phage delivery by comparing the plaque forming assay results from each of the lysates after incubation with each cell line and washing steps. Cells were treated with 5 mL of F12K/10% FBS containing 1.0×10^9 plaque forming units (pfu)/mL of $(Ypep)_5$- phage. This equates to a solution with a concentration of 1.7 pM phage. Thus, cell-penetration at this concentration indicates very high potency. After incubation with phage, cells were washed to remove cell-surface-bound phage, and cells were lysed as previously described. In addition to titering the cell lysate, aliquots from each final wash solution were titered to ensure that all surface-bound phage were completely removed before cell lysis. No phage were found in any of the final washing solutions (Experimental Methods). In contrast, high levels of $(Ypep)_5$-phage was found in the PC-3 cell lysate (**Figure 2.5C**). However, unlike the previously described protein fusions, appreciable levels of $(Ypep)_5$-phage were not observed in off-target cell lines. Appreciable levels (>25 pfu/mL) of phage were not

observed with cell lysates from LNCaP, HEK-293T, Hs 697.Sp, or MRC-9 cells. In contrast, >1,500 pfu/ml were observed in *E. coli* treated with PC-3 cell lysate. This represents a drastic change in the cell-selectivity of Ypep-dependent delivery.

Although these data suggest that multivalency effects likely play a role in the cell-selectivity of uptake, the architecture of Ypep display in the context of fusion to GFP and fusion to the N-terminus of phage coat protein p3 differ greatly. We cannot dismiss the possibility that these architectural changes may play an important role in the cell-selectivity profiles we observe. Nonetheless, the cell-selectivity and potency profiles displayed by bivalent Ypep-GFP fusions and $(Ypep)_5$-phage make Ypep well suited for targeted bioimaging applications, as well as phage-based approaches to biomedical science.

2.8 Mechanism of Ypep Internalization

Knowledge about the mechanism of PTD delivery is essential in predicting and engineering peptides with desirable cell entry properties; therefore, there has been a great interest in elucidating the mechanism by which these peptides are internalized. PTDs can achieve internalization through either an energy-dependent endocytotic mechanism, or via direct translocation. Initially studies of Tat, Antp, and transportan demonstrated peptide internalization at both 37 °C and 4 °C, which indicated an

energy-independent translocation mechanism.[9,11,15] However, others have observed an interaction with cell-surface proteoglycans that facilitated internalization in a concentration and temperature-dependent way, indicating an endocytotic mechanism.[49–51] Conversely, studies have also demonstrated that internalization is not mediated by proteoglycan interaction, proteoglycans were merely facilitating an electrostatic interaction.[52,53] It is now generally accepted that most PTDs induce uptake through some endocytotic mechanism of internalization.[50,51] The seemingly contradictory results can be attributed to the PTD delivery dependence on the attached cargo.[54] For instance, when Tat is conjugated to protein cargo, it undergoes lipid raft-mediated endocytosis[55], but when conjugated to a small molecule fluorophore, clathrin-dependent endocytosis is achieved.[56] Moreover, experimental artifacts, such as the fixation of cells, has also hindered the study of the uptake of these reagents.[57,58] The controversy surrounding the study of the mechanism of entry for PTDs continues, but it is now widely accepted that the mechanism is dependent on both the conjugated cargo (small molecule, protein, fluorophore, or nanoparticle)[54,56], as well as the cell type[59].

In comparison to other PTDs, Ypep only has a charge of +1, which made us particularly interested in the mechanism of uptake. In addition to the low positive charge that Ypep has, multivalency seems to play a key role in internalization of the Ypep constructs. Given these characteristics, we were interested in establishing the mechanism of internalization for Ypep-GFP, Ypep-GFP-Ypep, and $(Ypep)_5$-phage. To

probe the mechanism of internalization, we performed experiments to block certain transduction pathways. We began by determining if the internalization was through direct transduction across the plasma membrane. We did not observe internalization when PC-3 cells were cooled to 4 °C before and during treatment with either 15 μM Ypep-GFP or 10 μM Ypep-GFP-Ypep (**Figures 2.6B & 2.6I**, respectively). These results suggest that cell penetration of Ypep-GFP and Ypep-GFP-Ypep requires an energy-dependent process, consistent with endocytosis.

We next evaluated the cell-penetration of each Ypep variant under conditions that block a particular component of an endocytotic pathway. PC-3 cells were incubated with relatively high concentrations of Ypep-GFP or Ypep-GFP-Ypep to ensure that changes in cell fluorescence were due to inhibition of cell penetration as opposed to relatively small changes in uptake of low concentrations of GFP fusions that may or may not be associated with inhibition of endocytosis. Moreover, cells were not fixed before microscopy analysis, as some fixatives have been reported to alter internalization studies. Cells were pretreated with the small molecule inhibitor for 10 minutes prior to incubation with the inhibitor and the protein fusion. Treatment with 5 μg/mL chlorpromazine, showed no change in GFP, indicating that uptake was not a clathrin-mediated endocytotic mechanism (**Figures 2.6F & 2.6M**). Additionally, when cells were treated with 10 μg/mL cytochalasin D, an actin polymerization inhibitor, little inhibition was observed (**Figures 2.6G & 2.6N**).

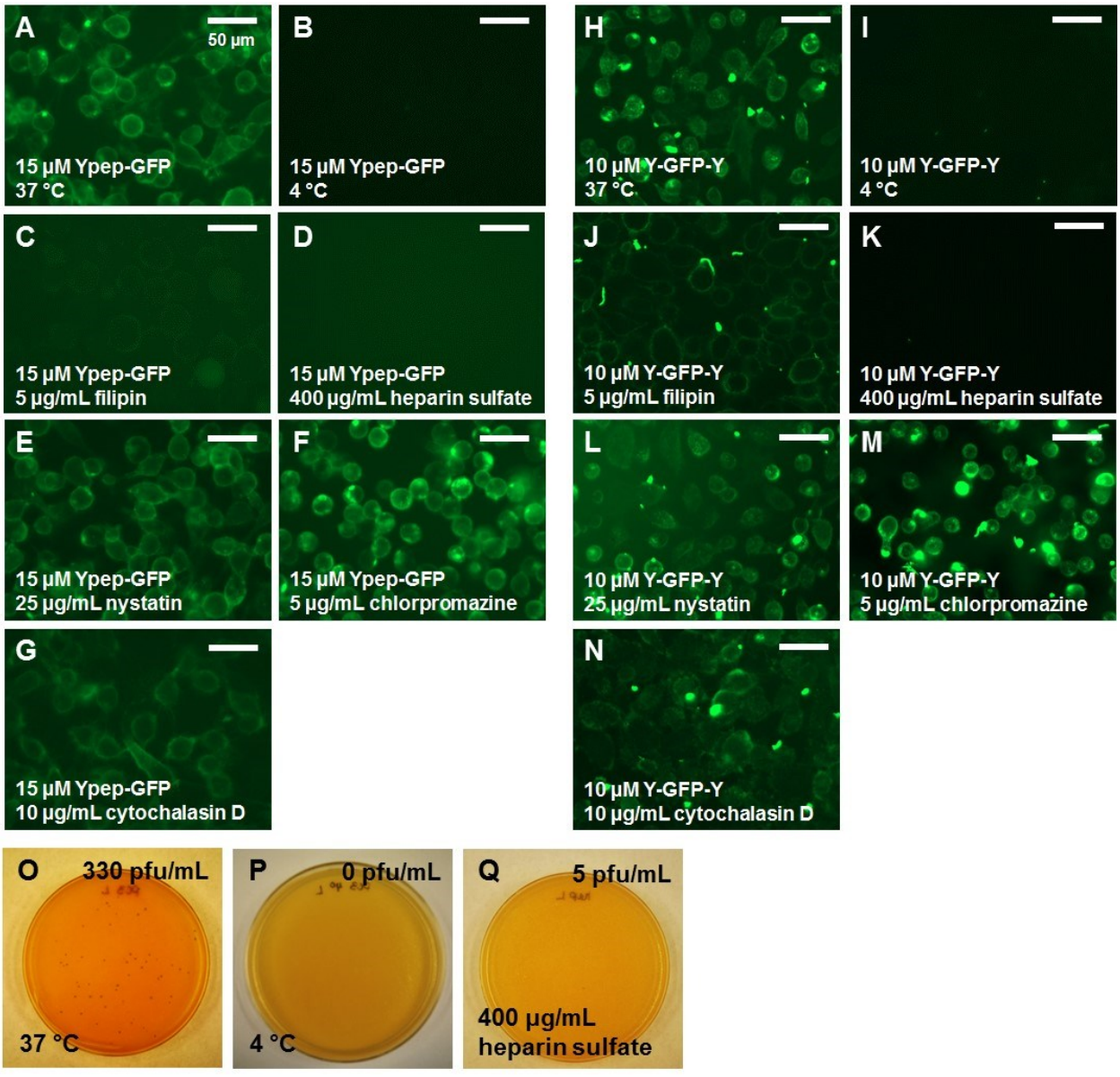

Figure 2.6 Mechanistic probes of Ypep-GFP, Ypep-GFP-Ypep, and $(Ypep)_5$-phage internalization. PC-3 cells treated with: A) 15 µM Ypep-GFP at 37 °C. B) 15 µM Ypep-GFP at 4 °C. C) 15 µM Ypep-GFP and 5µg/ml filipin, a known inhibitor of lipid-raft mediated endocytosis. D) 15 µM Ypep-GFP and 400 µg/ml heparin sulfate. E) 15 µM Ypep-GFP and 25 µg/ml nystatin, an inhibitor of caveolae-mediated endocytosis. F) 15 µM Ypep-GFP and 5 µg/ml chlorpromazine, an inhibitor of clathrin-mediated endocytosis. G) 15 µM Ypep-GFP and 10 µg/ml cytochalasin D, a known inhibitor of actin polymerization. H-N) The conditions are the same in Figures 2.6H-2.6N, except cells were treated with 10 µM Ypep-GFP-Ypep. All fluorescence images were obtained with a 200 ms exposure, 20% lamp intensity. Scale bars in each image is 50 µm. Plaque forming assays were performed on PC-3 cells treated with O) 1×10^9 pfu/mL $(Ypep)_5$-phage at 37 °C. P) 1×10^9 pfu/mL $(Ypep)_5$-phage at 4 °C. Q) 1×10^9 pfu/mL $(Ypep)_5$-phage and 400 µg/ml heparin sulfate.

However, treatment with 5 μg/mL filipin, a small molecule known to inhibit lipid-raft or caveolae-dependent endocytosis, showed much lower GFP uptake compared to cells that were not treated with the inhibitor molecule (**Figures 2.6C & 2.6J**). In addition, treatment with 400 μg/mL heparin sulfate also inhibited internalization. Based on previous studies, this suggests that internalization requires interaction(s) with one or more glycosaminoglycans on the surface of PC-3 cells. Interestingly, treatment with 25 μg/mL nystatin, which is often used interchangeably with filipin and is also an inhibitor of caveolae-dependent endocytosis but not lipid-raft-mediated endocytosis, does not show inhibition of fusion protein internalization (**Figures 2.6E & 2.6L**). These data suggest that this process is lipid-raft mediated process that does not require caveolae, but does require the interaction of cell surface glycosaminoglycans on the surface of PC-3 cells.

We next applied the inhibition conditions described above to PC-3 cells treated with $(Ypep)_5$-phage. Unlike Ypep-GFP and Ypep-GFP-Ypep fusions, which can be removed using a relatively simple washing procedure and for which internalization can be immediately imaged, phage experiments require a relatively substantial washing procedure to ensure that all phage are completely removed from the cell surface. Unfortunately, following treatment with filipin, cytochalasin D, nystatin, and chlorpromazine, PC-3 cells did not withstand the washing protocol. We observed significant loss of cells throughout the experiment due to cytotoxicity. Therefore, we

were unable to obtain meaningful data from those experiments. Because of this, studies on the mechanism of $(Ypep)_5$-phage penetration in PC-3 cells were limited to conditions that were not cytotoxic to the cells during the course of the experiments.

As shown in **Figure 2.6P**, experiments conducted at 4 °C did not show phage internalization when compared to the 37 °C results (**Figure 2.6O**). This suggests that cell penetration of $(Ypep)_5$-phage requires an energy-dependent process, consistent with endocytosis. In addition, internalization of $(Ypep)_5$-phage was inhibited by heparin sulfate (**Figure 2.6Q**), suggesting that internalization requires interaction with cell-surface glycosaminoglycans on PC-3 cells.

2.9 Cytotoxicity and Robustness of Ypep-dependent Delivery

To assess the cytotoxicity of Ypep variants under conditions required for appreciable uptake, we performed an MTT (3-[4,5-dimethylthiazol-2-yl]-2,5-diphenyltetrazolium bromide) assay on PC-3 cells after treatment with 0.5, 1, or 5 μM Ypep-GFP or Ypep-GFP-Ypep or 1×10^9 pfu/ml $(Ypep)_5$-phage. As shown in **Figure 2.7A-C**, no apparent cytotoxicity to PC-3 cells was observed for any of the Ypep variants.

Phage selections were performed in a complex solution consisting of F12K cell culture media and 10% fetal bovine serum (FBS). In order for a PTD to be used *in vivo*, it

must penetrate the target cell in the presence of a complex solution, such as whole blood. We treated PC-3 cells with either 10 μM Ypep-GFP or Ypep-GFP-Ypep in F12K/10% FBS solution containing 50% whole human blood. Cells were then washed as described, and red blood cells were removed using standard methods. Cell fluorescence was measured by flow cytometry. Ypep-GFP-Ypep, but not Ypep-GFP penetrates PC-3 cells in a solution containing human blood (**Figure 2.8D & 2.8E**). In addition, when PC-3 cells were treated with 1×10^9 pfu/mL $(Ypep)_5$-phage in F12K/10% FBS solution

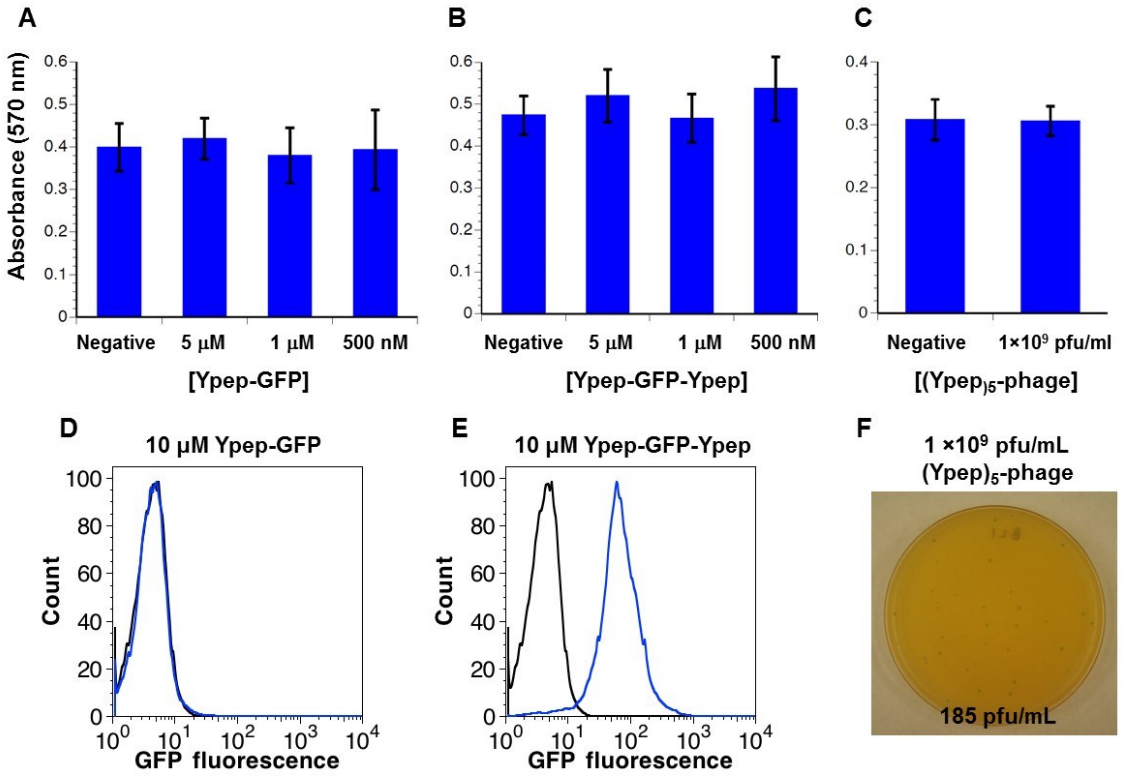

Figure 2.7 Cytotoxicity and delivery in complex solution. A-C) MTT assays of PC-3 cells treated with various concentrations of Ypep-GFP, Ypep-GFP-Ypep, or $(Ypep)_5$-phage. The values and error bars represent the mean and standard deviation of three separate experiments. D-E) GFP uptake of 10 μM Ypep-GFP and Ypep-GFP-Ypep after incubation with PC-3 in whole blood and F12K/10% FBS. F) Plaque forming assay of PC-3 cells treated with 1×10^9 pfu/ml $(Ypep)_5$-phage in whole blood and F12K/10% FBS.

containing 50% whole blood, appreciable levels of phage were found in cell lysate (**Figure 2.8F**). Taken together, these data suggest that multivalent Ypep-dependent cell-penetration is functional in blood. The high potency of $(Ypep)_5$-phage is not abrogated in the presence of human blood.

2.10 Conclusions

Using phage evolution, we identified a novel PTD (Ypep) whose potency and selectivity for targeted PC-3 prostate cancer cells is tightly controlled through multivalency. A single copy of Ypep attached to the N-terminus of GFP (Ypep-GFP) penetrates a diverse set of human cells with modest potency and poor selectivity. The addition of a second copy of Ypep attached to the C-terminus of GFP (Ypep-GFP-Ypep), enhanced potency by ~9- to ~29-fold over the same set of human cells. The cell-selectivity of Ypep-GFP-Ypep also increased. Although the same approximate level of Ypep-GFP was found in PC-3 and MRC-9 cell lines, ~4-fold more Ypep-GFP-Ypep was found in PC-3 cells over a range of concentrations. However, phage that display five copies of Ypep ($(Ypep)_5$-phage) very potently and selectively penetrate PC-3 cells. When a diverse set of human cells were treated with 1.7 pM phage, cellular uptake was observed in PC-3 cells, but not LNCaP (prostate cancer, PSMA-pos), HEK293T (kidney), Hs 697.Sp (spleen), and MRC-9 (lung) cells. Collectively, our results reveal Ypep as a

novel PTD capable of delivering protein (GFP) or nanometer-sized cargo (phage), with cell-penetrating properties that are tightly controlled through multivalency effects. Both Ypep-GFP-Ypep and $(Ypep)_5$-phage penetrate cells in the presence of human blood. All Ypep-dependent cell penetration is non-cytotoxic at conditions required for uptake and proceeds via endocytosis. Both Ypep-GFP and Ypep-GFP-Ypep penetrate PC-3 cells through a caveolae-independent lipid-raft mediated endocytosis.

2.11 Experimental Methods

Materials

Phosphate buffered saline (PBS) - Hyclone/Thermo Scientific
0.25% Trypsin - Hyclone/Thermo Scientific
Brilliant Blue R-250 - J.T.Baker
Bovin serum albumin - Sigma Aldrich
Fetal bovin serum (FBS) - PAA Laboratories
Triton X-100 - Fisher Scientific
Dulbecco's modified Eagle medium (DMEM) - Hyclone/Thermo Scientific
RPMI-1640 media - Hyclone/Thermo Scientific
F-12K medium – Cellgro/MediaTech
Mammalian cell culture dishes - Fisher Scientific
Ph.D.-12 Phage Display Library - New England BioLabs
Sodium Deoxycholate - Sigma Aldrich
B-PER Bacterial Protein Extraction Reagent - Thermo Scientific
Imidazole - Sigma Aldrich
Heparin sulfate – Sigma Aldrich
Modified Lowry Protein Assay Kit - Pierce/Thermo Scientific
cOmplete Mini Protease Cocktail tablets – Roche
TACS MTT reagent –Trevigen
Ni-NTA agarose resin - QIAGEN
Whole blood – Innovative research

Instrumentation

Fluorescence microscopy images were taken on an EVOS fluorescence inverted microscope from the Advanced Microscopy Group (AMG). MTT assay readings were taken on a Synergy Mx microplate reader from BioTek Instruments (Winooski, VT, USA). Flow cytometry experiments were performed on a MoFlo (Dako Colorado, Fort Collins, CO, USA) flow cytometer using a solid-state iCyt 488 nm (blue) laser to measure GFP fluorescence.

Mammalian Cell Culture

Human prostate adenocarcinoma cells (PC-3) cells were cultured in F12K with 10% fetal bovine serum (FBS). Human prostate carcinoma cells (LNCaP) and human embryonic lung fibroblasts (MRC-9) cells were cultured in RPMI-1640 media with 10% FBS; human spleen fibroblasts (Hs 697.Sp) and HEK-293T cells were cultured in high glucose Dulbecco's modified Eagle's medium (DMEM) with 10% fetal bovine serum (FBS). PC-3, LNCaP, and MRC-9 cells were incubated at 37 °C with 5% CO_2 environment. Hs 697.Sp cells were incubated at 37 °C with 10% CO_2 environment. All cells were obtained from the American Type Culture Collection.

Phage Selection

Positive Selection: A 10 mL solution of F12K/10% FBS containing 5×10^9 pfu phage library members (Ph.D.-12 Phage Display Library, NEB) was added to 80% confluent PC-3 cells grown as a monolayer in a T25 culture flask and incubated at 37 °C under 5%

CO_2 environment for 3 hours. After incubation, cells were then placed on ice for 5 minutes and washed with 4 °C PBS five times while on ice. Cells were then washed three times with 4 °C Tris-buffered saline (TBS)/0.1% v/v Tween-20 for 3 minutes each while on ice. The remaining surface-bound phage was proteolyzed by addition of a 5 mL TBS/subtilisin (3 mg/mL) for 45 minutes at 4 °C. Cells were then transferred into a 15 mL plastic tube and pelleted for 5 minutes at 3,000 rpm and at 4 °C. Supernatant was removed and cells were resuspended in 5 mL PBS/protease inhibitor for 15 minutes at 4 °C and then pelleted for 5 minutes at 3,000 rpm and 4 °C. Supernatant was removed, and cells were resuspended in 1 mL of PBS and pelleted for 5 minutes at 3,000 rpm and 4 °C. Supernatant was removed and saved as the last wash solution for subsequent titering. Cells were lysed with 0.5 mL of lysis buffer (2% sodium deoxycholate, 10 mM Tris-HCl, and 2 mM EDTA) and 0.5 mL of TBS for 1 hour at room temperature. After cell lysis, internalized phage was amplified in a 150 mL flask containing 30 mL LB, 360 mL 0.1 M $CaCl_2$, 20 mg/mL tetracycline, and 0.15 mL of *E. coli* (ER2837) that had been grown to optical density OD_{600} ~0.5. The final wash solution (200 mL) or the cell lysate was then added, and this solution was incubated at 37 °C, 250 rpm for 5 hours. *E. coli* was pelleted for 10 minutes at 10,000 rpm and 4 °C. Supernatant containing phage was transferred to another tube, and *E. coli* cell debris was pelleted at 10,000 rpm for 10 minutes at 4 °C. Phage from the supernatant was precipitated by addition of 5 mL 20% PEG-8000/2.5 M NaCl. Phage was only amplified after positive selection rounds; the

phage-containing media from negative selections was directly added to positive cell lines without amplification of the phage.

Negative selection: A 10 mL solution containing 1×10^9 pfu/mL amplified from the positive selection was added to a T25 culture flask and incubated at 37 °C with 5% CO2 environment for 1 hour. Rounds of positive and negative selection were performed three times.

Plasmid Construction

All constructs were cloned into pET plasmids. DNAs encoding cell-penetrating peptide fusions with sfGFP were assembled using oligonucleotide overlap gene construction and PCR.

Protein purification

BL21-DE3 *E. coli* were typically grown in 500 ml LB cultures at 37 °C to OD_{600} ~0.6 and induced with 1mM IPTG at 30 °C overnight. Cells were then pelleted by centrifugation and lysed with 25 mL B-PER. Cell lysate was cleared by centrifugation (17,000 rpm, 30 minutes), and supernatant was mixed with 1 mL of Ni-NTA agarose resin for 1 hour at 4 °C under agitation. Resin was collected by centrifugation (4,950 rpm, 10 minutes). Ni-NTA agarose resin was washed with 50 mL of PBS containing 300 mM NaCl and then 50 ml of PBS containing 20 mM imidazole. Protein was then eluted with 5 mL PBS containing 300 mM NaCl and 500 mM imidazole. Eluted protein was dialyzed against

PBS and analyzed for purity by SDS-PAGE followed by staining with Coomassie Blue. Protein concentrations were measured using a modified Lowry Protein Assay Kit.

Flow Cytometry

Mammalian cells were grown to ~80% confluency in a 6-well plate. Cells were washed once with PBS and PBS containing Ypep-GFP, (Ypep)2-GFP, or Ypep-GFP-Ypep was added. Cells were incubated with each PBS/protein solution for 3 hours at 37 °C under 5% CO_2 environment and then washed twice with PBS and three times with PBS-HS (heparin sulfate 20 U/mL) for 10 minutes each at 37 °C. Cells were then removed from the tissue culture plate by addition of 0.5 mL of 0.25% trypsin and pelleted by centrifugation. Cell pellet was resuspended in PBS/10% FBS, and cell fluorescence was analyzed by flow cytometry.

Mechanism of Cell Penetration

PC-3 cells were grown to ~80% confluency in a 12-well tissue culture plate. Cells were then washed once with PBS and incubated with the small molecule inhibitor in PBS for 10 minutes at 37 °C under 5% CO_2 environment. The PBS-small molecule solution was then removed, and a PBS solution containing either 15 mM Ypep-GFP or 10 mM Ypep-GFP-Ypep with a small molecule inhibitor in PBS was added to the cells. Cells were incubated in each solution for 30 minutes at 37 °C under 5% CO_2 environment. Cells were washed twice with PBS, once with PBS-HS (heparin sulfate 20 U/mL), and imaged on an EVOS fl fluorescence.

Cell-Selectivity Experiments

For experiments involving Ypep-GFP and Ypep-GFP-Ypep, cell penetration was measured using flow cytometry, as described above (see Flow Cytometry). For cell selectivity experiments involving $(Ypep)_5$-phage, cells were grown to ~80% confluency and then treated with 5 mL of media supplemented with 10% FBS and 1×10^9 pfu/mL $(Ypep)_5$-phage for 3 hours at 37 °C and 5% CO_2 environment. Cells were washed and lysed as previously described (see Phage Selection). An aliquot of the final wash solution was kept for titering. Following cell lysis (see Phage Selection), aliquots from cell lysate and the last wash before lysis were titered. Titering was carried out as described above (see Phage Selection). After this time, the entire *E. coli* mixture was plated on IPTG/X-gal LB-agar plates and incubated at 37 °C for 18 hours.

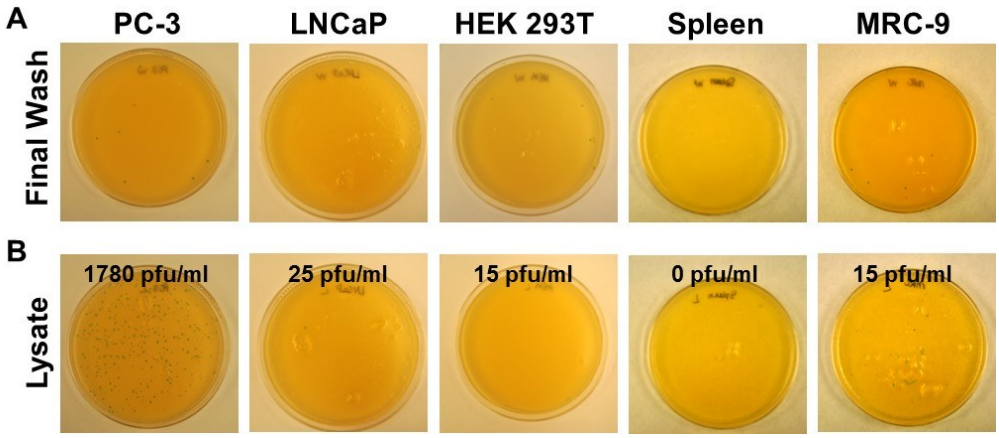

Figure 2.8 Plaque forming assay data representative of Figure 2.5. Phage plaque-forming units generated from A) aliquots from the final wash solution of each cell line tested following incubation with *E. coli* for 5 minutes at 37 °C then grown on an IPTG/x-gal plate for 18 hours B) aliquots of cell lysate of each cell line tested, following the same incubation. Phage express β-galactosidase, thus phage present on each plate are seen as blue plaques.

MTT Cell Viability Assay

PC-3 cells were grown to ~80% confluency in a 12-well tissue culture plate. Cells were then washed once with PBS and incubated with 0.5–5 mM Ypep-GFP or Ypep-GFP-Ypep in PBS for 3 hours at 37 °C under a 5% CO_2 environment. Cells were washed three times with PBS-HS (20 U/mL heparin sulfate) and then incubated with 500 μL media containing 50 μL of MTT reagent for 4.5 hours. After such time, a 250 μL detergent reagent was added to the cells, and they were incubated for an additional 30 minutes at 37 °C under a 5% CO_2 environment. Absorbance was measured at 570 nm on a Synergy Mx microplate reader. Cell viability of cells treated with $(Ypep)_5$-phage was determined after a 3 hours incubation with 5 mL of 1×10^9 pfu/mL Ypep-phage (1.67 pM) in F12K medium supplemented with 10% FBS at 37 °C under a 5% CO_2 environment. PC-3 cells were washed twice with PBS, and the MTT assay was performed as described above.

Ypep-GFP and Ypep-GFP-Ypep Internalization in the Presence of Human Blood

PC-3 cells were grown to ~80% confluency in a 6-well plate. Whole blood was diluted in half with F12K/10% FBS. To this solution either Ypep-GFP or Ypep- GFP-Ypep was added to final concentrations of 10 mM. Cells were incubated with these solutions for 1 hour, washed once with PBS, and then washed twice with a red blood cell lysis buffer (0.15 M NH_4Cl, 0.01 M $KHCO_3$, and 0.0001 M EDTA, pH 7.7) to remove all red blood cells. Cells were washed three times with PBS-HS (20 U/mL heparin sulfate) and imaged on an EVOS fl fluorescence microscope.

$(Ypep)_5$-Phage Internalization in the Presence of Human Blood

PC-3 cells were grown to ~80% confluency in a 6-well plate. Whole blood was diluted in half with F12K/10% FBS. To this solution, 1×10^9 pfu/mL $(Ypep)_5$-phage (1.67 pM) was added. Cells were incubated in this solution for 3 hr at 37 C under a 5% CO_2 environment. Cells were washed twice with red blood cell lysis buffer, twice with PBS, and three times with Tris-buffered saline (TBS)/ 0.1% v/v Tween-20 for 3 minutes each on ice. Cells were then washed as described. Aliquots from final wash and cell lysate solutions were titered as described previously (see Phage Selection: Positive Selection).

Sequence Information

sfGFP
MGGASKGEELFTGVVPILVELDGDVNGHKFSVRGEGEGDATNGKLTLKFICTTGKLP
VPWPTLVTTLTYGVQCFSRYPDHMKQHDFFKSAMPEGYVQERTISFKDDGTYKTRAE
VKFEGDTLVNRIELKGIDFKEDGNILGHKLEYNFNSHNVYITADKQKNGIKANFKIR
HNVEDGSVQLADHYQQNTPIGDGPVLLPDNHYLSTQSALSKDPNEKRDHMVLLEF
VTAAGITHGMDELYKHHHHHH

Ypep-GFP
MGYTFGLKTSFNVQGGSGGSGGSGGSMGGASKGEELFTGVVPILVELDGDVNGHKF
SVRGEGEGDATNGKLTLKFICTTGKLPVPWPTLVTTLTYGVQCFSRYPDHMKQHDFF
KSAMPEGYVQERTISFKDDGTYKTRAEVKFEGDTLVNRIELKGIDFKEDGNILGHKLE
YNFNSHNVYITADKQKNGIKANFKIRHNVEDGSVQLADHYQQNTPIGDGPVLLPDN
HYLSTQSALSKDPNEKRDHMVLLEFVTAARITHGMDELYKHHHHHH

Tat-GFP
MGYGRKKRRQRRRGGSGGSGGSGGSMGGASKGEELFTGVVPILVELDGDVNGHKFS
VRGEGEGDATNGKLTLKFICTTGKLPVPWPTLVTTLTYGVQCFSRYPDHMKQHDFFK
SAMPEGYVQERTISFKDDGTYKTRAEVKFEGDTLVNRIELKGIDFKEDGNILGHKLEY

NFNSHNVYITADKQKNGIKANFKIRHNVEDGSVQLADHYQQNTPIGDGPVLLPDN
HYLSTPSALSKDPNEKRDHMVLLEFVTAAGITHGMDELYKHHHHHH

Pen-GFP

MGRQIKIWFQNRRMKWKKGGSGGSGGSGGSMGGASKGEELFTGVVPILVELDGDV
NGHKFSVRGEGEGDATNGKLTLKFICTTGKLPVPWPTLVTTLTYGVQCFSRYPDHMK
QHDFFKSAMPEGYVQERTISFKDDGTYKTRAEVKFEGDTLVNRIELKGIDFKEDGNIL
GHKLEYNFNSHNVYITADKQKNGIKANFKIRHNVEDGSVQLADHYQQNTPIGDGP
VLLPDNHYLSTQSALSKDPNEKRDHMVLLEFVTAAGITHGMDELYKHHHHHH

Ypep-GFP-Ypep

MGYTFGLKTSFNVQGGSGGSGGSGGSMGGASKGEELFTGVVPILVELDGDVNGHKF
SVRGEGEGDATNGKLTLKFICTTGKLPVPWPTLVTTLTYGVQCFSRYPDHMKQHDFF
KSAMPEGYVQERTISFKDDGTYKTRAEVKFEGDTLVNRIELKGIDFKEDGNILGHKLE
YNFNSHNVYITADKQKNGIKANFKIRHNVEDGSVQLADHYQQNTPIGDGPVLLPDN
HYLSTQSALSKDPNEKRDHMVLLEFVTAAGITHGMDELYKHHHHHHGGSGGSGGS
MYTFGLKTSFNVQ

Pen-GFP-Pen

MGRQIKIWFQNRRMKWKKGGSGGSGGSGGSMGGASKGEELFTGVVPILVELDGDV
NGHKFSVRGEGEGDATNGKLTLKFICTTGKLPVPWPTLVTTLTYGVQCFSRYPDHMK
QHDFFKSAMPEGYVQERTISFKDDGTYKTRAEVKFEGDTLVNRIELKGIDFKEDGNIL
GHKLEYNFNSHNVYITADKQKNGIKANFKIRHNVEDGSVQLADHYQQNTPIGDGP
VLLPDNHYLSTQSALSKDPNEKRDHMVLLEFVTAAGITHGMDELYKHHHHHHGGS
GGSGGSMRQIKIWFQNRRMK

Tat-GFP-Tat

MGYGRKKRRQRRRGGSGGSGGSGGSMGGASKGEELFTGVVPILVELDGDVNGHKFS
VRGEGEGDATNGKLTLKFICTTGKLPVPWPTLVTTLTYGVQCFSRYPDHMKQHDFFK
SAMPEGYVQERTISFKDDGTYKTRAEVKFEGDTLVNRIELKGIDFKEDGNILGHKLEY
NFNSHNVYITADKQKNGIKANFKIRHNVEDGSVQLADHYQQNTPIGDGPVLLPDN
HYLSTQSALSKDPNEKRDHMVLLEFVTAAGITHGMDELYKHHHHHHGGSGGSGGS
MYGRKKRRQRRR

Ypep$_2$-GFP

MGYTFGLKTSFNVQGGSGGSGGSGGSYTFGLKTSFNVQGGSGGSGGSGGSMGGASK
GEELFTGVVPILVELDGDVNGHKFSVRGEGEGDATNGKLTLKFICTTGKLPVPWPTL
VTTLTYGVQCFSRYPDHMKQHDFFKSAMPEGYVQERTISFKDDGTYKTRAEVKFEGD
TLVNRIELKGIDFKEDGNILGHKLEYNFNSHNVYITADKQKNGIKANFKIRHNVEDG
SVQLADHYQQNTPIGDGPVLLPDNHYLSTQSALSKDPNEKRDHMVLLEFVTAAGIT
HGMDELYKHHHHHH

REFERENCES

(1) Favoreel, H. W., Nauwynck, H. J., Halewyck, H. M., Van Oostveldt, P., Mettenleiter, T. C., and Pensaert, M. B. (1999) Antibody-induced endocytosis of viral glycoproteins and major histocompatibility complex class I on pseudorabies virus-infected monocytes. *J. Gen. Virol. 80 (Pt 5)*, 1283–91.

(2) Muller, S., Zhao, Y., Brown, T. L., Morgan, A. C., and Kohler, H. (2005) TransMabs: cell-penetrating antibodies, the next generation. *Expert Opin. Biol. Ther. 5*, 237–41.

(3) Hughes, B. (2010) Antibody-drug conjugates for cancer: poised to deliver? *Nat. Rev. Drug Discov. 9*, 665–7.

(4) Wu, A. M., and Senter, P. D. (2005) Arming antibodies: prospects and challenges for immunoconjugates. *Nat. Biotechnol. 23*, 1137–46.

(5) Deshayes, S., Morris, M. C., Divita, G., and Heitz, F. (2005) Cell-penetrating peptides: tools for intracellular delivery of therapeutics. *Cell. Mol. Life Sci. 62*, 1839–49.

(6) Ford, K. G., Souberbielle, B. E., Darling, D., and Farzaneh, F. (2001) Protein transduction: an alternative to genetic intervention? *Gene Ther. 8*, 1–4.

(7) Mäe, M., and Langel, U. (2006) Cell-penetrating peptides as vectors for peptide, protein and oligonucleotide delivery. *Curr. Opin. Pharmacol. 6*, 509–14.

(8) Tréhin, R., and Merkle, H. P. (2004) Chances and pitfalls of cell penetrating peptides for cellular drug delivery. *Eur. J. Pharm. Biopharm. 58*, 209–23.

(9) Pooga, M., Hällbrink, M., Zorko, M., and Langel, U. (1998) Cell penetration by transportan. *FASEB J. 12*, 67–77.

(10) Oehlke, J. (1998) Cellular uptake of an α-helical amphipathic model peptide with the potential to deliver polar compounds into the cell interior non-endocytically. *Biochim. Biophys. Acta - Biomembr. 1414*, 127–139.

(11) Vivès, E., Brodin, P., and Lebleu, B. (1997) A truncated HIV-1 Tat protein basic domain rapidly translocates through the plasma membrane and accumulates in the cell nucleus. *J. Biol. Chem. 272*, 16010–7.

(12) Mitchell, D. J., Steinman, L., Kim, D. T., Fathman, C. G., and Rothbard, J. B. (2000) Polyarginine enters cells more efficiently than other polycationic homopolymers. *J. Pept. Res. 56*, 318–325.

(13) Futaki, S., Suzuki, T., Ohashi, W., Yagami, T., Tanaka, S., Ueda, K., and Sugiura, Y. (2001) Arginine-rich peptides. An abundant source of membrane-permeable peptides having potential as carriers for intracellular protein delivery. *J. Biol. Chem. 276*, 5836–40.

(14) Elliott, G., and O'Hare, P. (1997) Intercellular trafficking and protein delivery by a herpesvirus structural protein. *Cell 88*, 223–33.

(15) Derossi, D., Joliot, A. H., Chassaing, G., and Prochiantz, A. (1994) The third helix of the Antennapedia homeodomain translocates through biological membranes. *J. Biol. Chem. 269*, 10444–50.

(16) Fischer, P. M., Zhelev, N. Z., Wang, S., Melville, J. E., Fåhraeus, R., and Lane, D. P. (2000) Structure-activity relationship of truncated and substituted analogues of the intracellular delivery vector Penetratin. *J. Pept. Res. 55*, 163–72.

(17) Lin, Y. Z., Yao, S. Y., and Hawiger, J. (1996) Role of the nuclear localization sequence in fibroblast growth factor-1-stimulated mitogenic pathways. *J. Biol. Chem. 271*, 5305–8.

(18) Lin, Y. Z., Yao, S. Y., Veach, R. A., Torgerson, T. R., and Hawiger, J. (1995) Inhibition of nuclear translocation of transcription factor NF-kappa B by a synthetic peptide containing a cell membrane-permeable motif and nuclear localization sequence. *J. Biol. Chem. 270*, 14255–8.

(19) Zhang, L., Torgerson, T. R., Liu, X. Y., Timmons, S., Colosia, A. D., Hawiger, J., and Tam, J. P. (1998) Preparation of functionally active cell-permeable peptides by single-step ligation of two peptide modules. *Proc. Natl. Acad. Sci. U. S. A. 95*, 9184–9.

(20) Morris, M. C., Vidal, P., Chaloin, L., Heitz, F., and Divita, G. (1997) A new peptide vector for efficient delivery of oligonucleotides into mammalian cells. *Nucleic Acids Res. 25*, 2730–6.

(21) Chaloin, L., Vidal, P., Lory, P., Méry, J., Lautredou, N., Divita, G., and Heitz, F. (1998) Design of carrier peptide-oligonucleotide conjugates with rapid membrane translocation and nuclear localization properties. *Biochem. Biophys. Res. Commun. 243*, 601–8.

(22) Lapidus, R. G., Tiffany, C. W., Isaacs, J. T., and Slusher, B. S. (2000) Prostate-specific membrane antigen (PSMA) enzyme activity is elevated in prostate cancer cells. *Prostate 45*, 350–4.

(23) Bostwick, D. G., Pacelli, A., Blute, M., Roche, P., and Murphy, G. P. (1998) Prostate specific membrane antigen expression in prostatic intraepithelial neoplasia and adenocarcinoma: a study of 184 cases. *Cancer 82*, 2256–61.

(24) Henry, M. D., Wen, S., Silva, M. D., Chandra, S., Milton, M., and Worland, P. J. (2004) A prostate-specific membrane antigen-targeted monoclonal antibody-chemotherapeutic conjugate designed for the treatment of prostate cancer. *Cancer Res. 64*, 7995–8001.

(25) Nanus, D. M., Milowsky, M. I., Kostakoglu, L., Smith-Jones, P. M., Vallabahajosula, S., Goldsmith, S. J., and Bander, N. H. (2003) Clinical use of monoclonal antibody HuJ591 therapy: targeting prostate specific membrane antigen. *J. Urol. 170*, S84–8; discussion S88–9.

(26) Patri, A. K., Myc, A., Beals, J., Thomas, T. P., Bander, N. H., and Baker, J. R. Synthesis and in vitro testing of J591 antibody-dendrimer conjugates for targeted prostate cancer therapy. *Bioconjug. Chem. 15*, 1174–81.

(27) Dassie, J. P., Liu, X.-Y., Thomas, G. S., Whitaker, R. M., Thiel, K. W., Stockdale, K. R., Meyerholz, D. K., McCaffrey, A. P., McNamara, J. O., and Giangrande, P. H. (2009) Systemic administration of optimized aptamer-siRNA chimeras promotes regression of PSMA-expressing tumors. *Nat. Biotechnol. 27*, 839–49.

(28) Murphy, G. P., Elgamal, A. A., Su, S. L., Bostwick, D. G., and Holmes, E. H. (1998) Current evaluation of the tissue localization and diagnostic utility of prostate specific membrane antigen. *Cancer 83*, 2259–69.

(29) Silver, D. A., Pellicer, I., Fair, W. R., Heston, W. D., and Cordon-Cardo, C. (1997) Prostate-specific membrane antigen expression in normal and malignant human tissues. *Clin. Cancer Res. 3*, 81–5.

(30) Beckett, M. Lou, Cazares, L. H., Vlahou, A., Schellhammer, P. F., and Wright, G. L. . J. (1999) Prostate-specific Membrane Antigen Levels in Sera from Healthy Men and Patients with Benign Prostate Hyperplasia or Prostate Cancer. *Clin. Cancer Res. 5*, 4034–4040.

(31) Clackson, T., and Lowman, H. B. (2004) Phage Display: A Practical Approach. Oxford University Press.

(32) Barbas, C. F. I., Burton, D. R., Scott, J. K., and Silverman, G. J. (2004) Phage Display: A Laboratory Manual. CSHL Press.

(33) Gao, C., Mao, S., Ditzel, H. J., Farnaes, L., Wirsching, P., Lerner, R. A., and Janda, K. D. (2002) A cell-penetrating peptide from a novel pVII-pIX phage-displayed random peptide library. *Bioorg. Med. Chem. 10*, 4057–65.

(34) Ivanenkov, V. V., Felici, F., and Menon, A. G. (1999) Uptake and intracellular fate of phage display vectors in mammalian cells. *Biochim. Biophys. Acta - Mol. Cell Res. 1448*, 450–462.

(35) Ivanenkov, V. V, Felici, F., and Menon, A. G. (1999) Targeted delivery of multivalent phage display vectors into mammalian cells. *Biochim. Biophys. Acta 1448*, 463–72.

(36) Kim, Y., Lillo, A. M., Steiniger, S. C. J., Liu, Y., Ballatore, C., Anichini, A., Mortarini, R., Kaufmann, G. F., Zhou, B., Felding-Habermann, B., and Janda, K. D. (2006) Targeting heat shock proteins on cancer cells: selection, characterization, and cell-penetrating properties of a peptidic GRP78 ligand. *Biochemistry 45*, 9434–44.

(37) Nomura, T., Kawamura, M., Shibata, H., Abe, Y., Ohkawa, A., Mukai, Y., Sugita, T., Imai, S., Nagano, K., Okamoto, T., Tsutsumi, Y., Kamada, H., Nakagawa, S., and Tsunoda, S. (2007) Creation of a novel cell penetrating peptide, using a random 18mer peptides library. *Pharmazie 62*, 569–73.

(38) Tsien, R. Y. (1998) The green fluorescent protein. *Annu. Rev. Biochem. 67*, 509–44.

(39) Cronican, J. J., Beier, K. T., Davis, T. N., Tseng, J.-C., Li, W., Thompson, D. B., Shih, A. F., May, E. M., Cepko, C. L., Kung, A. L., Zhou, Q., and Liu, D. R. (2011) A class of human proteins that deliver functional proteins into mammalian cells in vitro and in vivo. *Chem. Biol. 18*, 833–8.

(40) Cronican, J. J., Thompson, D. B., Beier, K. T., McNaughton, B. R., Cepko, C. L., and Liu, D. R. (2010) Potent delivery of functional proteins into Mammalian cells in vitro and in vivo using a supercharged protein. *ACS Chem. Biol. 5*, 747–52.

(41) McNaughton, B. R., Cronican, J. J., Thompson, D. B., and Liu, D. R. (2009) Mammalian cell penetration, siRNA transfection, and DNA transfection by supercharged proteins. *Proc. Natl. Acad. Sci. U. S. A. 106*, 6111–6.

(42) Meade, B. R., and Dowdy, S. F. (2008) Enhancing the cellular uptake of siRNA duplexes following noncovalent packaging with protein transduction domain peptides. *Adv. Drug Deliv. Rev. 60*, 530–6.

(43) Mammen, M., Choi, S.-K., and Whitesides, G. M. (1998) Polyvalent Interactions in Biological Systems: Implications for Design and Use of Multivalent Ligands and Inhibitors. *Angew. Chemie Int. Ed. 37*, 2754–2794.

(44) Moss, J. A., Lillo, A., Kim, Y. S., Gao, C., Ditzel, H., and Janda, K. D. (2005) A dimerization "switch" in the internalization mechanism of a cell-penetrating peptide. *J. Am. Chem. Soc. 127*, 538–9.

(45) Krishnamurthy, V. M., Estroff, L. A., and Whitesides, G. M. (2006) Fragment-based Approaches in Drug Discovery (Jahnke, W., and Erlanson, D. A., Eds.), pp 11–53. Wiley-VCH Verlag GmbH & Co. KGaA, Weinheim, FRG.

(46) Tseng, Y.-L., Liu, J.-J., and Hong, R.-L. (2002) Translocation of liposomes into cancer cells by cell-penetrating peptides penetratin and tat: a kinetic and efficacy study. *Mol. Pharmacol. 62*, 864–72.

(47) Li, S., McGuire, M. J., Lin, M., Liu, Y.-H., Oyama, T., Sun, X., and Brown, K. C. (2009) Synthesis and characterization of a high-affinity {alpha}v{beta}6-specific ligand for in vitro and in vivo applications. *Mol. Cancer Ther. 8*, 1239–49.

(48) Sung, M., Poon, G. M. K., and Gariépy, J. (2006) The importance of valency in enhancing the import and cell routing potential of protein transduction domain-containing molecules. *Biochim. Biophys. Acta 1758*, 355–63.

(49) Tyagi, M., Rusnati, M., Presta, M., and Giacca, M. (2001) Internalization of HIV-1 tat requires cell surface heparan sulfate proteoglycans. *J. Biol. Chem. 276*, 3254–61.

(50) Sandgren, S., Cheng, F., and Belting, M. (2002) Nuclear targeting of macromolecular polyanions by an HIV-Tat derived peptide. Role for cell-surface proteoglycans. *J. Biol. Chem. 277*, 38877–83.

(51) Console, S., Marty, C., García-Echeverría, C., Schwendener, R., and Ballmer-Hofer, K. (2003) Antennapedia and HIV transactivator of transcription (TAT) "protein

transduction domains" promote endocytosis of high molecular weight cargo upon binding to cell surface glycosaminoglycans. *J. Biol. Chem. 278*, 35109–14.

(52) Violini, S., Sharma, V., Prior, J. L., Dyszlewski, M., and Piwnica-Worms, D. (2002) Evidence for a plasma membrane-mediated permeability barrier to Tat basic domain in well-differentiated epithelial cells: lack of correlation with heparan sulfate. *Biochemistry 41*, 12652–61.

(53) Mai, J. C., Shen, H., Watkins, S. C., Cheng, T., and Robbins, P. D. (2002) Efficiency of protein transduction is cell type-dependent and is enhanced by dextran sulfate. *J. Biol. Chem. 277*, 30208–18.

(54) Maiolo, J. R., Ferrer, M., and Ottinger, E. a. (2005) Effects of cargo molecules on the cellular uptake of arginine-rich cell-penetrating peptides. *Biochim. Biophys. Acta 1712*, 161–72.

(55) Fittipaldi, A., Ferrari, A., Zoppé, M., Arcangeli, C., Pellegrini, V., Beltram, F., and Giacca, M. (2003) Cell membrane lipid rafts mediate caveolar endocytosis of HIV-1 Tat fusion proteins. *J. Biol. Chem. 278*, 34141–9.

(56) Richard, J. P., Melikov, K., Brooks, H., Prevot, P., Lebleu, B., and Chernomordik, L. V. (2005) Cellular uptake of unconjugated TAT peptide involves clathrin-dependent endocytosis and heparan sulfate receptors. *J. Biol. Chem. 280*, 15300–6.

(57) Melan, M. A., and Sluder, G. (1992) Redistribution and differential extraction of soluble proteins in permeabilized cultured cells. Implications for immunofluorescence microscopy. *J. Cell Sci. 101 (Pt 4*, 731–43.

(58) Pichon, C., Monsigny, M., and Roche, A. C. (1999) Intracellular localization of oligonucleotides: influence of fixative protocols. *Antisense Nucleic Acid Drug Dev. 9*, 89–93.

(59) Zhang, X., Wan, L., Pooyan, S., Su, Y., Gardner, C. R., Leibowitz, M. J., Stein, S., and Sinko, P. J. (2004) Quantitative Assessment of the Cell Penetrating Properties of RI-Tat-9: Evidence for a Cell Type-Specific Barrier at the Plasma Membrane of Epithelial Cells. *Mol. Pharm. 1*, 145–155.

CHAPTER THREE

MUTAGENESIS MODULATES THE UPTAKE EFFICIENCY, CELL-SELECTIVITY, AND FUNCTIONAL ENZYME DELIVERY OF A PROTEIN TRANSDUCTION DOMAIN

3.1 Introduction

In Chapter 2 we described our efforts to develop a prostate cancer cell-selective protein transduction domain, which penetrates PC-3 prostate cancer cells in a manner that is controlled by multivalency effects.[1] In order to better understand the requirements for uptake of Ypep by PC-3 cells, as well as to optimize the potency and cell-selectivity of our evolved PTD, we prepared a significant number of Ypep mutants to screen cellular uptake. We assayed these variants for the ability to deliver functional fluorescent protein or enzyme to PC-3 cells. We show that the best mutant delivers ~19-fold more fused protein to PC-3 cells and cell-selectivity increased by ~4-fold. In addition, the most potent and cell-selective mutant delivers large quantities of functional enzyme to human prostate cancer cells. This chapter details those efforts to further develop our cell-selective PTD as a targeting reagent for prostate cancer cells.

3.2 Alanine Scanning Illuminates the Specific Contribution Each Residue Plays in Ypep Uptake by PC-3 Cells

Initially, we used phage display to evolve our cell-selective protein transduction domain, Ypep. While the complexity of the 12-mer phage display library is approximately 10^9 independent clones, that is only a small amount of the 20^{12} (4.1×10^{15}) possible peptide sequences. Moreover, the probability of encoding each amino acid is not equal due to codon degeneracy.[2] For equal probability of encoding all amino acids, a library of 64^{12} (4.7×10^{21}) is required. Additionally, some amino acid sequences are preferentially displayed on the phage or amplified in *E. coli*, which may also limit the diversity of the screened library. Therefore, it was necessary to further optimize the peptide evolved from the phage display library.

To assess the specific contribution each residue in Ypep plays in cell uptake efficiency, we made a library of Ypep alanine mutants and expressed these peptides as N-terminal fusions to green fluorescent protein (GFP) (**Figure 3.1A**). PC-3 cells were treated with 5 μM of each Ypep-GFP mutant, a concentration previously shown to be sufficient for appreciable Ypep-GFP uptake.[1] Cell were then exhaustively washed using conditions that we,[1] and others,[3–6] have previously shown to remove cell surface-bound protein. The amount of internalized GFP was measured by flow cytometry. As shown in **Figure 3.1B**, most mutations resulted in significantly lower GFP deliver. However,

the Gly4Ala and Thr7Ala mutations delivered ~3.8- and ~6.8-fold more GFP to PC-3 cells compared to native Ypep, respectively. Moreover, we were interested in the effect of removal of the single positively charged residue (Lys6) because of the low theoretical net charge of Ypep compared to other common PTDs (as discussed in Chapter 2.8). Mutation of the lysine to an alanine did result in decreased GFP uptake ~4-fold (Figure 3.1). Based on these initial findings, we prepared a focused library of mutants with molecularly diverse residues at position 4 and/or 7.

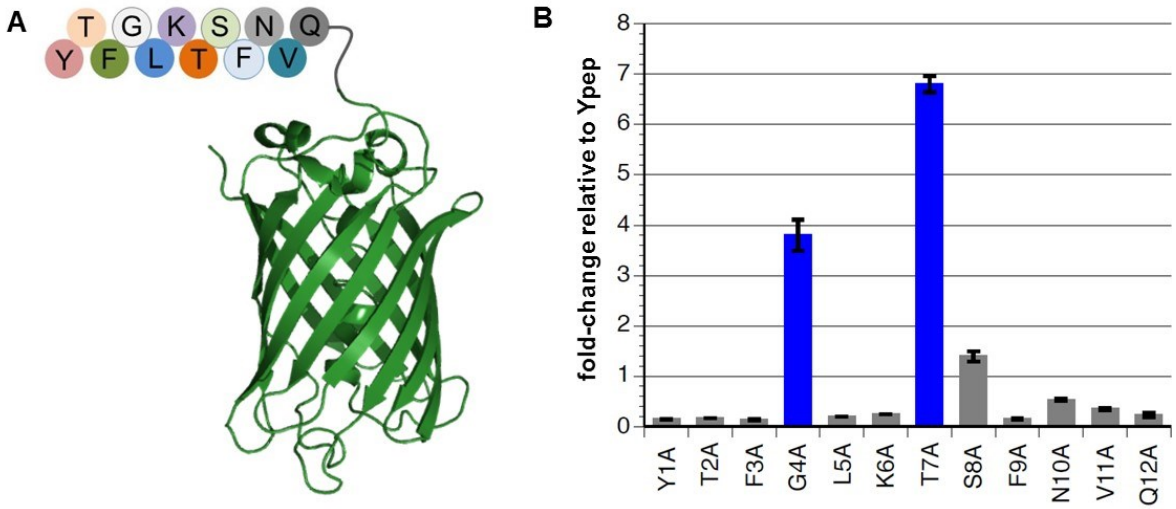

Figure 3.1 Alanine scan of Ypep transduction. A) Amino acid sequence of Ypep displayed on N-terminus of GFP. B) Fold-change in GFP uptake for alanine mutants of Ypep-GFP, relative to Ypep-GFP. PC-3 cells were treated with 5 μM mutant Ypep-GFP, and then washed to remove cell surface-bound protein. GFP internalization was measured by flow cytometry. Values and error bars represent the mean and standard deviation of three independent experiments.

3.3 Optimizing Cellular Uptake of a Prostate Cancer Cell-Selective Protein Transduction Domain

Ypep mutants containing either negatively charged (aspartic acid), positively charged (lysine), aromatic (phenylalanine), hydrogen bond donated (serine), or amide (asparagine) functional groups at positions 4 or 7 were expressed as N-terminal fusions to GFP. As shown in **Figure 3.2A**, the Gly4Asp mutant exhibited significantly lower uptake, and Gly4Phe and Gly4Ser mutants achieved only slightly high uptake than Ypep-GFP. However, Gly4Lys and Gly4Asn mutants delivered ~3.2 and ~19.2-fold more GFP to PC-3 cells, compared to native Ypep-GFP. Interestingly, small structural changes at position 4 significantly lowered uptake. While the Gly4Gln mutant was ~6.6-fold improved over Ypep, it was ~2.8-fold less efficient than the Gly4Asn mutant. While the cell surface receptor of Ypep and Ypep mutants has not yet been elucidated, the fact that the addition of a methylene unit significantly lowers uptake supports a model wherein a well-defined interaction between Ypep(G4N)-GFP and a cell-surface receptor is required for efficient uptake. Further, the interaction is not only a function of the sequence-defined amide group display on the PTD, but also the spatial orientation of that group.

We next performed identical experiments to optimize residue 7. The Thr7Asp mutant exhibited essentially identical uptake efficiency as native Ypep (**Figure 3.2B**). However, Thr7Lys, Thr7Ser, and Thr7Asn mutants all showed significantly lower transduction efficiencies. In contrast, the Thr7Phe mutant was significantly improved, and was able to deliver ~7.6-fold more GFP to PC-3 cells, compared to native Ypep. Based on this finding, we measured uptake efficiencies for Ypep variants containing all possible proteinogenic aromatic residues at position 7. While both Thr7Tyr and Thr7Trp mutants significantly outperformed native Ypep, delivering ~6.8 and ~7.1-fold more GFP, respectively, neither outperformed the Thr7Phe mutant. In contrast, the Thr7His mutant showed significantly lower cell uptake compared to Thr7Tyr and Thr7Trp mutants, as well as native Ypep. Taken together, the reduced transduction we observed

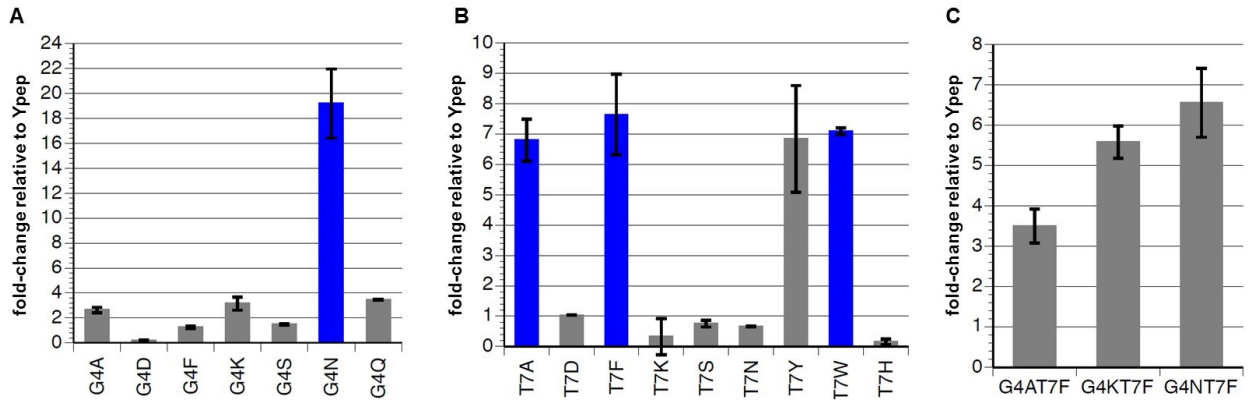

Figure 3.2 Optimizing cellular uptake of Ypep. A) Fold-change in GFP uptake for Ypep-GFP mutants at residue 4, relative to Ypep-GFP. B) Fold-change in GFP uptake for Ypep-GFP mutants at residue 7, relative to Ypep-GFP. C) Efficiency of GFP uptake for Ypep-GFP double mutants at residues 4 and 7. A-C) For each example, PC-3 cells were treated with 5 μM mutant Ypep-GFP, then washed to remove cell surface-bound protein. GFP internalization was measured by flow cytometry. Values and error bars represent the mean and standard deviation of three independent experiments. Blue bars represent the four most active mutants.

for the Thr7His and Thr7Lys mutants suggests that residues with positive charge, or partial positive charge may not be tolerated at this position.

The effect of double beneficial mutations on the uptake efficiency of PTD-GFP was next evaluated. Combined synergistic effects can play important roles in many biological processes and macromolecule-substrate interactions.[7] To assess if combinations of beneficial mutants are synergistic, we prepared three Ypep double mutants that contain combinations of the most beneficial single mutations at residues 4 and 7. Ypep double mutants that contain combinations of the most beneficial single mutations at residues 4, and phenylalanine at position 7 were expressed as N-terminal fusions to GFP and added to PC-3 cells as previously described. The Gly4Ala:Thr7Phe, Gly4Lys:Thr7Phe, and Gly4Asn:Thr7Phe double mutants were found to be ~3.5, ~5.6, and ~6.5-fold more efficient at GFP transduction than Ypep-GFP, respectively (**Figure 3.2C**). Interestingly, however, none of these double mutants exhibited higher uptake compared to the single mutant Ypep variants from which they were derived.

3.4 Ypep Mutants are Not Cytotoxic and are Internalized via Energy-Dependent Endocytosis

Based on these data, the Gly4Asn, Thr7Phe, Thr7Trp, and Thr7Ala mutants (bars are colored in blue in **Figure 3.2**) were most improved over Ypep, with increased

transduction efficiencies of ~19.2, ~7.6, ~7.1, and ~6.8-fold, respectively. To assess the cytotoxicity of Ypep variants under conditions required for appreciable uptake, we performed 3-(4,5-dimethylthiazol-2-yl)-2,5-diphenyltetrazolium bromide assay (MTT) on PC-3 cells after treatment with 5 μM Ypep(mutant)-GFP. These assays revealed no apparent cytotoxicity to PC-3 cells for any of the Ypep mutants (**Figure 3.3A**). GFP uptake was confirmed for these four mutants by live-cell fluorescence microscopy. While only a very small amount of internalized GFP was observed in PC-3 cells following treatment with 5 μM Ypep-GFP, large amounts of internalized GFP was

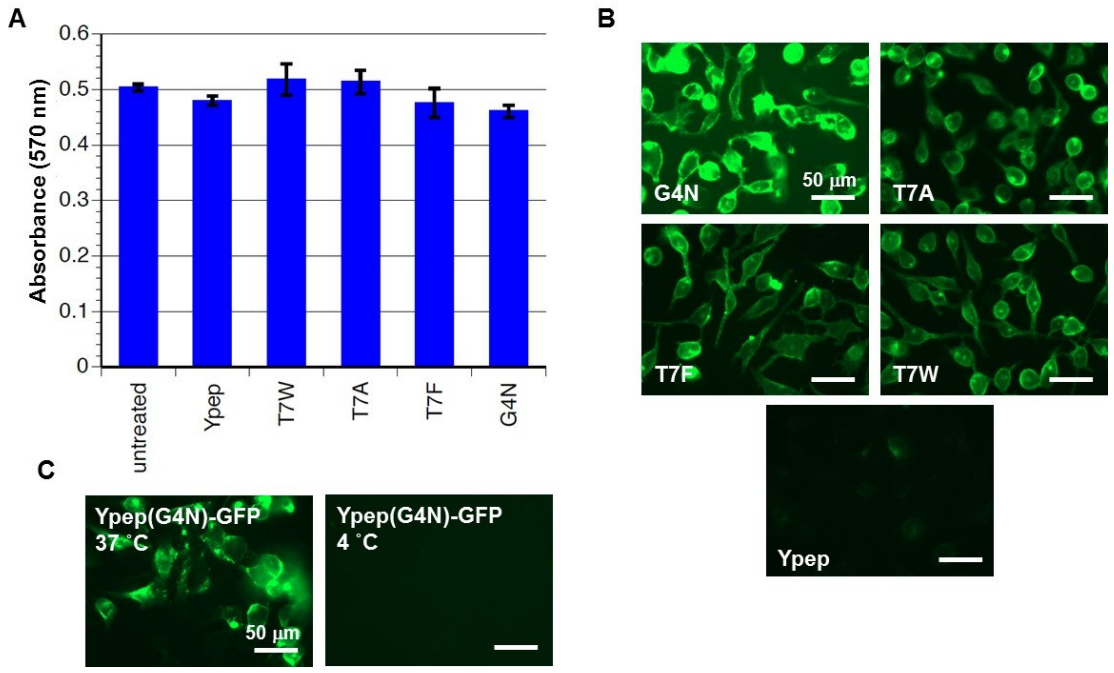

Figure 3.3 Cytotoxicity and mechanism of transduction for Ypep mutants. A) MTT cell viability assay data. B) Live cell fluorescence microscopy images of PC-3 cells following treatment with 5 μM of the most efficient mutant Ypep-GFP fusions, then washed to remove cell surface-bound protein. C) Cell penetration of Ypep(G4N)-GFP at 37 °C or 4 °C. Live cell fluorescence microscopy of images of PC-3 cells following treatment with 5 μM Ypep(G4N)-GFP fusions for 30 minutes at 37 °C or 4 °C. For all microscopy images lamp intensity was set at 50% with a 500 msec exposure.

observed in cells following treatment with the same concentration of the four most active Ypep-GFP fusions (**Figure 3.3B**). Consistent with our flow cytometry data, the Gly4Asn mutant delivered the highest amount of GFP to the cell interior.

Previously, we performed extensive studies to elucidate the mechanism of Ypep uptake (Chapter 2.8). We found that while Ypep is taken up at 37 °C, it is not appreciably internalized when PC-3 cells are incubated with a Ypep solution at 4 °C. This finding suggests that Ypep internalization proceeds via an energy-dependent endocytotic pathway. In order to determine if Ypep(G4N) uptake is consistent with the parent peptide, or if internalization proceeds via an alternative pathway, we incubated PC-3 cells with 1 μM Ypep(G4N)-GFP at either 37 °C or 4 °C, washed cells to remove surface-bound material and measured GFP internalization by microscopy and flow cytometry. Interestingly, similar to our findings for Ypep-GFP uptake, high levels of cell fluorescence is observed following treatment at 37 °C; however, no appreciable fluorescence is observed when cells are treated at 4 °C (**Figure 3.3C**). Taken together, these findings suggest that like the parent peptide, the Ypep(G4N) mutant also relies on energy-dependent endocytosis for internalization.

3.5 Gly4Asn Ypep Outperforms Tat and Penetratin Protein Transduction Domains

As described in Chapter 2.6, we observed that Ypep-GFP performed similarly to another widely used PTD, penetratin, and outperformed Tat. Again we sought to compare these new Ypep mutants to the commonly used PTDs, penetratin and Tat. We treated PC-3 cells with solutions containing either Tat-GFP, penetratin-GFP, or the four best Ypep variants identified as a result of mutagenesis studies. As shown in **Figure 3.4**, following treatment with 1 μM PTD-GFP fusion, and washing, all Ypep mutants delivered significantly more GFP to the interior of PC-3 cells, compared to Tat-GFP fusions. Most notably, uptake efficiency in PC-3 cells treated with 1 μM Ypep(G4N)-GFP was ~1.5-fold and 23-fold higher than cells treated with either penetratin-GFP or Tat-GFP fusions, respectively.

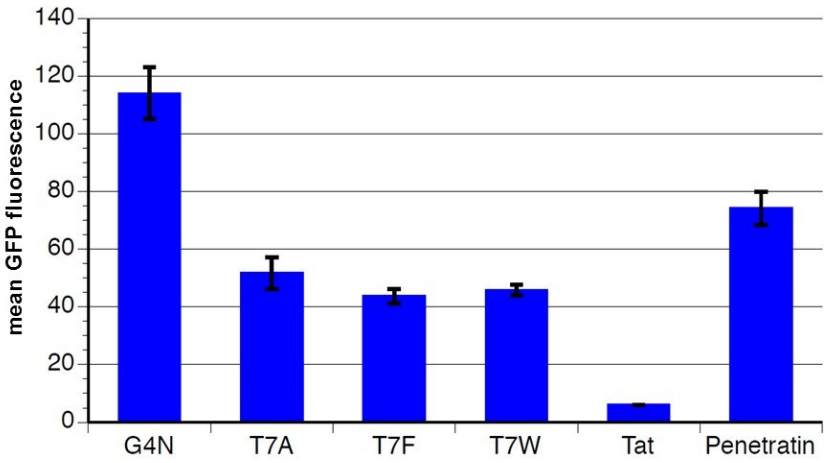

Figure 3.4 Cell uptake of Ypep mutants compared to Tat and penetratin. Flow cytometry data showing amounts of GFP delivered to PC-3 cells following treatment with 1 μM Ypep(mutant)-GFP fusions, Tat-GFP fusion, or penetratin-GFP fusion, then washed to remove cell surface-bound protein. Values and error bars represent the mean and standard deviation of three independent experiments.

3.6 Mutations Beneficial to Uptake Efficiency Also Increase the Cell-selectivity of Protein Delivery

While the above mutational studies on Ypep resulted in numerous variants with improved transduction efficiency, the effect of these beneficial mutations on cell-selectivity was unclear. In order to assess the impact of these mutations on cell-selectivity, we compared PTD-GFP fusion uptake in PC-3 (target) and off-target non-cancer human embryonic kidney cells (HEK-293T). Cells were treated with 0.1-1 μM PTD-GFP fusion, washed as previously described to remove cell surface-bound material, and internalized GFP was measured by flow cytometry. As shown in **Figure 3.5**, a majority of the most efficient Ypep mutants also exhibited increased selectivity for

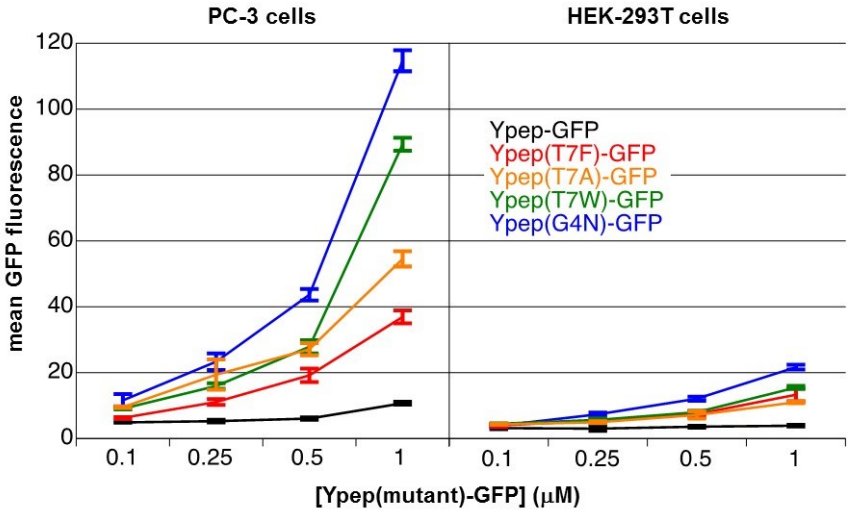

Figure 3.5 Cell-selectivity of Ypep mutants. Flow cytometry data showing the amount of internalized GFP in PC-3 cells or HEK-293T cells following treatment with 0.1, 0.25, 0.5, or 1 μM mutant Ypep-GFP, Ypep(T7A)-GFP, Ypep(T7W)-GFP, or Ypep(G4N)-GFP, then washed to remove cell surface-bound protein. Values and error bars represent the mean and standard deviation of three independent experiments.

PC-3 human prostate cancer cells. Consistent with our previous findings, Ypep delivered ~1.6, ~1.8, ~1.7, or ~2.8-fold more GFP to PC-3 cells compared to HEK-293 cells, following treatment with 0.1, 0.25, 0.5, or 1 μM solutions, respectively. While the Thr7Phe mutant exhibited similar selectivity for PC-3 cells (~1.6, ~2.0, ~2.6, and ~2.8-fold following 0.1-1 μM treatment), the Gly4Asn, Thr7Trp, and Thr7Ala mutants were significantly more selective for PC-3 cells. For example, Gly4Asn, Thr7Trp, and Thr7Ala Ypep mutants were ~5.3, ~5.8, and ~5.0-fold more selective for PC-3 prostate cancer cells compared to HEK-293T cells. Taken together, these studies demonstrate a significant improvement in both the transduction efficiency and PC-3 cell-selectivity of multiple Ypep mutants found as a result of these studies.

3.7 Gly4Asn Ypep Mutant Delivers Appreciable Levels of a Functional Enzyme to PC-3 Cells

Perhaps the ultimate test of a PTD is intracellular delivery of a functional enzyme. Luciferase is a class of enzymes that oxidize a photon-emitting substrate, resulting in bioluminescence. These enzymes are used extensively as reporters and cell imaging reagents because of their high sensitivity, broad dynamic range, and operational simplicity.[8] NanoLuc luciferase (nLuc) is a recently reported variant of the small luciferase subunit from the deep sea shrimp *Oplophorus gracilirostris*.[9] As a simple

test for functional intracellular enzyme delivery, we measured luciferase activity in PC-3 prostate cancer cells following treatment with 1 μM nLuc, Ypep-nLuc, or Ypep(G4N)-nLuc. Consistent with the overwhelming majority of proteins, appreciable amounts of nLuc do not penetrate mammalian cells. Cells treated with nLuc, washed to remove surface-bound protein, and treated with furimazine, exhibited very little luminescence (**Figure 3.6**). Similar to our previous findings, relatively modest functional enzyme delivery was achieved via Ypep-dependent delivery. Cells treated with Ypep-nLuc, then washed as described above, were ~6.1-fold more luminescent than cells treated with nLuc alone (**Figure 3.6**). In contrast, cells similarly treated with Ypep(G4N)-nLuc were ~41.6-fold more luminescent than cells treated with nLuc alone. These findings suggest that relatively large amounts of enzymatically active

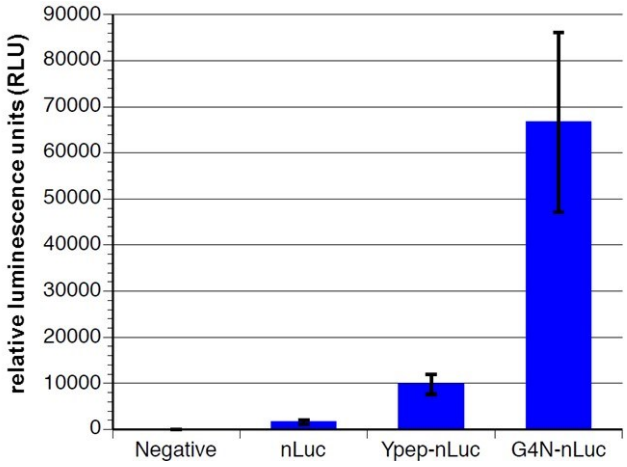

Figure 3.6 Efficiency of nanoluciferase (nLuc) delivery to human prostate cancer cells (PC-3). PC-3 cells were treated with either nLuc, Ypep-nLuc or Ypep(G4N)-nLuc, then washed to remove cell surface-bound protein. Functional nLuc and Ypep-nLuc does not appreciably penetrate PC-3 cells; however, relatively high levels of internalized functional nLuc are observed in cells following treatment with Ypep(G4N)-nLuc.

Ypep(G4N)-nLuc were delivered to the interior of PC-3 cells. Importantly, cells were not lysed at any point during the luciferase assay. Therefore, luminescence generated during these experiments is the action of active nLuc enzyme within the cell interior.

3.8 Conclusions

In summary we developed a novel prostate cancer cell-selective PTD, with uptake efficiency and cell-selectivity profiles that are dependent on multivalency effects. When a single copy of Ypep is fused to GFP, modest uptake efficiency and cell-selectivity was observed. Mutational studies have revealed a number of Ypep variants with significantly improved protein transduction efficiency and selectivity for PC-3 human prostate cancer cells. Amazingly, a single mutation to Ypep(G4N) delivered appreciable levels of nanoluciferase (nLuc) to the interior of PC-3 cells. Taken together, the findings described in this paper significantly improve the functional utility of Ypep-dependent delivery of exogenous proteins to the interior of PC-3 prostate cancer cells. Our data suggest that Ypep mutants described here are well suited to serve as reagents for PC-3 cell-selective delivery of imaging and enzymatic proteins for basic research and biomedical applications.

3.9 Experimental Methods

Materials

Phosphate buffered saline (PBS) - Hyclone/Thermo Scientific
0.25% Trypsin - Hyclone/Thermo Scientific
Brilliant Blue R-250 - J.T.Baker
Bovin serum albumin - Sigma Aldrich
Fetal bovin serum (FBS) - PAA Laboratories
Triton X-100 - Fisher Scientific
Dulbecco's modified Eagle medium (DMEM) - Hyclone/Thermo Scientific
F-12K Nutrient Mixture (Kaighn's Mod.) - Cellgro/Corning
RPMI-1640 media - Hyclone/Thermo Scientific
Mammalian cell culture dishes - Fisher Scientific
B-PER Bacterial Protein Extraction Reagent - Thermo Scientific
Imidazole - Sigma Aldrich
Modified Lowry Protein Assay Kit - Pierce/Thermo Scientific
Nano-Glo® Luciferase Assay - Promega
TACS MTT reagent- Trevigen
PageRuler Prestained Protein Ladder - Thermo Scientific

Instrumentation

All flow cytometry data was carried out on a MoFlo Flow Cytometer and High Speed Cell Sorter with a solid state iCyt 488nm laser. Relative luciferase units were measured on a Synergy Mx Microplate Reader from BioTek. MTT assay absorbance was measured on Synergy Mx Microplate Reader from BioTek. Fluorescence microscopy images were taken with EVOS FL from Advanced Microscopy Group.

Mammalian cell culture

Human prostate adenocarcinoma cells (PC-3) cells were cultured in F12K with 10% Fetal Bovine Serum (FBS) and HEK293T cells cultured in high glucose Dulbecco's

modified Eagle medium (DMEM) with 10% Fetal Bovine Serum (FBS). All cells were incubated at 37 °C with 5% CO_2 environment. All cells were obtained from ATCC.

Cloning

All plasmids were constructed on a pETDuet-1 backbone. All peptides and GGS linkers on the N-terminus and C-terminus of sfGFP were assembled from a set of overlapping oligonucleotides. The peptides were then amplified with the sfGFP or nLuc proteins and the plasmids were ligated into *Nco*I and *Kpn*I restriction enzyme cleavage sites in the pETDuet-1 plasmid.

Protein purification

Cells were grown in 500 mL LB cultures at 37 °C to OD_{600} ~0.6 and induced with 1 mM IPTG at 30 °C overnight. Cells were then collected by centrifugation and stored at -20 °C. Frozen pellets were thawed and 20 mL B-PER was added to lyse cells. The lysate was cleared by centrifugation (17000 rpm, 30 minutes) and the supernatant was mixed with 1 mL of Ni-NTA agarose resin for 1 hour. The resin was collected by centrifugation (4950 rpm, 10 minutes). The resin was washed with 50 mL of PBS with 300 mM NaCl and 20 mM imidazole. The protein was then eluted with 5 mL PBS containing 300 mM NaCl and 500 mM imidazole. The proteins were dialyzed against

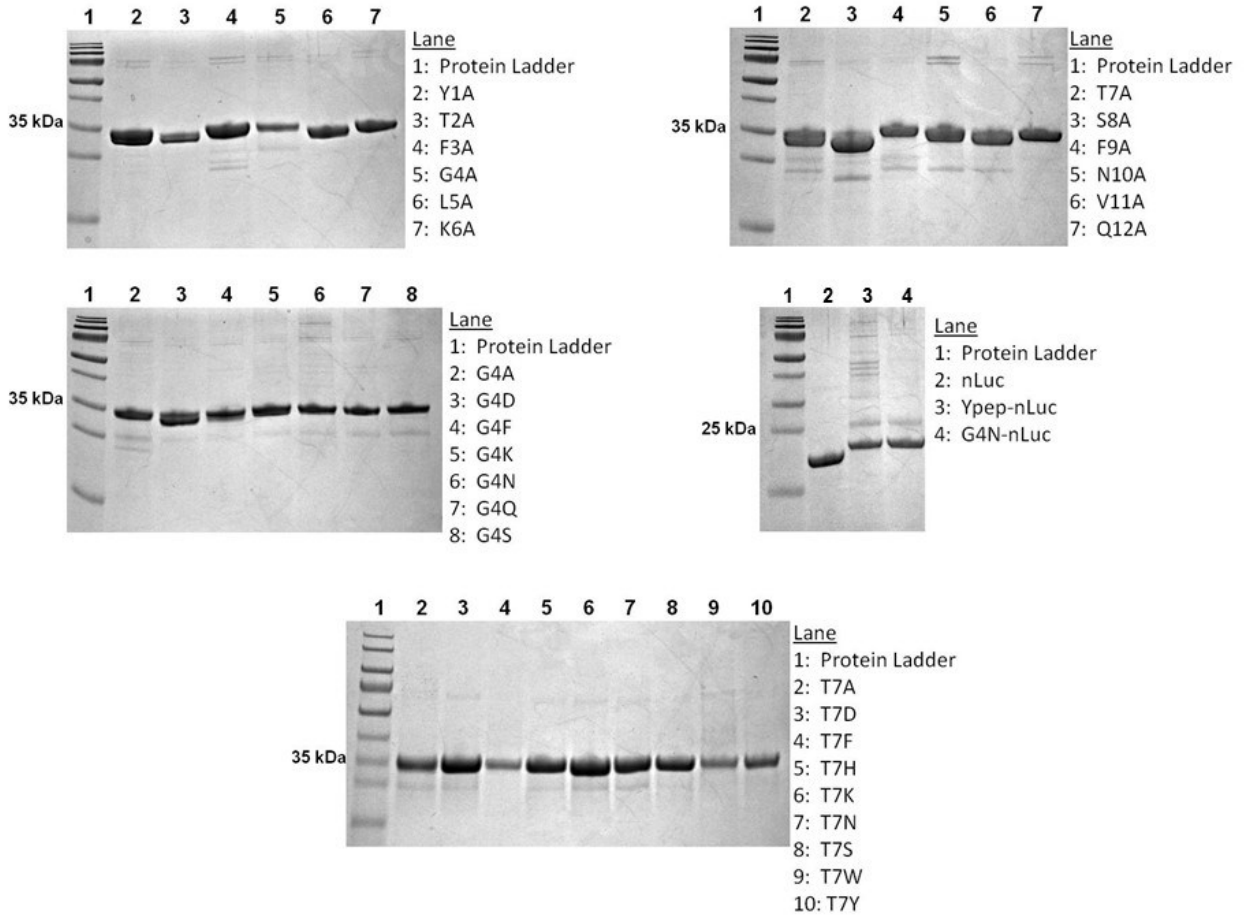

Figure 3.7 PAGE analysis of all proteins used in this chapter. Purified proteins were run on 15% Tris-HCl gels (BioRad), and stained with Coomassie Blue.

PBS and analyzed for purity by SDS-PAGE staining with Coomassie Blue (**Figure 3.7**). The proteins were then quantified using a modified Lowry protein assay kit. Nanoluciferase (nLuc) proteins were purified in the sample way, except washed with Tris buffers (25 mM Tris-HCl, 100 mM NaCl, pH 8.0) instead of phosphate buffers.

Flow cytometry analysis

Mammalian cells were grown to 90% confluency in a 12-well plate. Cells were then washed once with PBS and 500 µL of diluted protein in PBS was added. The cells were incubated with the protein solution for 3 hours at 37 °C, 5 % CO_2 environment. After

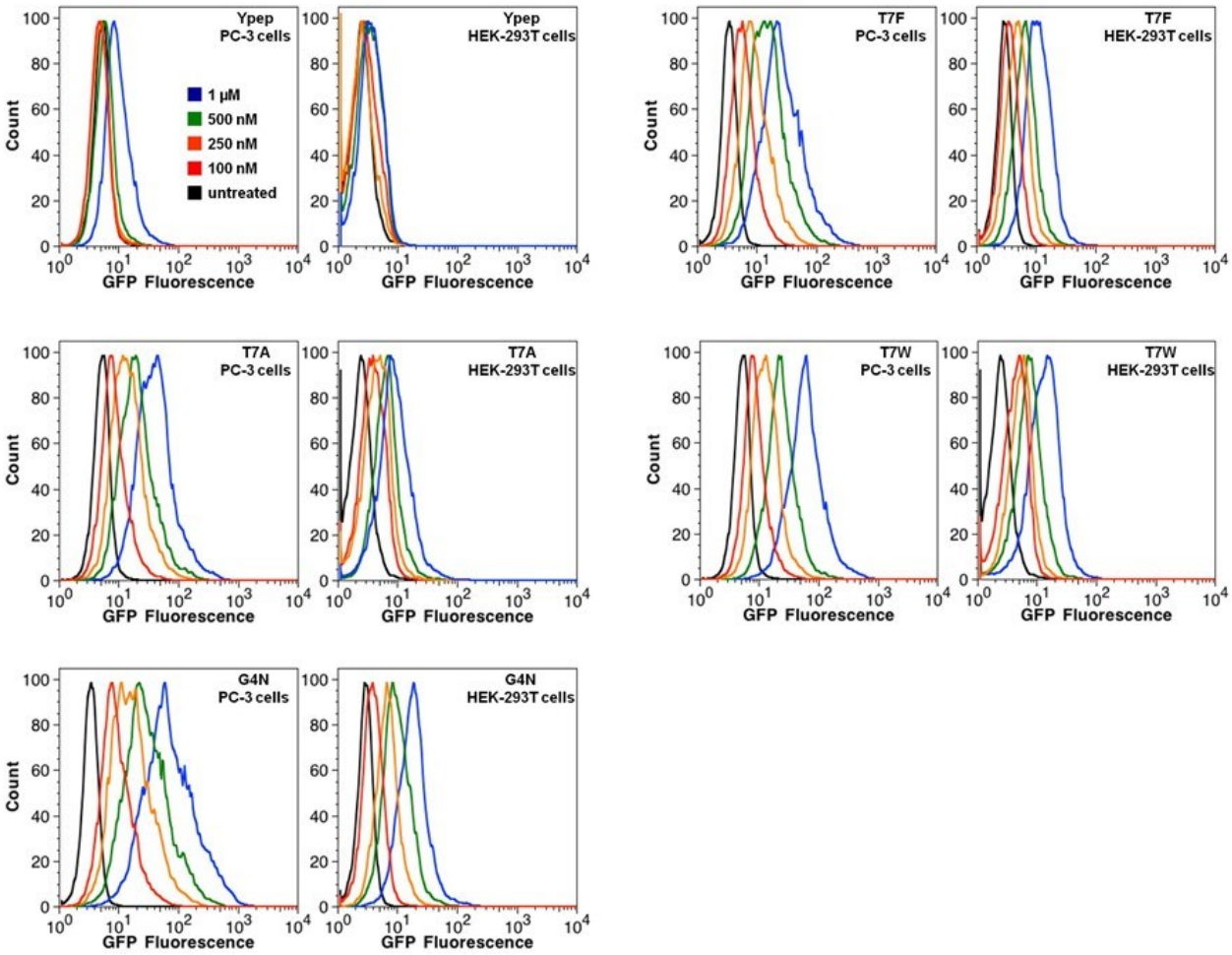

Figure 3.9 Representative flow cytometry data from Figure 3.5. Flow cytometry data showing the amount of internalized GFP in PC-3 cells or HEK-293T cells following treatment with 100 nM, 250 nM, 500 nM, or 1 µM Ypep-GFP, Ypep(T7F)-GFP, Ypep(T7A)-GFP, Ypep(T7W)-GFP, or Ypep(G4N)-GFP for 3 hours at 37 °C in PBS.

the incubation period, cells were then washed once with PBS and two times with PBS-HS (heparin sulfate 20 U/mL) for 10 minutes at 37 °C, 5% CO_2. The cells were then removed from dish with 0.5 mL of 0.25% Trypsin and collected by centrifugation. The cells were then resuspended in PBS-HS and analyzed by flow cytometry.

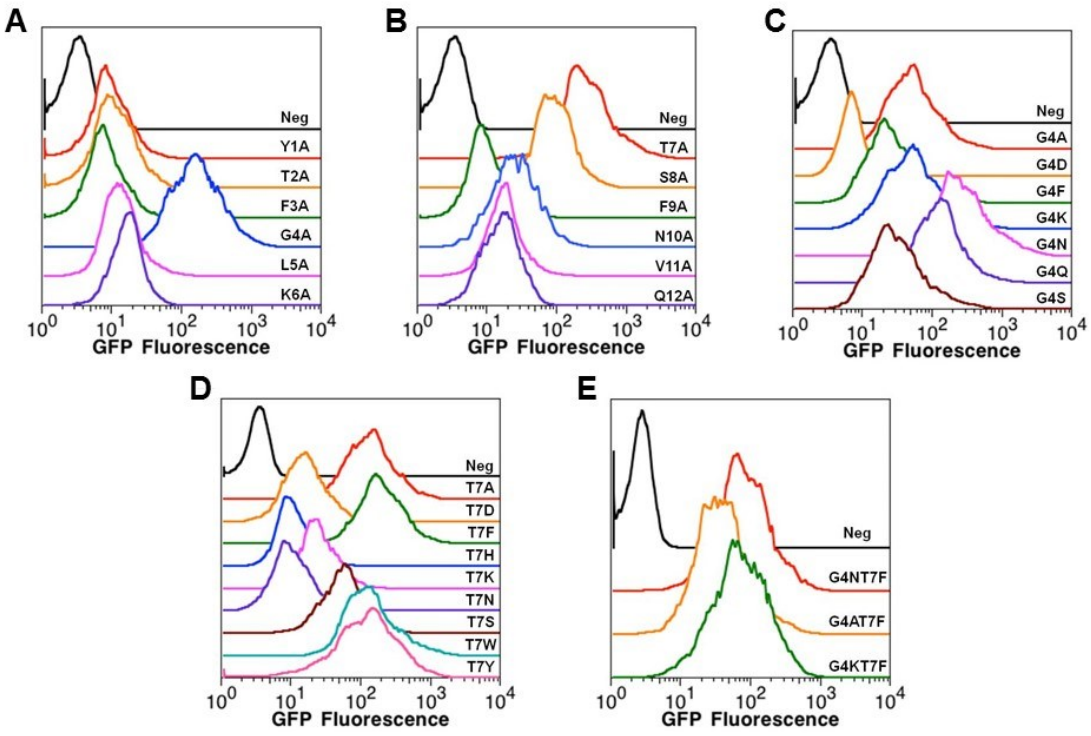

Figure 3.8 Representative flow cytometry data from Figure 3.1-3.2. A-B) Flow cytometry data showing GFP uptake for alanine mutants of Ypep-GFP. C) GFP uptake for Ypep-GFP mutants at residue 4. D) GFP uptake of Ypep-GFP mutants at residue 7. E) GFP uptake of Ypep-GFP double mutants at residue 4 and 7. A-E) PC-3 cells treated with 5 μM mutant Ypep-GFP for 3 hours at 37 °C, then washed as described above.

Live cell fluorescence microscopy

Mammalian cells were grown to 90% confluency in a 12-well plate. Cells were then washed once with PBS and 500 μL of 5 μM protein in PBS was added. The cells were incubated with the protein solution for 3 hours at 37 °C, 5% CO_2 environment. After the incubation period, cells were then washed once with PBS and three times with PBS-HS (heparan sulfate 20 U/mL) for 10 minutes at 37 °C, 5% CO_2. The cells were then imaged on the EVOS FL fluorescence microscope. For 4 ˚C experiments, the PC-3 cells were

incubated at 4 ˚C for 30 minutes prior to the addition of the diluted protein. The incubation period was carried out at 4 ˚C and washed as described above.

MTT assay

PC-3 cells were grown to 90% confluency in a 12-well plate. Cells were then washed once with PBS and incubated with the protein in PBS for 3 hours at 37 °C, 5% CO_2. The solution was removed and the cells were washed twice with PBS-HS (heparan sulfate 20 U/mL). The cells were then incubated with 0.5 mL media with 25 μL of MTT reagent for 4.5 hours. After the incubation, 250 μL detergent was added to the cells and they were incubated for an addition 30 minutes. MTT assay readings were taken with a Synergy Mx microplate reader at 570 nm.

NanoGlo luciferase assay

PC-3 cells were grown to ~80% confluency in a 24-well plate (clear bottom, black well). The nLuc proteins were diluted in TBS (25 mM Tris-HCl, 150 mM NaCl, pH 7.0) and added to the PC-3 cells. Cells were incubated with each solution for 3 hours at 37 ˚C under 5% CO_2 environment. The cells were then washed with TBS, TBS-0.1% tween-20, and TBS-HS (heparan sulfate 20 U/mL). This washing procedure was repeated a total of two times. Then, the cells were incubated with 200 μL TBS and 200 μL Nano-Glo Luciferase Assay Reagent for 10 minutes. Luminescence was measured on a Synergy Mx microplate reader.

Sequence information

Ypep-GFP

MGYTFGLKTSFNVQGGSGGSGGSGGSMGGASKGEELFTGVVPILVELDGDVNGHKF
SVRGEGEGDATNGKLTLKFICTTGKLPVPWPTLVTTLTYGVQCFSRYPDHMKQHDFF
KSAMPEGYVQERTISFKDDGTYKTRAEVKFEGDTLVNRIELKGIDFKEDGNILGHKLE
YNFNSHNVYITADKQKNGIKANFKIRHNVEDGSVQLADHYQQNTPIGDGPVLLPDN
HYLSTQSALSKDPNEKRDHMVLLEFVTAARITHGMDELYKHHHHHH

Tat-GFP

MGYGRKKRRQRRRGGSGGSGGSGGSMGGASKGEELFTGVVPILVELDGDVNGHKFS
VRGEGEGDATNGKLTLKFICTTGKLPVPWPTLVTTLTYGVQCFSRYPDHMKQHDFFK
SAMPEGYVQERTISFKDDGTYKTRAEVKFEGDTLVNRIELKGIDFKEDGNILGHKLEY
NFNSHNVYITADKQKNGIKANFKIRHNVEDGSVQLADHYQQNTPIGDGPVLLPDN
HYLSTPSALSKDPNEKRDHMVLLEFVTAAGITHGMDELYKHHHHHH

Pen-GFP

MGRQIKIWFQNRRMKWKKGGSGGSGGSGGSMGGASKGEELFTGVVPILVELDGDV
NGHKFSVRGEGEGDATNGKLTLKFICTTGKLPVPWPTLVTTLTYGVQCFSRYPDHMK
QHDFFKSAMPEGYVQERTISFKDDGTYKTRAEVKFEGDTLVNRIELKGIDFKEDGNIL
GHKLEYNFNSHNVYITADKQKNGIKANFKIRHNVEDGSVQLADHYQQNTPIGDGP
VLLPDNHYLSTQSALSKDPNEKRDHMVLLEFVTAAGITHGMDELYKHHHHHH

nLuc

MVFTLEDFVGDWRQTAGYNLDQVLEQGGVSSLFQNLGVSVTPIQRIVLSGENGLKID
IHVIIPYEGLSGDQMGQIEKIFKVVYPVDDHHFKVILHYGTLVIDGVTPNMIDYFGRPY
EGIAVFDGKKITVTGTLWNGNKIIDERLINPDGSLLFRVTINGVTGWRLCERILAHHH
HHH

Ypep-nLuc

YTFGLKTSFNVQGGSALALGMVFTLEDFVGDWRQTAGYNLDQVLEQGGVSSLFQNL
GVSVTPIQRIVLSGENGLKIDIHVIIPYEGLSGDQMGQIEKIFKVVYPVDDHHFKVILHY
GTLVIDGVTPNMIDYFGRPYEGIAVFDGKKITVTGTLWNGNKIIDERLINPDGSLLFRV
TINGVTGWRLCERILAHHHHHH

REFERENCES

(1) DePorter, S. M., Lui, I., Mohan, U., and McNaughton, B. R. (2013) A protein transduction domain with cell uptake and selectivity profiles that are controlled by multivalency effects. *Chem. Biol. 20*, 434–44.

(2) Denault, M., and Pelletier, J. N. (2007) Protein library design and screening: working out the probabilities. *Methods Mol. Biol. 352*, 127–54.

(3) Cronican, J. J., Beier, K. T., Davis, T. N., Tseng, J.-C., Li, W., Thompson, D. B., Shih, A. F., May, E. M., Cepko, C. L., Kung, A. L., Zhou, Q., and Liu, D. R. (2011) A class of human proteins that deliver functional proteins into mammalian cells in vitro and in vivo. *Chem. Biol. 18*, 833–8.

(4) Cronican, J. J., Thompson, D. B., Beier, K. T., McNaughton, B. R., Cepko, C. L., and Liu, D. R. (2010) Potent delivery of functional proteins into Mammalian cells in vitro and in vivo using a supercharged protein. *ACS Chem. Biol. 5*, 747–52.

(5) McNaughton, B. R., Cronican, J. J., Thompson, D. B., and Liu, D. R. (2009) Mammalian cell penetration, siRNA transfection, and DNA transfection by supercharged proteins. *Proc. Natl. Acad. Sci. U. S. A. 106*, 6111–6.

(6) Thompson, D. B., Cronican, J. J., and Liu, D. R. (2012) Engineering and identifying supercharged proteins for macromolecule delivery into mammalian cells. *Methods Enzymol. 503*, 293–319.

(7) Mammen, M., Choi, S.-K., and Whitesides, G. M. (1998) Polyvalent Interactions in Biological Systems: Implications for Design and Use of Multivalent Ligands and Inhibitors. *Angew. Chemie Int. Ed. 37*, 2754–2794.

(8) Thorne, N., Inglese, J., and Auld, D. S. (2010) Illuminating insights into firefly luciferase and other bioluminescent reporters used in chemical biology. *Chem. Biol. 17*, 646–57.

(9) Hall, M. P., Unch, J., Binkowski, B. F., Valley, M. P., Butler, B. L., Wood, M. G., Otto, P., Zimmerman, K., Vidugiris, G., Machleidt, T., Robers, M. B., Benink, H. A., Eggers, C. T., Slater, M. R., Meisenheimer, P. L., Klaubert, D. H., Fan, F., Encell, L. P., and Wood, K. V. (2012) Engineered luciferase reporter from a deep sea shrimp utilizing a novel imidazopyrazinone substrate. *ACS Chem. Biol. 7*, 1848–57.

CHAPTER FOUR

ENGINEERED M13 BACTERIOPHAGE NANOCARRIERS FOR INTRACELLULAR DELIVERY OF EXOGENOUS PROTEINS TO HUMAN PROSTATE CANCER CELLS

4.1 Introduction

Previously, we evolved a highly potent protein transduction domain, Ypep, with cell-selectivity and uptake profiles that are dependent on multivalent display. In Chapter 3, I described our efforts to further improve the potency and cell-selectivity of Ypep in PC-3 human prostate cancer cells. Solutions containing as little as ~1.6 pM phage that display Ypep mutants on the terminus of p3 were found to selectively recognize and penetrate PC-3 cells. Here, we describe the manipulation of this phage for intracellular delivery of functional proteins and enzymes to PC-3 prostate cancer cells.

4.2 Conjugation of Exogenous Proteins to Filamentous Bacteriophage Coat Proteins

There are a number of methods to conjugate proteins to phage, including genetic modification, phagemid incorporation, chemical coupling, and enzymatic ligation. Direct genetic modification of the phage genome is the most compelling method to display a protein on the surface of filamentous bacteriophage. While phage coat protein

3 (p3) can be genetically modified to display foreign peptides or proteins of varied size and structure, genetic fusion to the other coat proteins p6, p7, p8 and p9 is challenging. The major coat protein p8, which makes up the majority of the phage structure, is a small protein that requires precise folding to facilitate virion formation. Therefore, genetic modification of p8 often results in deleterious effects to the amplification or formation of the phage particle.[1,2] Additionally, genetic fusion to the minor coat proteins p7 and p9 requires separation of overlapping gene regions and the introduction of a signal sequence in order to display proteins and peptides larger than approximately 15 amino acids.[3,4] While phage can be engineered for improved display, higher efficiencies are dependent on the composition and size of the foreign peptide or protein.[1] An alternative to direct genetic modification is the use of a phagemid vector.

The most common way to display large proteins on the surface of phage is to use a phagemid. A phagemid is a phage derived vector that contains a plasmid origin of replication and the protein cargo genetically fused to the desired coat protein (**Figure 4.1A**).[5] Phagemids can be transformed into an F′ strain of *E. coli* where they can then be expressed and preferentially packaged to display on a helper phage. This process typically yields a heterogeneous population of phage that may display as few as one foreign protein.[5] Our work is focused on the delivery of multiple copies of protein cargo for imaging and therapeutic applications; therefore, phagemids are not an optimal method for display of our protein cargo.

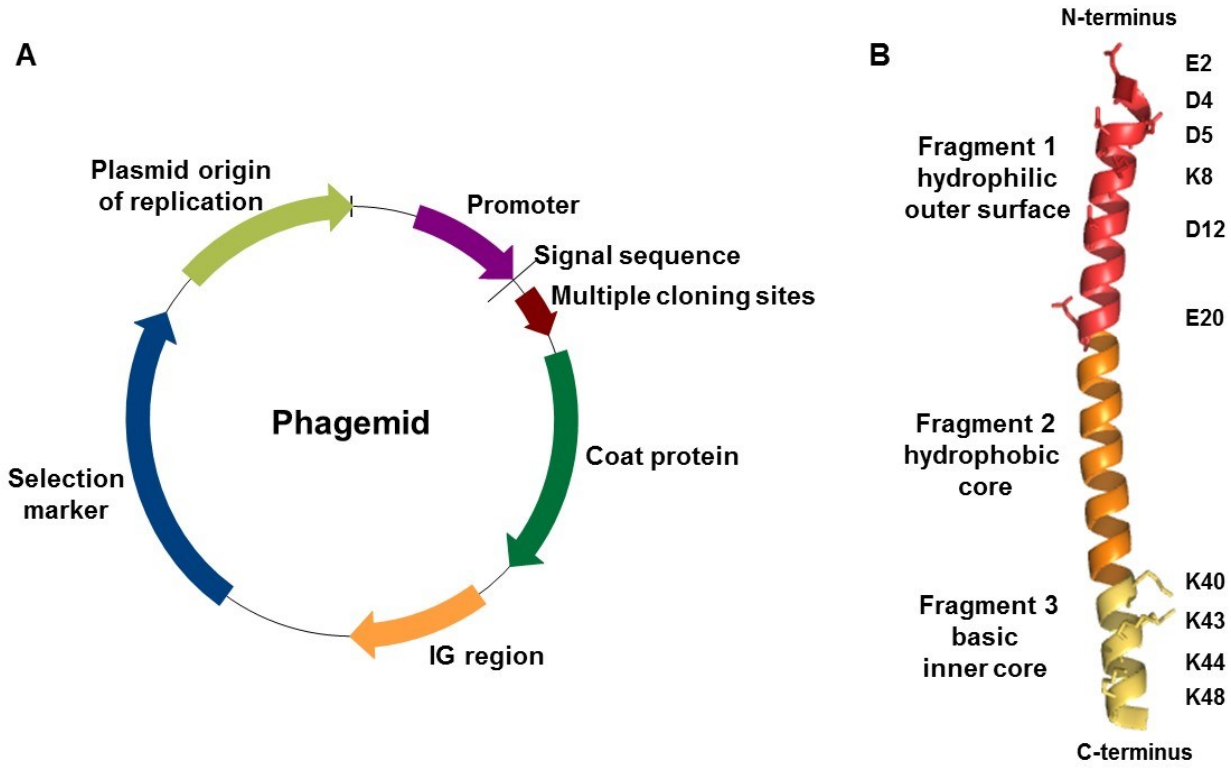

Figure 4.1 Phage conjugation methods. A) Scheme of phagemid vector. B) Structure of the major coat protein p8 with carboxylic and amine residues annotated.

An alternative approach is to chemically couple the protein cargo onto the coat proteins of the phage. There are a number of commercially available protein coupling reagents, which can be used to activate the exposed amines or carboxylic acids on the surface of the phage (**Figure 4.1B**) and protein cargo.[6] These reagents are an attractive option for protein coupling because they are used after the phage is isolated, so there is no effect on the assembly and amplification on the phage. However, chemical coupling is not selective for individual coat proteins and may bind to and inhibit the cell-penetrating moiety already displayed on the phage surface.

Another option is to utilize an enzyme that recognizes a particular sequence on the phage to facilitate protein cargo conjugation. There are enzymes that recognize an acceptor peptide sequence and conjugate a specific small molecule to that site. Some examples include biotin ligase[7], which covalently attaches biotin to a biotin acceptor peptide, or lipoic acid ligase[8,9], which ligates lipoic acid to a lipoic acid acceptor peptide. These types of enzymes do not directly attach a protein to the signal sequence, but they provide a site-specific chemical moiety for further conjugation or complexation. Direct conjugation of two proteins can be achieved with enzymes such as sortase A. Sortase A requires relatively short recognition sequences, which is particularly appealing when modifying phage coat proteins.[10] After evaluating all of these conjugation techniques, we determined that the best method to conjugate multiple copies of exogenous protein to the phage would be to employ a sortase mediated conjugation method.

4.3 Evaluation of Sortase A Conjugation Method for Protein Coupling to Phage Nanocarriers

In response to the challenges associated with genetic fusion of proteins to the majority of the phage coat proteins, we first attempted an enzymatic sortase-mediated conjugation strategy to develop prostate cancer cell-penetrating phage to deliver a foreign protein cargo. Sortase A has been widely used to enzymatically ligate a number

of reagents to proteins, including fluorophores, small molecules, lipids and other proteins.[10–14] Moreover, sortase is an attractive method of conjugation as the recognition peptides to be displayed on the phage surface are short enough to be inserted into the phage genome. As shown in **Figure 4.2A**, sortase A recognizes and cleaves after the threonine residue of LPETG or LPETA motifs. This results in a thioester bond between sortase A and the protein cargo, which is then ligated to the phage protein by nucleophilic attack of the exposed amine of the polyglycine or polyalanine tag displayed on the phage coat proteins. This method of sortase ligation has been used by Belcher and colleagues to label phage with GFP and to build a multiphage structure[15]; therefore, we sought to utilize this method for the conjugation of our protein cargo to the phage nanocarriers for intracellular delivery.

I began by preparing phage genetically engineered to display a prostate cancer cell penetrating component, Ypep on the N-terminus of p3 and two orthogonal sortase acceptor sequences displayed on the N-terminus of p8 and p9 (**Figure 4.2A**).[13,16] If successful, this would allow for sortase-mediated conjugation of two separate proteins onto the phage, which would enable multifunctionality to be built into the phage. For example, we could conjugate a fluorescent protein along with an endosomolytic protein for endosomal release after Ypep-mediated transduction. As an initial test of phage conjugation and phage nanocarrier delivery, I conjugated a fluorescently labeled peptide, FITC-GGS-LPETAA, onto p8 with sortase A from *Streptococcus pyogenes*

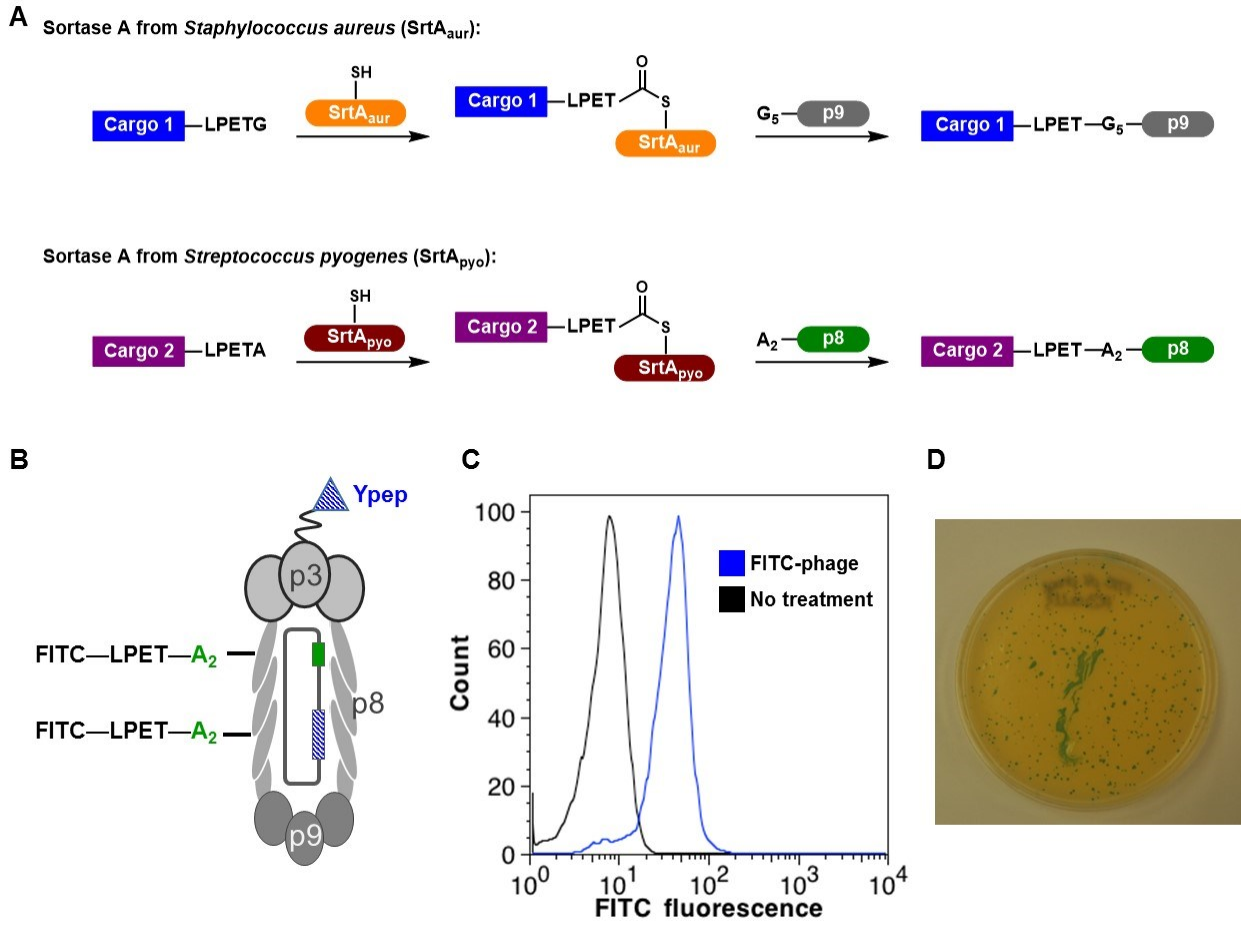

Figure 4.2 Sortase A conjugation technique. A) Sortase A reaction scheme for ligating 2 different protein cargoes to phage coat proteins p8 and p9. B) Phage displaying Ypep PTD are conjugated on p8 to a FITC-labeled peptide to test conjugation and PC-3 cell internalization. C) Flow cytometry data showing PC-3 cells are incubation with 1×10^8 pfu/ml FITC-labeled Ypep phage. D) Plaque forming assay of PC-3 cells after incubation with FITC-labeled Ypep phage confirms that phage are internalized.

($SrtA_{pyogenes}$). The resulting phage (1×10^8 pfu/ml, 1.6×10^{-13} M), termed Ypep-p8-FITC (**Figure 4.2B**), was incubated with PC-3 prostate cancer cells. After washing the cells, phage uptake was measured by flow cytometry. As shown in **Figure 4.2C,** we observe potent internalization of Ypep-p8-FITC, considering the low concentration of phage that was incubated with the PC-3 cells. The flow cytometry data was further verified with a

plaque forming assay to confirm that phage was internalized and not just the remaining FITC peptide. These data further confirm that Ypep phage are able to potently penetrate PC-3 prostate cancer cells at subpicomolar concentrations and the sortase A conjugation technique for conjugating peptides onto p8 of the phage.

Next we attempted to conjugate protein cargo to either p8 or p9. I began by repeating the conditions reported by Belcher and coworkers for the conjugation of GFP onto p8 or p9, but those conditions did not yield GFP conjugated phage.[15] Various attempts with either sortase A from *Staphylococcus aureus* or *Streptococcus pyogenes* and their respective acceptor sequences proved unsuccessful. Following these experiments, we moved on to a coat protein selective complexation strategy, which relies on selective biotinylation of phage, followed by complexation to streptavidin (SAV) fusion proteins.

4.4 Streptavidin-Biotin Complexation Strategy to Conjugate Proteins to Phage Nanocarriers

The biotin-streptavidin complex is incredibly high-affinity, with a dissociation constant (K_D) of approximately 10^{-14} M. Thus, such a strategy should result in a stable phage complex. Successful biotinylation of phage coat proteins p3, p7, p8, and p9 has been achieved by biotin acceptor peptide (BAP) display and *in vitro* biotinylation with biotin ligase (BirA).[17] Recently the Belcher lab used a biotin complexation strategy to

prepare phage that bear a SAV-fluorescein conjugate.[3] However, the use of phage nanocarriers for intracellular delivery of functional imaging proteins and enzymes has not yet been reported.

Toward this end, we genetically modified phage to display the Ypep(T7A) mutant on the N-terminus of p3 and the BAP (GLNDIFEAQKIEWHE) on the N-terminus of p9 (T7A-p9BAP). The Ypep(T7A) mutant was chosen because it was most easily amplified in *E. coli* and it was among the most potent mutants to facilitate PC-3 prostate cancer cell internalization. Unfortunately, the large size of the BAP did not allow for genetic insertion onto the N-terminus of p8, most likely due to protein misfolding. The T7A-p9BAP phage was then biotinylated *in vitro* by incubation with BirA and ATP (**Figure 4.3**).[18] As a proof-of-concept, I separately expressed and purified a streptavidin-green fluorescent protein (SAV-GFP) fusion, which was then incubated

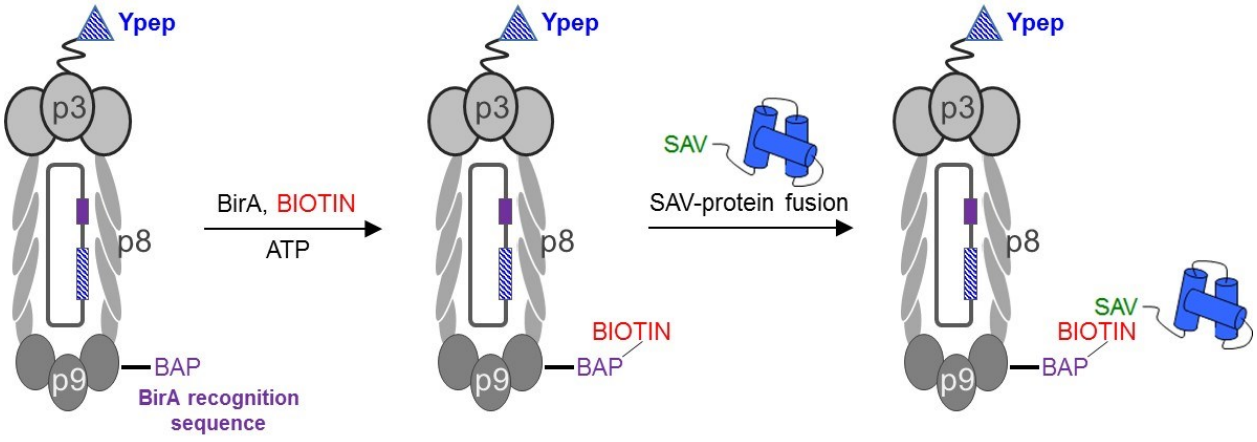

Figure 4.3 Scheme for streptavidin (SAV)-biotin complexation strategy. Phage is genetically modified to display a biotin acceptor peptide (BAP) on the N-terminus of p9. The BAP sequence is then site-specifically coupled to biotin via the lysine residue in BAP. Selective complexation is then achieved by streptavidin fusion to the protein cargo.

with biotinylated phage. Phage were then precipitated twice with PEG/NaCl and washed to remove any SAV-GFP that remained in the supernatant. These phage are herein referred to as T7A-p9SAV-GFP. SAV-GFP assembly was confirmed by Western blot (**Figure 4.4A**) and fluorescence analysis of the phage pellet, which appears bright green (**Figure 4.4B**).

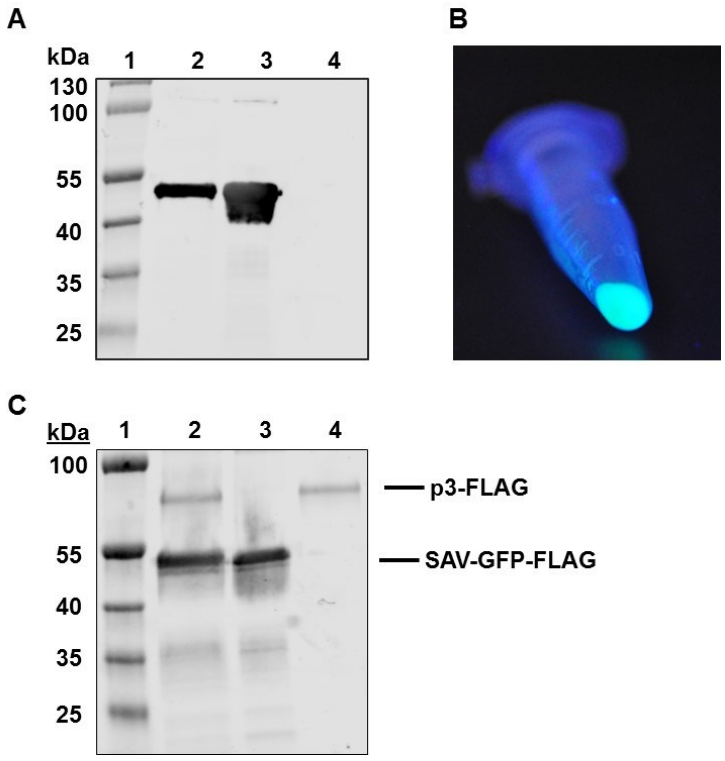

Figure 4.4 Verification of SAV-biotin complexation method. A) Anti-GFP western blot, showing: (*lane 1*) ladder; (*lane 2*) T7A-p9SAV-HRP phage; (*lane 3*) purified recombinant SAV-GFP; and (*lane 4*) supernatant from final precipitation of T7A-p9SAV-HRP phage. The expected molecular weight of the SAV-GFP fusion is ~44.3 kDa. B) Phage that display prostate cancer cell-penetrating component (Ypep(T7A)) on the N-terminus of p3, and biotin acceptor peptide (BAP) on the N-terminus of p9, following *in vitro* biotinylation of BirA and assembly with SAV-GFP, washing, and pelleting. Phage were illuminated with a long wave (365 nm) hand held lamp. C) Anti-FLAG western blot, showing: (*lane 1*) ladder; (*lane 2*) FLAG-p9SAV-GFP-FLAG; (*lane 3*) SAV-GFP-FLAG protein alone; (*lane* 4) FLAG-p9Avi (non-conjugated). Relative densitometry was estimated using LI-COR Image Studio software.

To determine the amount of complexed protein displayed on the phage, I constructed a FLAG tag (DYKDDDDK) on the N-terminus of p3 and the BAP on the N-terminus of p9, termed FLAG-p9BAP. I then separately expressed and purified a FLAG tagged SAV-GFP, SAV-GFP-FLAG. The FLAG-p9BAP was then biotinylated and conjugated with the SAV-GFP-FLAG and a western blot was performed on the resultant phage to measure the relative levels of p3-FLAG and SAV-GFP-FLAG (**Figure 4.4C**). On average, FLAG-p9BAP phage display 5 copies of FLAG on the N-terminus of p3. Based on densitometry ratios over three separate experiments, we estimated that each phage contains approximately 4 copies of SAV-GFP-FLAG per copy of p3-FLAG (**Figure 4.4C**). Since streptavidin is a homotetramer, and approximately the same number of copies of p3 and p9 are displayed on the phage, these findings suggest that each copy of p9 is biotinylated and complexed to a SAV-GFP-FLAG tetramer. Thus, at least in the case of GFP, each phage carries ~20 copies of the cargo protein (which is fused to SAV). These data demonstrate that this complexation strategy is a feasible method to attach multiple copies of protein cargo to our prostate cancer cell-penetrating phage.

4.5 Intracellular Delivery of Functional Enzymes to Prostate Cancer Cells with Bacteriophage Nanocarriers

Expanding on these initial findings, we tested the delivery of a functional enzyme using our phage nanocarrier strategy. We focused on the intracellular delivery of horseradish peroxidase (HRP), which is broadly utilized in bioimaging, and has therapeutic utility.[19] Assembly of SAV-HRP to biotinylated phage, and robust HRP enzymatic activity of the resulting reagent (T7A-p9SAV-HRP) was verified by incubating this phage with a known HRP substrate, 3,3′,5,5′-tetramethylbenzidine (TMB). While T7A-p9SAV-HRP phage act on TMB, resulting in a colorimetric reaction, supernatant taken after washing the precipitated phage pellet does not contain measurable levels of HRP (**Figure 4.5A**). These finding support a model wherein SAV-HRP assembles with biotinylated phage to generate enzymatically active nanorods.

Next SAV-HRP conjugated phage were added to PC-3 prostate cancer cells to evaluate the cell uptake of the phage nanocarriers. PC-3 cells were treated with solutions that contain 50×10^{9} to 1×10^{9} pfu/mL (~8.3×10^{-11} to 1.6×10^{-12} M) T7A-p9SAV-HRP phage and washed to remove cell surface-bound material. After rigorous washing, the cells were treated with TMB reagent for 2 hours. Impressively, cells treated with the three highest concentrations of phage were found to have appreciable levels of intracellular HRP, as determined by colorimetric analysis of PC-3 cells (**Figure 4.5B**).

These data are shown in **Figure 4.5C**, blue bars. In contrast, cells treated with ~1.6×10^{-9} M SAV-HRP (**Figure 4.5C**, red bar) were not found to contain appreciable levels of intracellular HRP. As a control, phage that display Ypep(T7A) on p3 and BAP on p9 (but not biotinylated with BirA) were incubated with SAV-HRP, and phage were

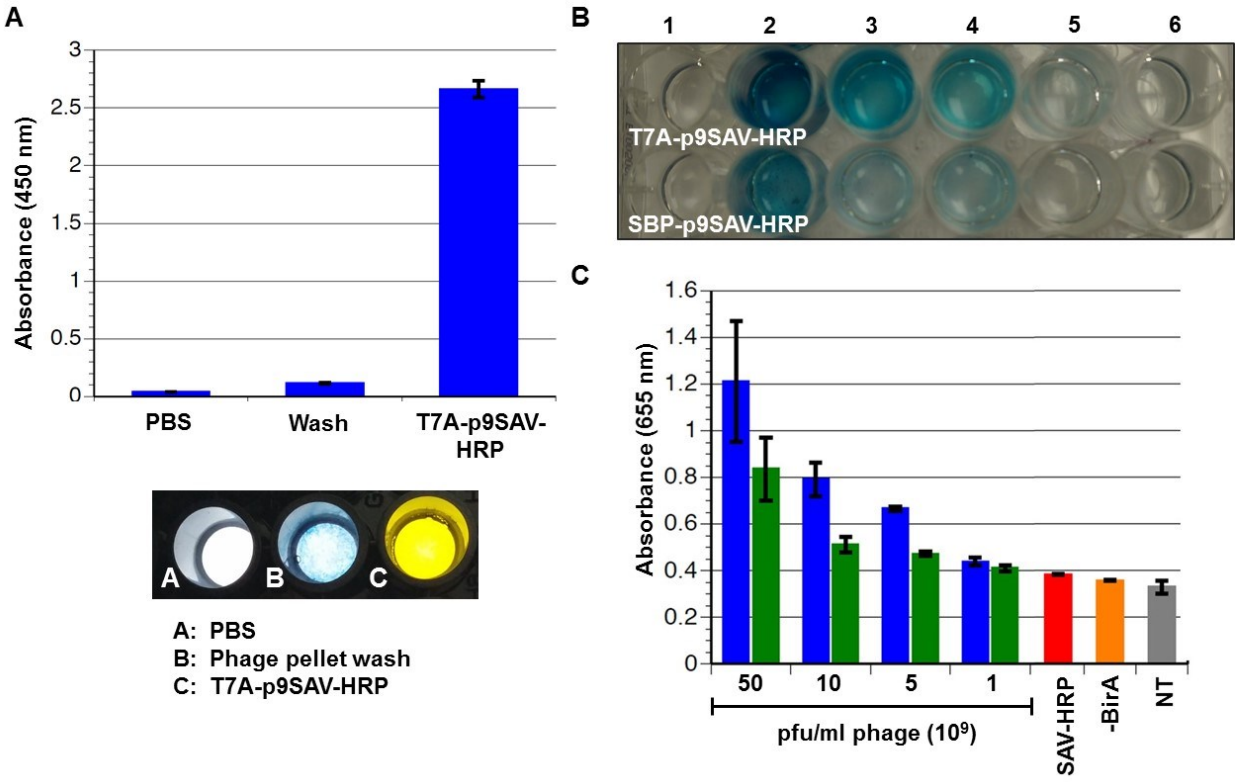

Figure 4.5 Conjugation and cell uptake of T7A-p9SAV-HRP. A) TMB assay of T7A-p9SAV-HRP complexation. PBS, T7A-p9SAV-HRP phage pellet wash and resuspended T7A-p9SAV-HRP phage was incubated with TMB One Solution for 20 minutes at room temperature. Absorbance was measured at 450 nm on the platereader. B) Image of a multi-well plate that contain a monolayer of PC-3 cells following: (*lane 1*) no treatment; (*lane 2*) 50×10^9; (*lane 3*) 10×10^9; (*lane 4*) 5×10^9; (*lane 5*) 1×10^9 T7A-p9SAV-HRP or SBP-p9SAV-HRP phage; or, (*lane 6*) ~1.6 nM (based on SAV concentration) recombinant SAV-HRP. B) Quantitated data from the image shown in A. Blue bars = HRP activity in PC-3 cells, following treatment with T7A-p9SAV-HRP; green bars = HRP activity in cells, following treatment with SBP-p9SAV-HRP; red bars = HRP activity in cells, following treatment with ~1.6 nM SAV-HRP; orange bar = HRP activity in cells, following treatment with phage that were not biotinylated prior to incubation with SAV-HRP; NT = no treatment.

precipitated and washed as before. When PC-3 cells were treated with these phage, no appreciable HRP activity was observed (**Figure 4.5C**, orange bar). These data indicate that assembly of SAV-HRP to biotinylated phage is required for phage-dependent delivery of the conjugated protein cargo.

4.6 Comparison to SPARC Binding Peptide Delivery

To assess the relative cell-penetrating and functional enzyme delivery efficiencies of T7A-p9SAV-HRP phage, we compared them to analogous phage that do not display Ypep(T7A), but display a recently reported cancer cell homing/cell-penetrating peptide (SPPTGIN) that binds to the matricellular protein SPARC (secreted protein, acidic, cysteine-rich). Overexpression of SPARC has been associated with a number of cancers, including prostate cancer.[20] This SPARC binding peptide, termed SBP, was previously reported by the Weissleder lab[21], and used by Belcher[22] and coworkers for phage-dependent delivery of iron oxide nanoparticles to PC-3 cells, which express appreciable levels of SPARC.

I constructed the phage to display SBP on p3 and conjugated SAV-HRP to the resulting phage, termed SBP-p9SAV-HRP. I measured HRP uptake following incubation with PC-3 cells in solutions containing ~50×10^{9} to 1×10^{9} pfu/mL (~8.3×10^{-11} to 1.6×10^{-12} M) SBP-p9SAV-HRP phage (**Figure 4.5B**, bottom row and **Figure 4.5C**, green

bars). Phage that display Ypep(T7A) generally deliver significantly more HRP to PC-3 cells, compared to analogous phage that contain SBP in place of Ypep(T7A). Treatment with a solution containing ~50 to 1×10^9 pfu/mL of T7A-p9SAV-HRP phage were found to have ~1.5-fold higher levels of HRP activity, compared to cells treated with the identical concentrations of the SBP-displayed variant. This demonstrates the potency of delivery of the Ypep(T7A) mutant phage over a previously described cell-penetrating phage.

4.7 Bacteriophage Nanocarriers as Targeted Enzyme Delivery for Prodrug Therapeutics

The ability of HRP to act on colorimetric and fluorescent substrates, including reagents that emit in the far-red (which is useful for deep tissue imaging), is well documented. Additionally, HRP can act on prodrug substrates, and thus, intracellular HRP and concomitant treatment of these substrates can lead to cell death. The plant hormone indole-3-acetic acid (IAA) is a prodrug that is acted on by HRP to form a peroxyl radical, which ultimately leads to radical-dependent cytotoxicity (**Figure 4.6A**).[23–25] The HRP IAA reaction does not require the addition of hydrogen peroxide and endogenous mammalian peroxidases are significantly less reactive with the IAA substrate.[26,27] Moreover, IAA alone is non-toxic up to 100 mg/kg[28]; therefore, this

enzyme-prodrug could potentially offer a route to prostate cancer cell death through cell-selective delivery of HRP.

To measure the functional utility of phage nanocarriers as delivery reagents for a therapeutic enzyme, we treated PC-3 cells with 6 mM IAA and ~5×10^{10} pfu/ml (~8.3×10^{-11} M) T7A-p9SAV-HRP phage. Following treatment, we assayed cytotoxicity using a commercially available thiazolyl blue tetrazolium bromide (MTT) cell viability assay. As shown in **Figure 4.6B** (red bar), we observed virtually complete cell death following treatment with both T7A-p9SAV-HRP and IAA, compared to untreated cells (**Figure 4.6B**, gray bar). In contrast, no appreciable toxicity was observed in cells following treatment with either 6 mM IAA (**Figure 4.6B**, orange bar), or ~1.6×10^{-8} M SAV-HRP, which is ~4 orders of magnitude more HRP than used in the phage-assisted delivery

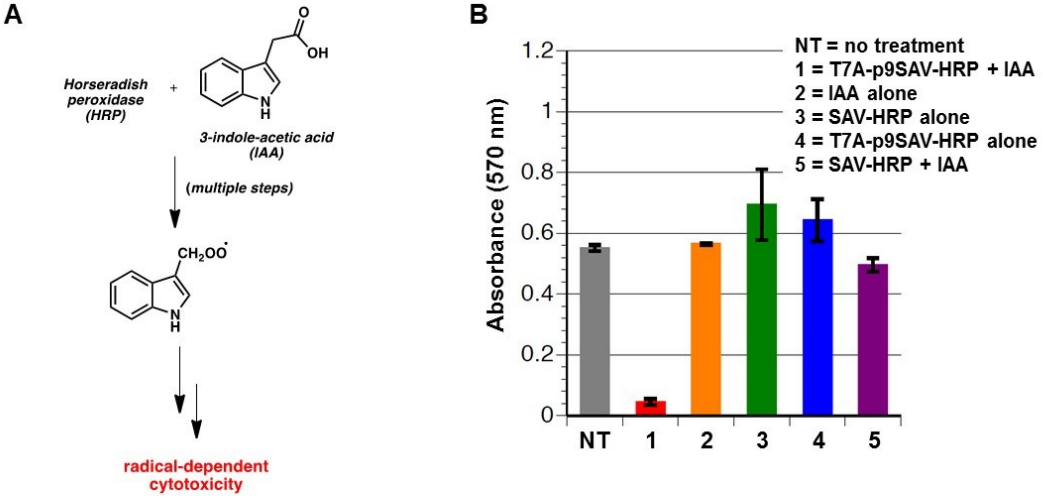

Figure 4.6 HRP-phage nanocarriers as a targeted enzyme-prodrug therapeutic reagent. A) HRP-dependent oxidation of indole-3-acetic acid (IAA) produces a peroxyl radical, which leads to toxicity in mammalian cells. B) Cell toxicity as a result of concomitant IAA treatment and intracellular delivery of HRP to PC-3 cells, via phage nanocarriers.

experiment (**Figure 4.6B**, green bar), or ~5×10^{10} pfu/mL T7A-p9SAV-HRP phage (**Figure 4.6B**, blue bar). Treatment with both 6 mM IAA and ~1.6×10^{-8} M SAV-HRP does not result in appreciable cell death (**Figure 4.6B**, purple bar). Thus, functional levels of SAV-HRP does not accumulate in the cell interior (via transduction), but HRP delivery and subsequent action on IAA is facilitated by T7A-p9SAV-HRP phage nanocarriers.

4.8 Conclusions

We engineered M13 bacteriophage as nanorod materials for the delivery of functional proteins to PC-3 human prostate cancer cells. Concomitant treatment with T7A-p9SAV-HRP phage and the prodrug, IAA, results in appreciable cell death, demonstrating that phage-assisted delivery of HRP has therapeutic utility. Throughout, our strategy relies on genetic modification of phage coat proteins p3 and p9, such that p3 displays a potent PC-3 cell-penetrating peptide (Ypep(T7A)), and p9 displays a biotin-acceptor peptide. Following *in vitro* biotinylation with *E. coli* biotin ligase (BirA), these phage were assembled with a protein fusion or conjugate to streptavidin, which tightly binds biotin. Previously, we have shown that phage bearing ~5 copies of Ypep peptides on the N-terminus of p3 potently penetrate PC-3 cells, in complex solutions. Here, we show that genetic and enzymatic manipulation of these phage, and decoration with exogenous protein assemblies on p9, leads to potent delivery of this protein cargo to PC-3 cells. This strategy is modular. Various previously reported cell-penetrating

reagents can be incorporated by genetic engineering, and diverse streptavidin-protein fusions and conjugates can easily be used. Since the phage genome predetermines the size and spatial localization of components that make up this nanomaterial, the phage can be genetically or enzymatically manipulated selectively. This approach overcomes some of the challenges associated with strategies that rely on the chemical synthesis and manipulation of synthetic nanocarriers for exogenous protein delivery.

4.9 Experimental Methods

Materials

PC-3 prostate cancer cells- ATCC
Phosphate buffered saline (PBS) - Hyclone/Thermo Scientific
0.25% Trypsin - Hyclone/Thermo Scientific
Brilliant Blue R-250 - J.T.Baker
Bovin serum albumin - Sigma Aldrich
Fetal bovin serum (FBS) - PAA Laboratories
Triton X-100 - Fisher Scientific
F-12K Nutrient Mixture (Kaighn's Mod.) - Cellgro/Corning
Mammalian cell culture dishes - Fisher Scientific
B-PER Bacterial Protein Extraction Reagent - Thermo Scientific
Imidazole - Sigma Aldrich
Modified Lowry Protein Assay Kit - Pierce/Thermo Scientific
Thiazolyl Blue Tetrazolium Bromide - Sigma Aldrich
PageRuler Prestained Protein Ladder - Thermo Scientific
NeutrAvidin-HRP - Thermo Scientific
TMB One Solution – Promega
15% Tris-HCl ready gel – Biorad
12% Mini-Protean TGX precast gels – Biorad
Anti-GFP antibody – Abcam
Anti-FLAG antibody – Abcam

Goat anti-rabbit IR Dye 800 CW – LI-COR
Odyssey blocking buffer – LI-COR

Instrumentation

MTT assay absorbance and TMB assay absorbance was measured on Synergy Mx Microplate Reader from BioTek. Western blots were imaged on LI-COR odyssey imager.

Mammalian Cell Culture

PC-3 human prostate cancer cells were cultured in F12K with 10% Fetal Bovine Serum (FBS) and incubated at 37 °C with a 5% CO_2 environment.

Genetic Modification of M13 Phage

M13KE filamentous phage vector was purchased from NEB. Ypep(T7A) and the SBP sequences were inserted onto the N-terminus of p3 between the KpnI and EagI restriction sites. The biotin acceptor peptide (BAP) was cloned in using overlapping PCR to separate the C-terminal end of p7 from the N-terminal end of p9 and to insert the BAP sequence (GLNDIFEAQKIEWHE) at the N-terminus of p9.

Phage Amplification and Purification

E. coli ER2738 was inoculated into an overnight culture for phage amplification. The next day, a fresh plaque of T7A-p9BAP or SBP-p9BAP phage was grown in LB containing a 1/100 dilution of the ER2738 culture and tetracycline. The phage were amplified overnight at 37 °C. The supernatant was collected and the amplified phage

were precipitated with PEG 8000/2.5 M NaCl overnight at 4 °C. After resuspension of the phage pellet in 1 mL PBS, the phage were filtered with a 0.45 μm Nalgene syringe filter to remove any remaining bacterial cells. The concentration of the phage was determined using a plaque forming assay.

Sortase-Mediated Coupling of FITC to p8

Purify M13-Ypep phage that display an A_2G_4 tag on p8 using standard methods. Dissolve the FITC peptide (FITC-Ahx-GGSLPETAA) into 20 μL dimethylsulfoxide. $SrtA_{pyogenes}$ (50 μM) to a solution of 2.0×10^{12} pfu/mL phage dissolved in PBS to a total volume of 230 μL. The FITC peptide solution was then added to the phage mixture and incubated for 3 hours at 37 °C. After incubation, 8 mL of Tris-buffered saline (TBS) was added and the phage was precipitated overnight at 4 °C with PEG/NaCl. The phage was collected, resuspended in TBS and precipitated for a second time. The phage were resuspended in 0.5 mL TBS for cell uptake studies.

Cell Uptake of FITC-Labeled Ypep Phage

Ypep-p8-FITC phage (1×10^8 pfu/mL) were diluted in F12K/10% FBS media and incubated with PC-3 cells for 3 hours at 37 °C. The cells were then washed twice with PBS and 3 times with TBS/0.1% tween-20. A solution of subtilisin (3 mg/mL) in PBS was then added to the cells and incubated for 45 minutes at 4 °C. The cells were collected by centrifugation and incubated with 500 μL protease inhibitor diluted in PBS. The cells were then resuspended in 300 μL PBS and fluorescence was analyzed by flow

cytometry. Approximately 100 μL of the cells were also lysed with a sodium deoxycholate solution (2% sodium deoxycholate, 10 mM Tris-HCl, 2 mM EDTA) and analyzed for phage internalization by plaque forming assay.

SAV-GFP Protein Purification

SAV-GFP-pETduet in BL21-DE3 *E. coli* was inoculated from an overnight culture into 1 L LB and grown at 37 °C to OD_{600} ~0.6. Protein expression was induced with 1 mM IPTG at 30 °C overnight. Cells were harvested by centrifugation, the pellet was resuspended in 10 mL B-PER and stored at -20 °C. The cells were thawed and 10 mL of Tris lysis buffer (25 mM Tris-HCl, 100 mM NaCl, 10 mM Imidazole, pH 8.0) was added to the solution. The cells were sonicated for 2 minutes and the lysate was cleared by centrifugation (15000 rpm, 30 minutes). The supernatant was mixed with 1 mL of Ni-NTA agarose resin for 1 hour and the resin was collected by centrifugation (4750 rpm, 10 minutes). The resin was washed with Tris wash buffer (25 mM Tris-HCl, 100 mM NaCl, 20 mM Imidazole, pH 8.0) and the protein was eluted with Tris elution buffer (25 mM Tris-HCl, 100 mM NaCl, 400 mM Imidazole, pH 8.0). The protein was dialyzed against 25 mM Tris-HCl, 100 mM NaCl, pH 8.0 and analyzed for purity by SDS-PAGE staining with Coomassie blue. The concentration of the protein was determined by Modified Lowry Protein Assay Kit. The SAV-GFP-FLAG construct was purified in the same manner.

In Vitro Phage Biotinylation

Phage (1×10^{12} pfu/mL) were precipitated with PEG/NaCl and resuspended in 633 μL PBS. The *in vitro* biotinylation was carried out with a commercially available kit from Avidity. Briefly, 80 μL of Biomix A and Biomix B were added to the phage solution and mixed. Then 7 μL of 3 mg/mL BirA biotin ligase was added to the solution. The mixture was incubated overnight at 30 °C. The phage were purified by precipitation with PEG/NaCl two times and resuspended in PBS. Phage titer was determined using a plaque forming assay.

Complexation of Streptavidin-Fusion Proteins

After biotinylation, the phage were incubated with either 20 μM SAV-GFP or 0.05 mg/mL NeutrAvidin-HRP in 500 μL PBS. The solutions were incubated for 3 hours at room temperature with rotation. The phage was purified by precipitation twice with PEG/NaCl at 4 °C and resuspended in 1 mL PBS. Phage titer was determined using a plaque forming assay.

Western Blot of Phage Conjugated to SAV-GFP

T7A-p9SAV-GFP phage, SAV-GFP, and phage wash samples were run on 12% TGX precast gels (BioRad), and transferred to PVDF membrane with iBlot transfer stack (invitrogen). The blot was incubated with anti-GFP primary antibody overnight at 4 °C, then incubated with goat-anti-rabbit IR Dye 800 CW secondary antibody for 1.5 hours at room temperature. The western blot was imaged on the LI-COR Odyssey Imager.

Determination of Complexation Stoichiometry

FLAG-p9BAP phage were purified and isolated as described above. Complexation of SAV-GFP-FLAG to FLAG-p9BAP phage was carried out as previously described. Samples were run on 12% TGX precast gels (BioRad), and transferred to PVDF membrane with iBlot transfer stack. The blot was blocked with milk for 45 minutes at room temperature, then incubated with anti-FLAG primary antibody for 15 minutes at 4 °C, then incubated with goat-anti-rabbit IR Dye 800 CW secondary antibody for 15 minutes at room temperature. The western blot was imaged on the LI-COR Odyssey Imager. Stoichiometry was determined by comparing band intensity of the FLAG(p3) and the SAV-GFP-FLAG bands.

TMB Assay of HRP Activity

PBS, wash from phage precipitation, and T7A-p9SAV-HRP phage were added (20 μL) to a 96-well black sides, clear bottom plate. To each well, 20 μL of TMB One solution was added and incubated for 5 minutes at room temperature. TMB absorbance was read at 450 nm (yellow) on the Synergy Mx microplate reader.

TMB Assay of Internalized HRP Phage

T7A-p9SAV-HRP and SBP-p9SAV-HRP phage were diluted to 50×10^9, 10×10^9, 5×10^9, and 1×10^9 pfu/mL in F12K/10% FBS media prewarmed to 37 °C. The solutions (0.4 mL to each well) were incubated with PC-3 prostate cancer cells in a 24-well plate for 3 hours at 37 °C, 5 % CO_2. Cells were then put on ice for 5 minutes before beginning washing

with cold reagents. Cells were washed twice with PBS, 3 times with TBS/0.1% tween-20, and 3 times with PBS/heparin sulfate. TMB One solution (250 μL) was added to each well and incubated at room temperature for 2 hours in the dark. Absorbance readings (655 nm) were taken on the Synergy Mx microplate reader.

MTT Assay of IAA-HRP Phage Cytotoxicity

Solutions of indole-3-acetic acid (IAA), T7A-p9SAV-HRP phage and SAV-HRP were prepared in F12K/10% FBS media prewarmed to 37 °C. The various solutions were added to 60% confluent PC-3 prostate cancer cells in a 24-well plate and incubated for 24 hours 37 °C, 5% CO_2. After incubation the cells were washed twice with PBS, and then MTT reagent diluted in prewarmed F12K/10% FBS was added to the cells. The cells were incubated for 3.5 hours with the MTT reagent at 37 °C, 5% CO_2. MTT detergent reagent (4 mM HCl, 0.1% Triton X-100 in isopropanol) was then added to the cells and the cells were incubated for an additional 30 minutes. Absorbance at 570 nm was then recorded with the Synergy Mx microplate reader.

Sequence Information

sfGFP

MGASKGEELFTGVVPILVELDGDVNGHKFSVRGEGEGDATNGKLTLKFICTTGKLPV
PWPTLVTTLTYGVQCFSRYPDHMKQHDFFKSAMPEGYVQERTISFKDDGTYKTRAEV
KFEGDTLVNRIELKGIDFKEDGNILGHKLEYNFNSHNVYITADKQKNGIKANFKIRH
NVEDGSVQLADHYQQNTPIGDGPVLLPDNHYLSTQSALSKDPNEKRDHMVLLEFVT
AAGITHGMDELYKHHHHHH

SAV-GFP

MASMTGGQQMGRDQAGITGTWYNQLGSTFIVTAGADGALTGTYESAVGNAESRYV
LTGRYDSAPATDGSGTALGWTVAWKNNYRNAHSATTWSGQYVGGAEARINTQWL
LTSGTTEANAWKSTLVGHDTFTKVKPSAASIDAAKKAGVNNGNPLDAVQQGGSGG
SGGSGGSSGGASKGEELFTGVVPILVELDGDVNGHKFSVRGEGEGDATNGKLTLKFIC
TTGKLPVPWPTLVTTLTYGVQCFSRYPDHMKQHDFFKSAMPEGYVQERTISFKDDGT
YKTRAEVKFEGDTLVNRIELKGIDFKEDGNILGHKLEYNFNSHNVYITADKQKNGIK
ANFKIRHNVEDGSVQLADHYQQNTPIGDGPVLLPDNHYLSTQSALSKDPNEKRDH
MVLLEFVTAAGITHGMDELYKHHHHHH

p9 BAP

MGLNDIFEAQKIEWHEGGSMSVLVYSFASFVLGWCLRSGITYFTRLMETSS

SAV-GFP-FLAG

MASMTGGQQMGRDQAGITGTWYNQLGSTFIVTAGADGALTGTYESAVGNAESRYV
LTGRYDSAPATDGSGTALGWTVAWKNNYRNAHSATTWSGQYVGGAEARINTQWL
LTSGTTEANAWKSTLVGHDTFTKVKPSAASIDAAKKAGVNNGNPLDAVQQGGSGG
SGGSGGSSGGASKGEELFTGVVPILVELDGDVNGHKFSVRGEGEGDATNGKLTLKFIC
TTGKLPVPWPTLVTTLTYGVQCFSRYPDHMKQHDFFKSAMPEGYVQERTISFKDDGT
YKTRAEVKFEGDTLVNRIELKGIDFKEDGNILGHKLEYNFNSHNVYITADKQKNGIK
ANFKIRHNVEDGSVQLADHYQQNTPIGDGPVLLPDNHYLSTQSALSKDPNEKRDH
MVLLEFVTAAGITHGMDELYKHHHHHHDYKDDDDK

REFERENCES

(1) Malik, P., Terry, T. D., Gowda, L. R., Langara, a, Petukhov, S. a, Symmons, M. F., Welsh, L. C., Marvin, D. a, and Perham, R. N. (1996) Role of capsid structure and membrane protein processing in determining the size and copy number of peptides displayed on the major coat protein of filamentous bacteriophage. *J. Mol. Biol. 260*, 9–21.

(2) Iannolo, G., Minenkova, O., Petruzzelli, R., and Cesareni, G. (1995) Modifying filamentous phage capsid: limits in the size of the major capsid protein. *J. Mol. Biol. 248*, 835–44.

(3) Ghosh, D., Kohli, A. G., Moser, F., Endy, D., and Belcher, A. M. (2012) Refactored M13 bacteriophage as a platform for tumor cell imaging and drug delivery. *ACS Synth. Biol. 1*, 576–82.

(4) Chan, L. Y., Kosuri, S., and Endy, D. (2005) Refactoring bacteriophage T7. *Mol. Syst. Biol. 1*, 2005.0018.

(5) Qi, H., Lu, H., Qiu, H.-J., Petrenko, V., and Liu, A. (2012) Phagemid vectors for phage display: properties, characteristics and construction. *J. Mol. Biol. 417*, 129–43.

(6) Hermanson, G. T. (2013) Bioconjugate Techniques, p 1200. Academic Press.

(7) Beckett, D., Kovaleva, E., and Schatz, P. J. (1999) A minimal peptide substrate in biotin holoenzyme synthetase-catalyzed biotinylation. *Protein Sci. 8*, 921–9.

(8) Fernández-Suárez, M., Baruah, H., Martínez-Hernández, L., Xie, K. T., Baskin, J. M., Bertozzi, C. R., and Ting, A. Y. (2007) Redirecting lipoic acid ligase for cell surface protein labeling with small-molecule probes. *Nat. Biotechnol. 25*, 1483–7.

(9) Cohen, J. D., Zou, P., and Ting, A. Y. (2012) Site-specific protein modification using lipoic acid ligase and bis-aryl hydrazone formation. *Chembiochem 13*, 888–94.

(10) Popp, M. W., Antos, J. M., Grotenbreg, G. M., Spooner, E., and Ploegh, H. L. (2007) Sortagging: a versatile method for protein labeling. *Nat. Chem. Biol. 3*, 707–8.

(11) Guimaraes, C. P., Carette, J. E., Varadarajan, M., Antos, J., Popp, M. W., Spooner, E., Brummelkamp, T. R., and Ploegh, H. L. (2011) Identification of host cell factors required for intoxication through use of modified cholera toxin. *J. Cell Biol. 195*, 751–64.

(12) Popp, M. W., Dougan, S. K., Chuang, T.-Y., Spooner, E., and Ploegh, H. L. (2011) Sortase-catalyzed transformations that improve the properties of cytokines. *Proc. Natl. Acad. Sci. U. S. A. 108*, 3169–74.

(13) Antos, J. M., Chew, G.-L., Guimaraes, C. P., Yoder, N. C., Grotenbreg, G. M., Popp, M. W.-L., and Ploegh, H. L. (2009) Site-specific N- and C-terminal labeling of a single polypeptide using sortases of different specificity. *J. Am. Chem. Soc. 131*, 10800–1.

(14) Antos, J. M., Miller, G. M., Grotenbreg, G. M., and Ploegh, H. L. (2008) Lipid modification of proteins through sortase-catalyzed transpeptidation. *J. Am. Chem. Soc. 130*, 16338–43.

(15) Hess, G. T. G., Cragnolini, J. J. J., Popp, M. W. M., Allen, M. A., Dougan, S. K., Spooner, E., Ploegh, H. L., Belcher, A. M., and Guimaraes, C. P. (2012) M13 bacteriophage display framework that allows sortase-mediated modification of surface-accessible phage proteins. *Bioconjug. Chem. 23*, 1478–1487.

(16) Race, P. R., Bentley, M. L., Melvin, J. A., Crow, A., Hughes, R. K., Smith, W. D., Sessions, R. B., Kehoe, M. A., McCafferty, D. G., and Banfield, M. J. (2009) Crystal structure of Streptococcus pyogenes sortase A: implications for sortase mechanism. *J. Biol. Chem. 284*, 6924–33.

(17) Smelyanski, L., and Gershoni, J. M. (2011) Site directed biotinylation of filamentous phage structural proteins. *Virol. J. 8*, 495.

(18) Scholle, M. D., Kriplani, U., Pabon, A., Sishtla, K., Glucksman, M. J., and Kay, B. K. (2006) Mapping protease substrates by using a biotinylated phage substrate library. *Chembiochem 7*, 834–8.

(19) Veitch, N. C. (2004) Horseradish peroxidase: a modern view of a classic enzyme. *Phytochemistry 65*, 249–259.

(20) Clark, C. J., and Sage, E. H. (2008) A prototypic matricellular protein in the tumor microenvironment--where there's SPARC, there's fire. *J. Cell. Biochem. 104*, 721–32.

(21) Kelly, K. A., Waterman, P., and Weissleder, R. (2006) In vivo imaging of molecularly targeted phage. *Neoplasia 8*, 1011–8.

(22) Ghosh, D., Lee, Y., Thomas, S., Kohli, A. G., Yun, D. S., Belcher, A. M., and Kelly, K. a. (2012) M13-templated magnetic nanoparticles for targeted in vivo imaging of prostate cancer. *Nat. Nanotechnol. 7*, 677–82.

(23) Greco, O., Folkes, L. K., Wardman, P., Tozer, G. M., and Dachs, G. U. (2000) Development of a novel enzyme/prodrug combination for gene therapy of cancer: horseradish peroxidase/indole-3-acetic acid. *Cancer Gene Ther. 7*, 1414–20.

(24) Kim, D.-S., Jeon, S.-E., and Park, K.-C. (2004) Oxidation of indole-3-acetic acid by horseradish peroxidase induces apoptosis in G361 human melanoma cells. *Cell. Signal. 16*, 81–8.

(25) Wardman, P. (2002) Indole-3-acetic acids and horseradish peroxidase: a new prodrug/enzyme combination for targeted cancer therapy. *Curr. Pharm. Des. 8*, 1363–74.

(26) Dunford, H. B. (1999) Heme peroxidases, pp 1–507. John Wiley.

(27) Folkes, L. K., Candeias, L. P., and Wardman, P. (1998) Toward targeted "oxidation therapy" of cancer: peroxidase-catalysed cytotoxicity of indole-3-acetic acids. *Int. J. Radiat. Oncol. 42*, 917–920.

(28) Diengott, D., and Mirsky, I. A. (1956) Hypoglycemic action of indole-3-acetic acid by mouth in patients with diabetes mellitus. *Proc. Soc. Exp. Biol. Med. 93*, 109–10.

CHAPTER FIVE

PART I:

PROGRAMMED MAMMALIAN CELL ADHESION AND GROWTH ON CELL IMPRINTED POLYACRYLAMIDE HYDROGELS

PART II:

ENGINEERING DINITROPHENYL CONJUGATED PROTEINS AS IMMUNOTHERAPEUTIC DRUG LEADS

5.1 Introduction

Although the majority of my research in the McNaughton lab has focused on the development of prostate cancer-selective protein transduction domains, and engineered bacteriophage nanocarriers for targeted delivery of proteinaceous reagents, I have also worked on a number of additional projects. That additional work resulted in both published[1,2] and ongoing projects, two of which are described in this chapter.

One of my early projects focused on the development of a simple and inexpensive method for spatially-defined cell adhesion and growth on 2-dimensional substrates (described in Part I of this chapter). More recently, I have been working in collaboration with Prof. David Spiegel's lab at Yale to engineer protein immunotherapeutics. These proteins are designed to both recognize the HER2 receptor

(which is overexpressed in, and displayed on the surface of, breast cancer cells), and trigger a native immune response, resulting in targeted cell death. I have genetically engineered these HER-2 binding proteins with a tag that can be used to site-specifically conjugate a dinitrophenyl (DNP) moiety that induces antibody-dependent cellular cytotoxicity. This work is described in Part II of this chapter.

Part I: Programmed Mammalian Cell Adhesion and Growth on Cell-Imprinted Polyacrylamide Hydrogels

5.2 Methods for Controlling Mammalian Cell Adhesion and Growth

Gaining precise control over mammalian cell adhesion and growth is a critical step in microscale tissue engineering, as well as biosensor fabrication, applied cell biology, and the development of cell-based screening assays.[3–5] Control over mammalian cell adhesion and growth is typically achieved by covalently patterning spatially-defined small molecule[6], carbohydrate[7], membrane[8], peptide[9–12], nucleic acid[13–16], protein[17–19], or antibody[20] reagents with affinity for a cell surface receptor onto a non-adhesive surface. However, these reagents are often susceptible to environmental and/or enzymatic degradation, which decrease their shelf-life. Moreover, preparation, purification, and conjugation of the substrate increases the overall cost and complexity of surface fabrication. Finally, application of these reagents to form a surface that

controls mammalian cell adhesion and growth often requires multi-step and expensive microfabrication techniques, such as microcontact printing or replica molding and microarraying, photolithography, and soft lithography (**Figure 5.1**).[21–24] In addition,

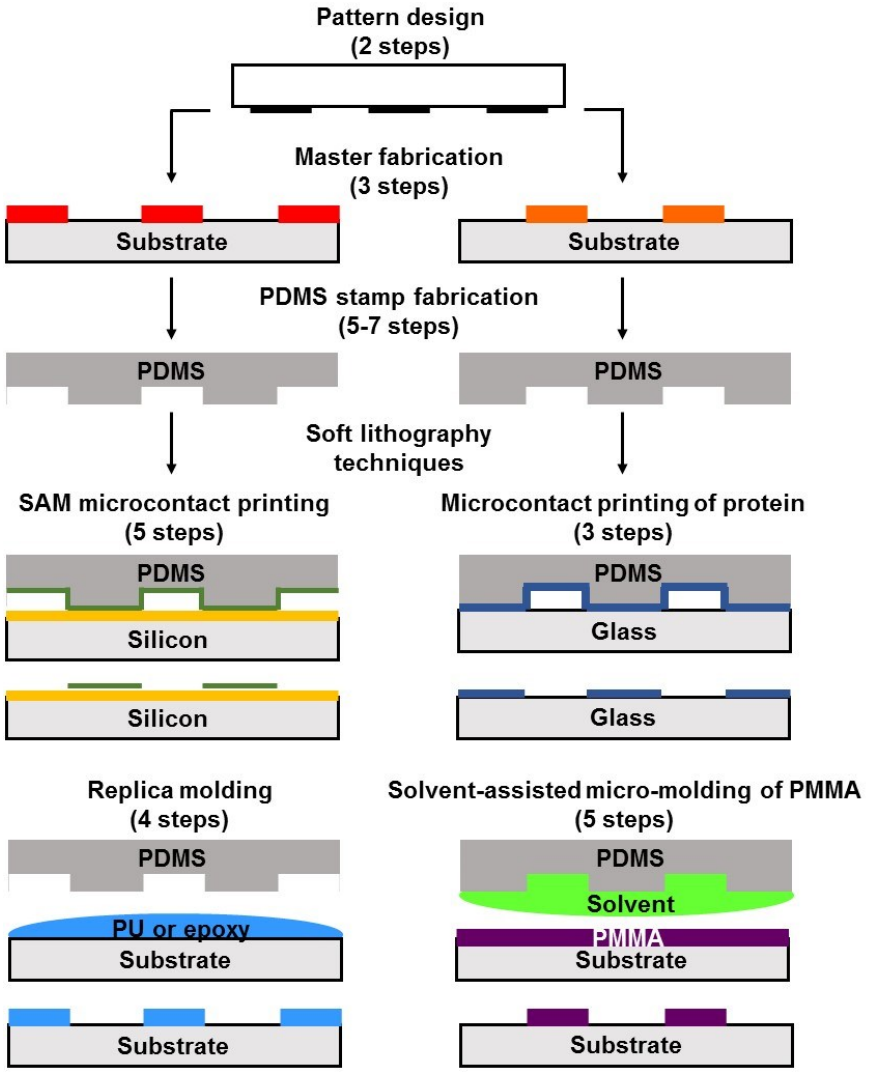

Figure 5.1 Scheme of soft lithography process. First, the pattern is designed on CAD software, then a photomask is created. A master is then fabricated using photolithography. The poly(dimethyl siloxane) (PDMS) stamp can then prepared and utilized to transfer patterns for soft lithography. Four major soft lithography techniques are described above: microcontact printing of self-assembled monolayers (SAMs) of alkanethiol patterns on gold, silver, copper, or palladium (yellow) on silicon substrates, microcontact printing to pattern cell adhesive proteins onto a glass substrate, replica molding, and solvent-assisted micromolding (SAMIM). This figure was adapted from *Nature Protocols* **2010,** *5*, 491.[22]

specialized methods such as laser photoablation[25], 3-D printing[26], ion implantation[27], and microfluidics[28] have been used. The cost and technical complexity associated with many of these methods can limit their use to a relatively small number of laboratories. In addition, the number of surfaces that can be fabricated for cell adhesion using these approaches is limited.

In addition to chemical-based cues, surface topography can modulate cell adhesion and growth.[29] For example, the topography of the extracellular matrix influences cell orientation, migration and organized cytoskeletal arrangements through contact cue guidance.[30] Moreover, recent studies have indicated that cell adhesion and cell spreading on engineered materials can be controlled by well-defined surface features.[30–32] However, fabricating precise features on a 2-dimensional surface often requires specialized techniques and reagents, as well as multi-step protocols (**Figure 5.1**). For example, soft lithography techniques like microcontact printing or replica molding require separate steps that involve photolithography to prepare the master template, creation of a polydimethylsiloxane (PDMS) stamp, inking the PDMS stamp with affinity reagent (such as those described above), and applying that stamp to a substrate surface.

In response to the above challenges, we set out to develop a simple, inexpensive, and robust method for controlling cell adhesion and growth on a 2-dimensional surface.

We also anticipated that these studies might lead to an improved understanding of the dictates for defined mammalian cell adhesion on a synthetic substrate. In contrast to methods that rely on controlling cell adhesion through the use of affinity reagents, our approach relies on cell-imprinted features on a hydrogel substrate.

Other studies have shown that bacterial or viral imprinted features can be utilized for cell recognition in solution, which can be used in bioanalytical devices for cell detection from complex solutions.[33,34] Additionally, Dickert and coworkers have used erythrocyte stamps as part of a microcontact printing protocol to prepare polyurethane surfaces that recognize erythrocytes from solution.[35] This work inspired us to utilize mammalian cells to create cell-imprinted topology that would facilitate cell adhesion and proliferation. We envisioned that hydrogels could be cast on a monolayer of mammalian cells, then removed and utilized as a substrate for mammalian cell adhesion (**Figure 5.2**). Hydrogels are an ideal material to produce cell-imprinted

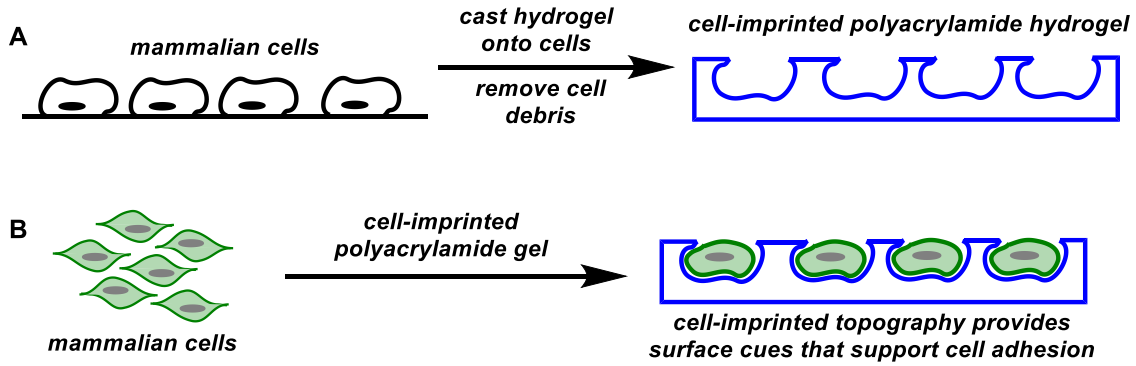

Figure 5.2 Programmed cell adhesion and growth by cell-imprinting. A) A polyacrylamide gel is cast on a monolayer of adherent mammalian cells, thereby generating a gel with cell-imprinted topography that complements the imprinted cells' morphology. B) Cell-imprinted features can provide surface cues that support cell adhesion and control cell growth.

substrates because they are inexpensive, easy to prepare, non-cytotoxic, and the mechanical properties are highly tunable.[36–41] Additionally, we questioned whether changes in cell morphology (and thus the imprint) might influence cell-selective recognition, adhesion, and growth.

5.3 Fabrication of Cell-Imprinted Polyacrylamide Hydrogels

As a proof-of-concept, we set out to prepare cell-imprinted polyacrylamide hydrogels and test their ability to act as substrates for mammalian cell adhesion and proliferation. We anticipated two major obstacles in their preparation and use. First, radical-induced polymerization of acrylamide and bisacrylamide is likely toxic to cells. Therefore, the gelation and cell-imprinted process competes with toxicity-dependent changes in cell morphology and detachment of cells from the tissue culture plate. As a result, the topology of the imprinted surface may not closely resemble the morphology of the imprinted cell, and detached dead cells may become irreversibly encapsulated within the hydrogel matrix. Second, a washing procedure would likely need to be developed to remove cell debris from the cell-imprinted surface.

Cell-imprinted polyacrylamide hydrogels were initially cast from a subconfluent monolayer of HeLa (human cervical cancer) cells grown in a 6-well tissue culture plate. Briefly, a premixed solution of 30% acrylamide, 1% bisacrylamide (wt/vol),

tetramethylethylene-diamine (TEMED), and ammonium persulfate (APS) was incubated with HeLa cells at room temperature. Gelation was typically complete after 20 minutes. We attempted to remove any intact cells or cell debris from the imprinted gel surface using a washing procedure that involved incubating the gel in 1 M aqueous sodium hydroxide for 1 hour at 37 °C, then an additional hour incubation in 0.6 M sodium dodecyl sulfate (SDS) at 37 °C. After these washing steps the gels were rinsed three times with phosphate buffered saline (PBS). Gel topology was assessed by scanning electron microscopy (SEM). Examination of the SEM images revealed that we were able to form cell-imprinted features; however, a large amount of cell debris remained on the imprinted hydrogel surface (**Figure 5.3A**). Additional analysis with Coomassie staining, which non-selectively stains proteins, confirmed the presence of

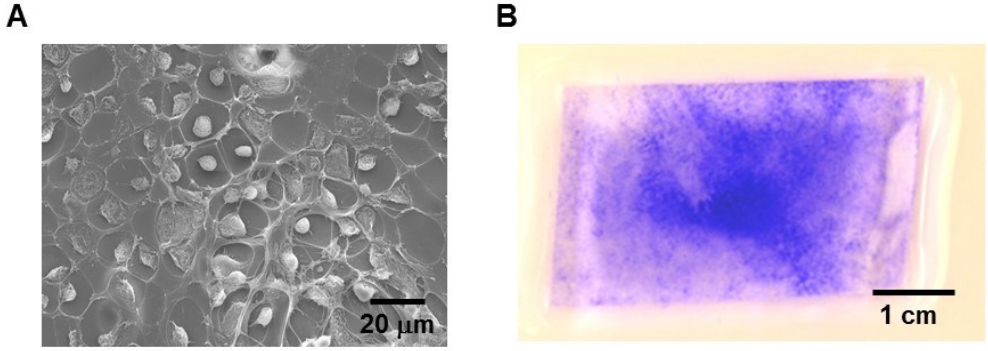

Figure 5.3 Initial results of cell-imprinting polyacrylamide hydrogels from a subconfluent monolayer of adherent HeLa cells. A) Scanning electron microscopy (SEM) image showing the cell-imprinted surface of the polyacrylamide hydrogel as well as a significant amount of intact HeLa cells and cell debris. B) A hydrogel imprinted with a monolayer of HeLa cells, then washed as described above, and stained with Coomassie. Staining clearly shows cell debris present on the surface of the hydrogel.

cellular proteins and/or cellular debris on the surface or within the hydrogel matrix, as shown in **Figure 5.3B**.

To resolve this issue, we chose to fix the cells before radical-induced gelation of the hydrogels. We hypothesized that fixation would help to maintain cell morphology during the harsh cell-imprinting process and reduce cell detachment during solidification of the hydrogel. We also reasoned that since fixation should minimize changes in cell morphology during the gelation process, imprinted features should more closely resemble features of cultured mammalian cells. To test whether pre-fixing cells allows us to transfer cell size and morphology to the imprinted hydrogel surface feature, our second-generation attempts at cell-imprinting hydrogel surfaces were performed using cells with epithelial-like and fibroblast-like morphology. HeLa (human cervical cancer, epithelial-like morphology), HEK-293T (human embryonic kidney, epithelial-like morphology), and MRC-9 (human embryonic kidney, fibroblast-like morphology) cells were used as templates for the cell-imprinted polyacrylamide gels. The cells were grown to subconfluent monolayers in a 6-well tissue culture place, and then fixed with 4% formaldehyde/PBS solution for five minutes. The fixed cells were then incubated with a pre-mixed solution of 30% acrylamide, 1% bisacrylamide (wt/vol), TEMED, and APS at 37 °C. We then used an optimized washing procedure to remove cell debris from the imprinted gel. Briefly, the hydrogels were incubated in a 0.25% trypsin solution for 1 hour at 37 °C, washed three times with PBS, incubated in a

1 M aqueous hydrochloric acid solution for 6 hours at 37 °C, and washed an additional three times with PBS. Gels were stored in PBS at 4 °C.

Following cell-imprinting and washing, cell-imprinted hydrogels were stained with Coomassie to verify that intact cells and cell debris was removed. As shown in **Figure 5.4A**, Coomassie does not appreciably stain cell-imprinted regions of the gel. Low levels of Coomassie stain remained on the edge of the gel, most noticeably in the HEK-293T-imprinted gel, but not in the center of the gel where cell-imprinted features exist. This edge staining affect is commonly observed when staining polyacrylamide gels after protein electrophoresis. Therefore, we analyzed Coomassie staining in the middle of the gels, which contain cell imprints. We further verified removal of cellular

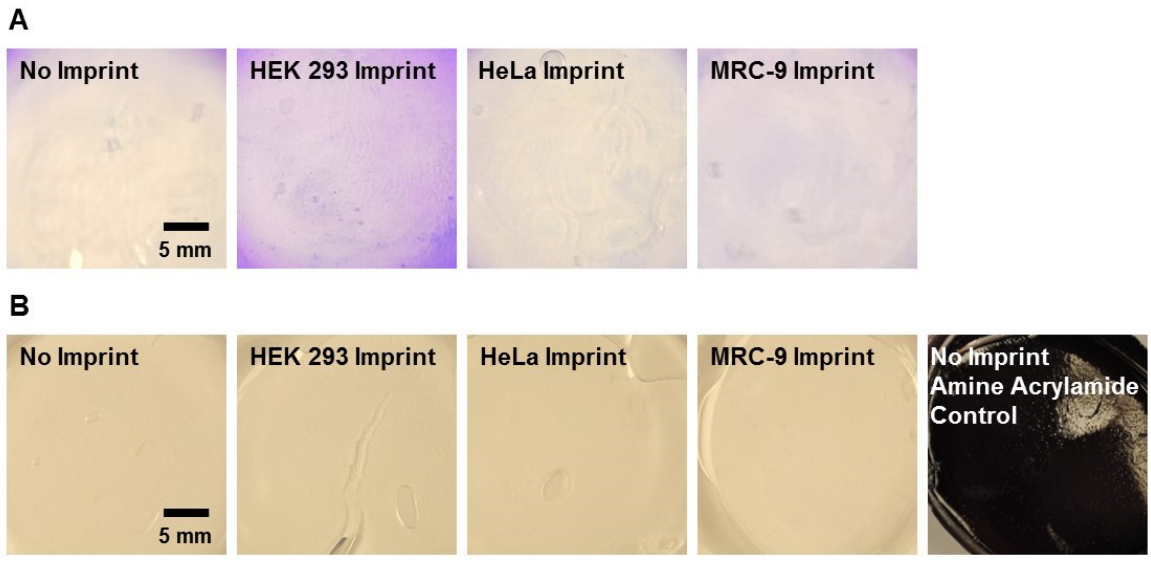

Figure 5.4 Verification of complete removal of cellular debris. A) Cell-imprinted gels washed with 0.25% trypsin and 1 M aqueous HCl, then stained with Coomassie and destained. Coomassie does not appreciably stain cell-imprinted regions of the gel. B) Ninhydrin does not appreciably stain cell-imprinted polyacrylamide gels, but does stain amino-functionalized gels prepared from poly-*N*-(aminopropyl)-methacrylamide.

proteins by ninhydrin staining. Ninhydrin stains free amines, as a result, it can be utilized to stain proteins containing lysine or aminoglycans. We prepared a positive control hydrogel with poly-*N*-3-(aminopropyl)-methacrylamide, which did stain with ninhydrin (**Figure 5.4B**). The cell-imprinted hydrogels did not stain with ninhydrin, demonstrating that the hydrogel surface is free of cellular protein or peptide debris (**Figure 5.4B**). Therefore, any cell adhesion or growth on the cell-imprinted hydrogels is not due to interaction with cellular debris, but likely the result of surface contact cue guidance.

Next we characterized the cell imprinted features by SEM. As shown in **Figure 5.5**, the shape and size of the imprints is consistent with the morphology of the imprinted cell. For instance, HeLa cells and HEK 293T cells, which exhibit epithelial-like morphology, form imprints that are elliptical and polygonal. Whereas imprints from MRC-9 cells, which have fibroblast morphology, show elongated and fibrous features, consistent with the topology of MRC-9 cells. In contrast, non-imprinted hydrogels do not show well-defined features. These data indicate that polyacrylamide gels can be prepared to mimic the topography of mammalian cells and could possibly facilitate adhesion based on surface guidance.

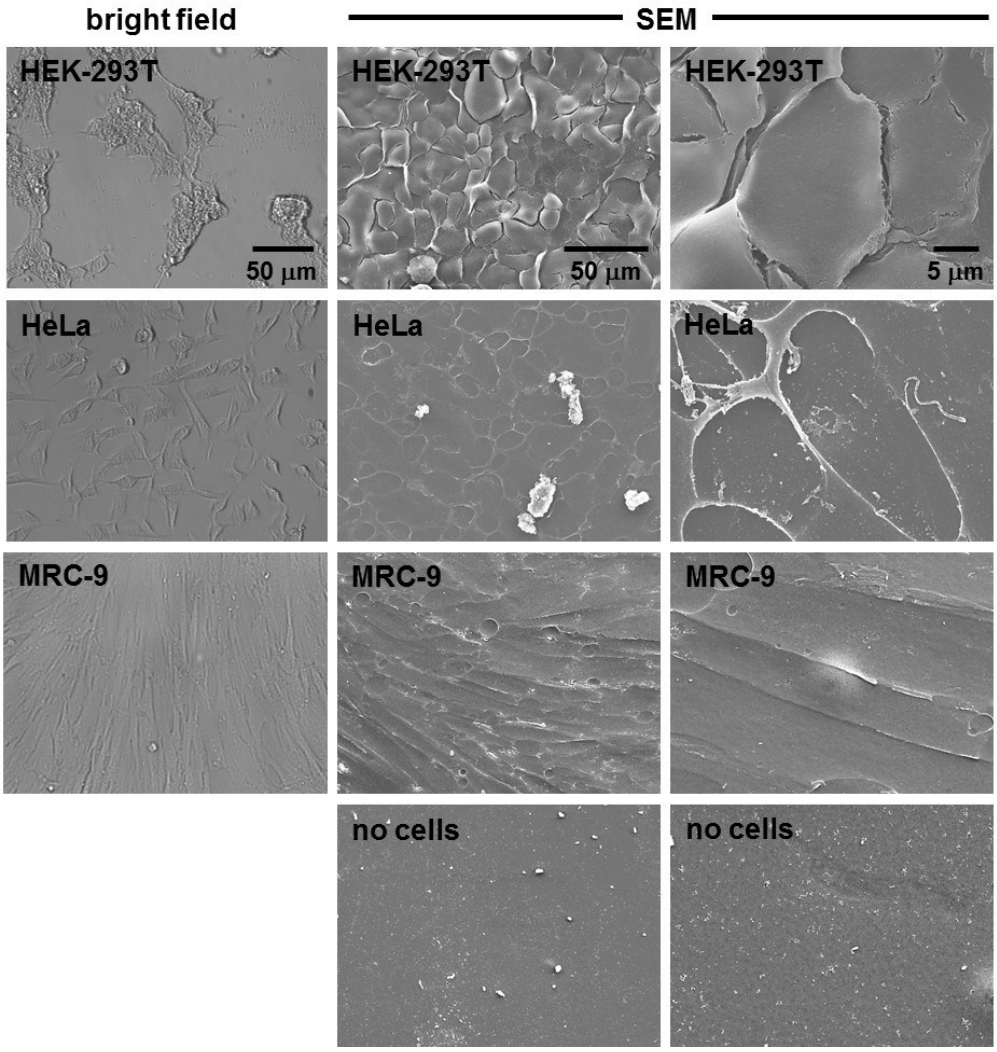

Figure 5.5 Bright field and SEM images of cells and cell imprints. (Left column) Bright field images of HEK-293T, HeLa and MRC-9 cells grown as a monolayer on polystyrene tissue culture plates. (Middle and right columns) Scanning Electron Microscopy (SEM) images of the surface of polyacrylamide gels imprinted with fixed HEK-293T, HeLa or MRC-9 cells then washed with 0.25% trypsin solution of 1 hour at 37 °C, then 1 M aqueous hydrochloric acid solution for 6 hours at 37 °C. The bottom row shows SEM images of a non-imprinted polyacrylamide hydrogel.

5.4 Cell-Imprinted Polyacrylamide Hydrogels for Mammalian Cell Adhesion

To assess whether the cell-imprinted hydrogels support the adhesion of mammalian cells, we added HeLa, HEK-293T, and MRC-9 cells to the cell-imprinted

hydrogels. We used HeLa-GFP and HEK-293T-GFP cells that constitutively express green fluorescent protein (GFP) to identify cell adhesion through fluorescence on the gel surface. MRC-9 cells do not express GFP; therefore, MRC-9 cell attachment was measured by staining the hydrogel with DAPI, which stains the nuclei of cells. Before incubation with cells, the cell-imprinted hydrogels were washed with the corresponding cell media. HeLa-GFP, HEK-293T-GFP, or MRC-9 cells were then added to both cell-imprinted and non-imprinted gels and incubated at 37 °C, 5% CO_2 for 12 hours. The gels were then washed three time with media to remove any non-adherent cells. Fluorescence images of the gels after incubation with the HeLa-GFP and HEK-293T-GFP cells were taken on a Typhoon Trio imager. We observe no fluorescence on non-imprinted polyacrylamide gels demonstrating that cells do not adhere to the gel itself (**Figure 5.6**). However, HeLa-GFP cells were able to attach to cell-imprinted hydrogels prepared from HeLa, HEK-293T, and MRC-9 cells. This result is unsurprising because HeLa cells are well-known to adhere and grow on a variety of surfaces. HEK-293T-GFP cells show attachment only to hydrogels imprinted with HeLa or HEK-293T cells. They were not able to adhere to MRC-9 imprinted gels, which exhibit fibroblast morphology, most likely due to the elongated and fibrous structure. MRC-9 cells were adherent to all three types of cell-imprinted surfaces, but they attached the best to HeLa and HEK-293T-imprinted hydrogels. Interestingly, MRC-9 cells that were adherent to the hydrogels did not have normal fibroblast-like morphology. Moreover, in the

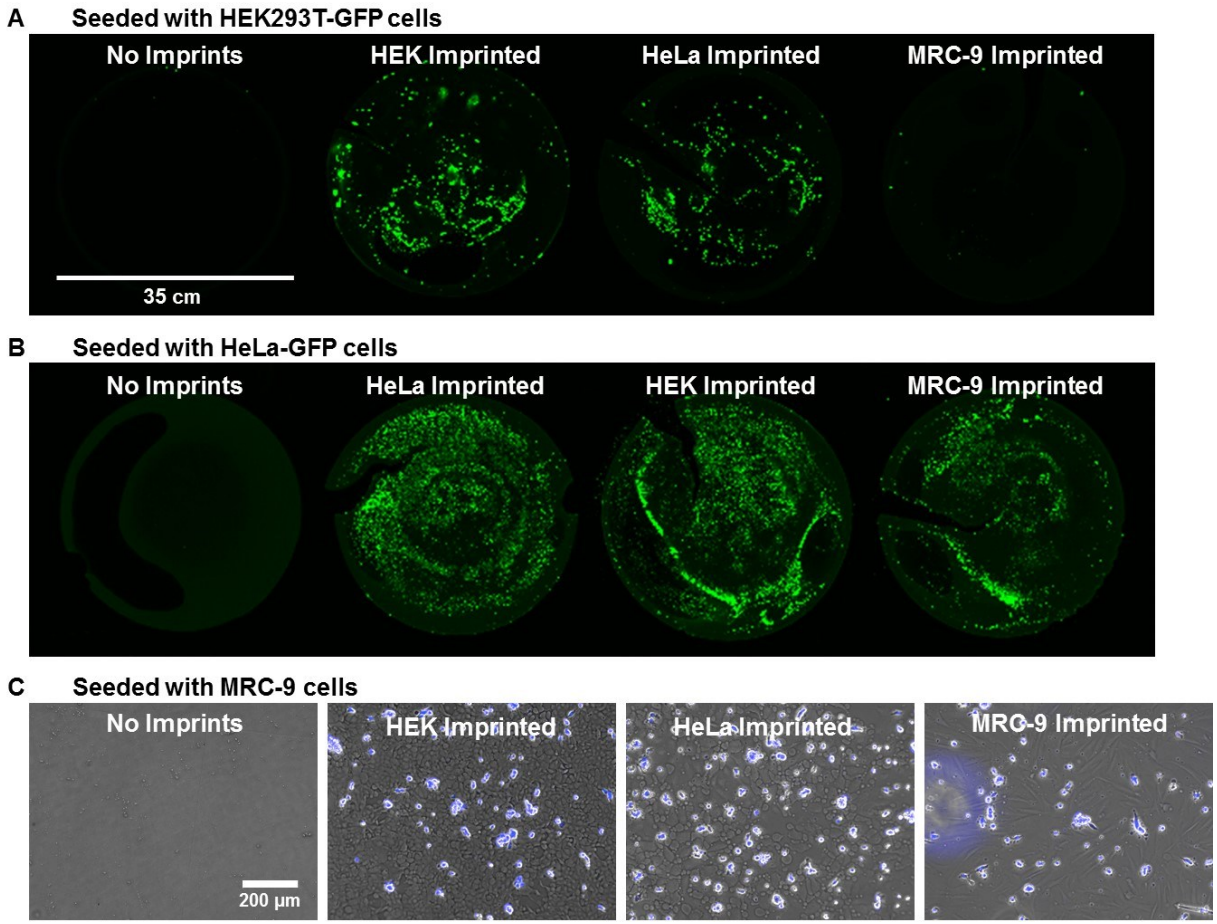

Figure 5.6 Mammalian cell adhesion on cell-imprinted hydrogels. Cell-imprinted polyacrylamide hydrogels that are seeded with either (A) HEK-293T-GFP, (B) HeLa-GFP, or (C) MRC-9 cells. (A) and (B) were imaged in a Typhoon Trio imager. (C) Cells were stained with DAPI and cell adhesion was assessed by fluorescence microscopy.

absence of fetal bovine serum, none of the cells lines tested adhered to any cell-imprinted hydrogel. This observation suggests that serum protein is required for cell adhesion and growth on the cell-imprinted gels. Overall, these data indicate that cell-imprinted topography can facilitate attachment of various mammalian cell lines. In the case of HEK-293T cells, the cell-imprinted features have a dramatic effect on cell adhesion. Consequently, cell-imprinted features have the possibility to be used for programmed cell-selective adhesion to a surface.

5.5 Analysis of Cellular F-actin in HeLa and HEK-293T Cells to Determine Cytoskeletal Arrangement on Cell-Imprinted Hydrogels

Our findings suggest that HEK-293T cells appear to selectively adhere to surfaces with epithelial-like cell-imprinted features. In order to investigate how HeLa and HEK-293T cells adhere to and spread on their respective cell-imprinted surfaces and if binding to topologically different surfaces results in appreciable rearrangement of the cytoskeleton, we compared their cytoskeletal arrangement when grown on a cell-imprinted hydrogel or a polystyrene tissue culture plate. Total cellular F-actin was stained with Alexa Fluor 555 phalloidin and cells were imaged by live cell fluorescence microscopy. As shown in **Figure 5.7**, in comparison to cells grown on a tissue culture plate, HeLa cells grown on a HeLa cell-imprinted gel have a condensed F-actin

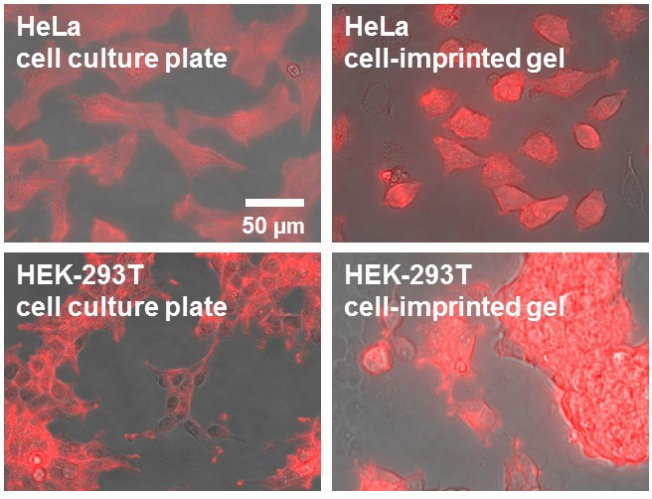

Figure 5.7 Comparison of cytoskeletal arrangement on cell culture plates and cell-imprinted polymers. Fluorescence microscopy images of HeLa and HEK-293T cells grown on a cell culture plate (left) or a cell-imprinted polyacrylamide gel (right). Cellular F-actin was stained with Alexa Fluor 555 phalloidin. Images are an overlay of fluorescence and bright field images.

cytoskeleton. Similar to HEK-293T cells that were grown on a polystyrene tissue culture dish, HEK-293T cells grown on HEK-293T-imprinted hydrogels formed large globular colonies. However, these cells have less distinguishable morphology and cytoskeletal features. In both cases, HeLa and HEK-293T cells grown on cell-imprinted gels were generally restricted to cell-imprinted features. These data suggest that cells grown on cell-imprinted polyacrylamide gels recognize surface contact cues present in the cell-imprinted topography and the cytoskeletal arrangement is affected by the interactions involving the cell surface and the imprinted feature. Condensation of the actin cytoskeleton may be required to allow these cells to fit within the confines of the cell-imprinted pits, and in the case of HEK-293T cells, this is limited to imprints from cells with epithelial-like cell morphology. This suggests that, at least for HEK-293T cells, a significant amount of cytoskeletal rearrangement is required to recognize and fit into a surface feature that resembles fibroblast-like morphology, and this is a significant barrier to adhesion and proliferation.

5.6 Using Spatially-Defined Cell-Imprints to Control the Adhesion and Proliferation of HeLa Cells on a Cell-Imprinted Hydrogel Surface

We hypothesized that we could develop this technology to utilize the spatially-defined cell-imprinted features to pattern cells on a hydrogel surface. This method

would be particularly attractive because it doesn't rely on specialized or expensive equipment to pattern the hydrogels with cell-imprinted topography. We began by creating a checkerboard pattern of UGlu® tape, which is an adhesive that can be applied to and removed from polystyrene surfaces, onto a tissue culture dish. We then added HeLa cells to the dish and allowed them to reach subconfluent levels on the exposed polystyrene surface. We then removed the tape from the dish and cast a polyacrylamide gel as described previously, thereby fabricating a well-defined checkerboard pattern of HeLa cell-imprinted features (summarized in **Figure 5.8A**). The cell-imprinted hydrogel was then washed as previously described and HeLa-GFP cells were incubated with the patterned gel. After a 12 hour incubation at 37 °C, the hydrogel was washed with DMEM/10% FBS media to remove non-adherent cells. The media was then replaced and the bound cells continued to proliferate for an additional 12 or 36 hours. The patterned hydrogel was then washed with PBS and fluorescence images of the surface were obtained. As shown in **Figure 5.8B**, there is a distinct checkerboard pattern of HeLa cells on the surface of the gel. We observe a high density of HeLa-GFP cells in the areas containing the cell-imprinted features, but not in the areas that were not cell-imprinted. Moreover, we monitored the proliferation of the HeLa-GFP cells on the patterned hydrogels over two days and observed increased cell density within the cell-imprinted features (**Figure 5.8C**). Further analysis of cell population revealed that cell densities

present on the imprinted regions of the hydrogels were similar to those seen on polystyrene culture dishes.

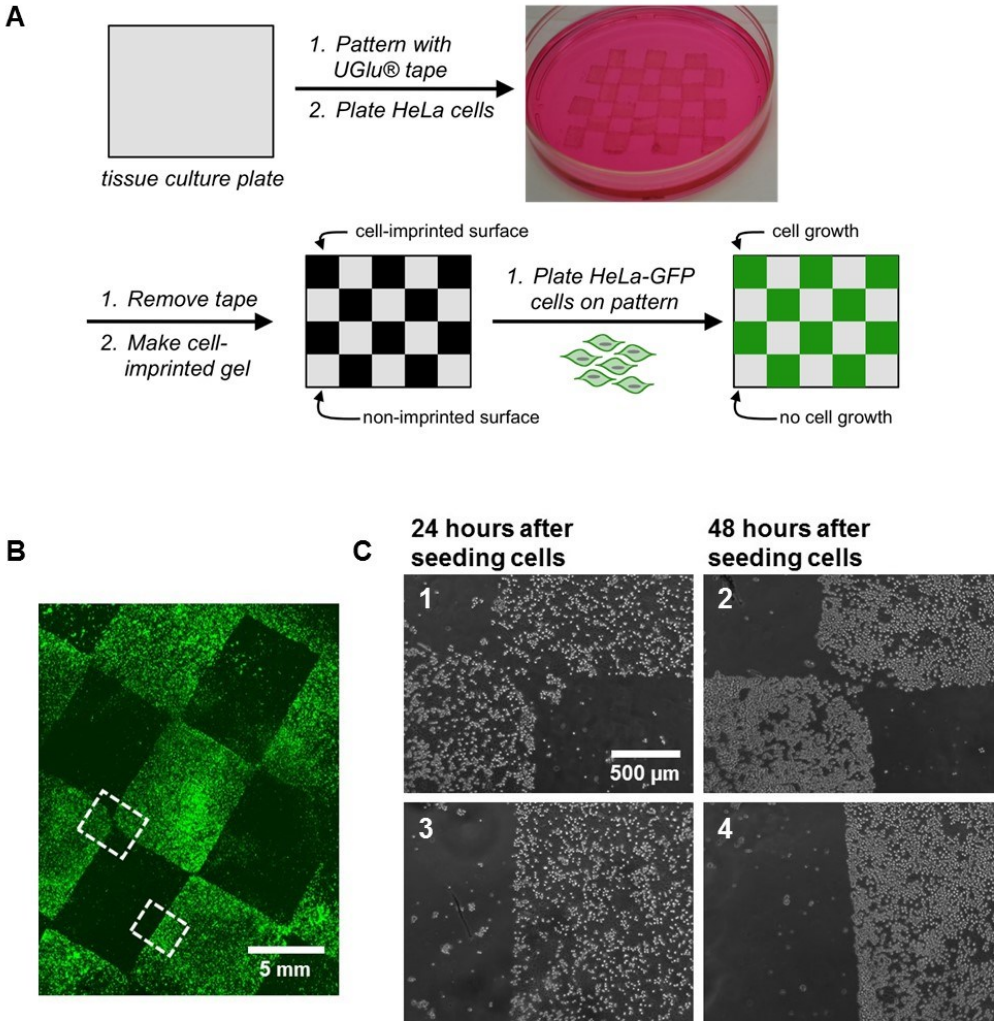

Figure 5.8 Patterning of HeLa-GFP cells on a cell-imprinted polyacrylamide gel. A) A checkerboard pattern of HeLa cells was prepared on a polystyrene tissue culture dish using UGlu® tape. A cell-imprinted polyacrylamide gel was cast onto these cells and spatially defined cell imprints were transferred to the gel. B) Fluorescence image of a checkerboard imprinted gel after treatment with HeLa-GFP cells. C) Bright field microscopy images showing cell growth 24 and 48 hours after cell seeding. Dotted boxes in (B) represent the general areas imaged in (C). In (C), images 1 and 2 are in the general area highlight by the larger dotted box. Images 3 and 4 are in the general area highlighted by the smaller dotted box. The images in (C) are rotated slightly counter-clockwise compared to (B).

5.7 Conclusions

We have developed a simple and inexpensive procedure for the fabrication of cell-imprinted polyacrylamide hydrogels. Using this technology, we have demonstrated that cell-imprinted features can support the adhesion and proliferation of mammalian cells. Interestingly, in the case of HEK-293T-GFP cells, the topology of the imprinted cells are important for cell attachment. Overall, these data indicate that cell-imprinted features can be utilized to control cell adhesion and growth. Additionally, by patterning a hydrogel with cell-imprinted regions, cell growth can be tightly controlled on the hydrogel surface. This method of cell imprinting could have a more general use in the fields of tissue engineering, diagnostics, and biomaterials science because of the relatively simple and inexpensive preparation of the polyacrylamide hydrogels.

5.8 Experimental Methods

Materials

Acrylamide - Aldrich
Bisacrylamide - Promega
Ammonium persulfate (APS) - Mallinckrodt Chemicals
Tetramethylethylenediamine (TEMED) - IBI Scientific
RNase/DNase-free water - Teknova
Phosphate buffered saline (PBS) - Hyclone/Thermo Scientific
0.25% Trypsin - Hyclone/Thermo Scientific
Hydrochloric acid - Mallinckrodt Chemicals
Brilliant Blue R-250 - J.T.Baker
Ninhydrin - Sigma Aldrich

Bovin serum albumin - Sigma Aldrich
Fetal bovin serum (FBS) - PAA Laboratories
Triton X-100 - Fisher Scientific
Dulbecco's modified Eagle medium (DMEM) - Hyclone/Thermo Scientific
RPMI-1640 media - Hyclone/Thermo Scientific
Mammalian cell culture dishes - Fisher Scientific
Glutaraldehyde - Fisher Scientific
N-(3-Aminopropyl)methacrylamide hydrochloride - Polysciences, Inc
Alexa Fluor 555 phalloidin – Invitrogen

Instrumentation

Scanning electron microscopy (SEM) images were taken on a JEOL JSM-6500 F field emission scanning electron microscope (FESEM). All microscopy images were taken on an EVOS fl fluorescence microscope from Advanced Microscopy Group (AMG). Fluorescence images of whole gels were obtained on a Typhoon Trio imager.

Mammalian Cell Culture

HEK293T, HEK 293T-GFP, HeLa and HeLa-GFP cells were cultured in high glucose Dulbecco's modified Eagle medium (DMEM) with 10% Fetal Bovine Serum (FBS) in a 37 °C incubator with 5% CO_2 environment. Human embryonic lung fibroblasts (MRC-9) were cultured in RPMI-1640 media and 10% FBS in a 37 °C incubator with 5% CO_2 environment.

Preparation of Cell-Imprinted Hydrogels

Cells were grown in a 6-well tissue culture dish until approximately 80% confluent. Cells were washed once with 37 °C phosphate buffered saline (PBS), fixed with 4% paraformaldehyde in 37 °C PBS for 5 minutes and washed two times with 37 °C PBS.

Polyacrylamide gels were prepared by mixing 5.33 mL of a 31% acrylamide solution (30% acrylamide and 1% bisacrylamide (wt/vol)) with 2.0 mL PBS and 0.5 mL RNase/DNase free-water. Gelation was initiated by the addition of 8 μL of TEMED and 80 μL of APS, followed by gentle mixing. 1.5 mL of the polyacrylamide solution was added to fixed cells in a 6-well tissue culture dish and incubated at 37 °C, 5% CO_2 for 20 minutes. The hydrogels were then removed from the cell culture dish, placed cell-imprint up in another 6-well plate and each gel was incubated with 3 mL of 0.25% trypsin solution for 1 hour at 37 °C. Following trypsin treatment gels were washed three times with room temperature PBS and then treated with 1 M aqueous HCl for 6 hours at 37 °C. Hydrogels were then washed three times with room temperature PBS, and incubated overnight in PBS at 37 °C / 5% CO_2.

Mammalian Cell Growth on Cell-Imprinted Hydrogels

Cell-imprinted hydrogels were washed twice with 37 °C high glucose Dulbecco's modified Eagle medium (DMEM). 2 mL of DMEM / 10% FBS containing either HEK 293T-GFP or HeLa-GFP cells was added to each gel containing approximately 3.0×10^5 cells/mL. The gels were incubated overnight at 37 °C and 5% CO_2. Hydrogels were then washed twice with 5 mL of 37 °C DMEM to remove any dead or non-adhered cells. Cells typically grew on the cell-imprinted hydrogels for 1-4 days before imaging.

Scanning Electron Microscopy (SEM)

Hydrogels were cut into 3mm × 3mm pieces and incubated in 200 μL of a 25% glutaraldehyde / PBS solution for 1 hour. Hydrogels were then washed three times for 30 minutes each with PBS and twice with water for 30 minutes each. Hydrogels were then dried by sequential incubation in 500 μL of 50:50, 70:30, 80:20, 90:10, and 95:5 ethanol:water for 10 minutes each. Dehydrated gels were then washed three times with absolute ethanol for 10 minutes each and dried using a critical point drier. Gels were imaged on a JEOL JSM-6500 F field emission scanning electron microscope (FESEM).

Coomassie Staining

Cell-imprinted and non-cell-imprinted hydrogels were washed as described above. The hydrogels were then stained with a 50% methanol, 10% acetic acid and 0.05% Brilliant Blue R-250 solution for 1 hour at 25 °C. Gels were then washed twice with water and destained using a 50% methanol, 40% water, and 10% acetic acid solution for 1 hour. Gels were then washed with water and images were taken using a Nikon D5000 digital camera.

Ninhydrin Staining

Cell-imprinted hydrogels prepared as previously described. Non-imprinted amino hydrogels prepared with 3 mL of 32% acrylamide solution (30% N-(3-Aminopropyl)methacrylamide hydrochloride and 2% bisacrylamide (wt/vol)) and polymerized with 60 μL APS and 6 μL TEMED. All gels were prepared and washed as

described above. Hydrogels were then incubated in 10 mL of a 1.5 g ninhydrin, 100 mL n-butanol, 3 mL acetic acid solution and heated to 100 °C for 30-40 minutes. The gels were then washed with three times with water and images were taken using a Nikon D5000 digital camera.

Actin Staining

Cells that were plated on gels and tissue culture dishes were washed with PBS. The cells were then fixed with 5 mL of 4% paraformaldehyde in PBS, pH 7.4 at 37 °C for 10 minutes. The cells were then washed twice with PBS and incubated with 0.1% Triton X-100 in PBS for 5 minutes. The cells were washed with PBS twice, incubated with 1 % BSA in PBS for 5 minutes and then washed with PBS. The cells were then stained for actin using 50 μL Alexa Fluor 555 phalloidin in 2 mL PBS for 30 min. at room temperature. The cells were then washed twice with PBS and imaged with the EVOS fl microscope.

Part II: Engineering Dinitrophenyl Conjugated Proteins as Immunotherapeutic Drug Leads (In collaboration with the Spiegel lab, Yale University)

5.9 Harnessing the Immune System to Target and Kill Cancer Cells

Targeted cancer therapeutics enable selective treatment of diseased cells without the toxicity of traditional chemotherapeutics. Small molecule therapeutics, in particular, are an appealing tool for the targeted treatment of cancer because they are relatively simple to produce and have the ability to cross the membrane of mammalian cells, thereby allowing these reagents to access intracellular targets. However – as described previously – small molecule therapeutics have significant limitations. Foremost among these is the limited functional diversity of small molecule drugs. Additionally, the screening and development of new small molecule reagents is difficult, costly, and laborious. High throughput methods of screening small molecule libraries often result in binders that are not selective and may require additional time-consuming optimization to improve affinity and specificity. Earlier in this thesis, I made the case for proteinaceous reagents as basic research tools and therapeutics, by virtue of the fact that proteins can often overcome many of the limitations faced by small molecules. However, the reality is that no one technology or set of reagents will represent a final destination in our search for approaches to cure human disease. Thus, researchers are best served by assessing and advancing a variety of technologies.

Regardless of whether the therapeutic reagent is a small molecule or protein, the basic paradigm is that the reagent binds to, or otherwise acts on, a cellular receptor, leading to a change in disease-relevant cell function and fate. An alternative approach is to develop reagents to *do not* act on a cellular receptor in a manner that induces a change in cell function or fate, but triggers the native immune response to selectively destroy that (diseased) cell. Reagents that act in this manner are referred to as immunotherapeutics. Immune system-mediated cytotoxicity can occur through a number of mechanisms, including phagocytosis, complement-dependent cytotoxicity (CDC), antibody-dependent cellular cytotoxicity (ADCC), modified T-cells targeted to single-chain variable fragment (scFv), and cross-presentation of antigen to dendritic cells (summarized in **Figure 5.9**).[42] Direct lysis of the target cell can be achieved by activating complement proteins, such as C1q, which then begins proteolytic events in CDC. Alternatively, cytotoxicity may be mediated by natural killer (NK) cells, macrophages, or neutrophils as is the case for antibody-dependent cellular cytotoxicity (ADCC).[43] ADCC occurs when immune cells recognize and bind to the crystallizable fragment (Fc) of the antibody and release toxic proteins, such as granzyme and perforin, to induce cell death.[44] Importantly, these types of immune responses have the potential to induce long-term adaptive immunity against tumors.[45–48]

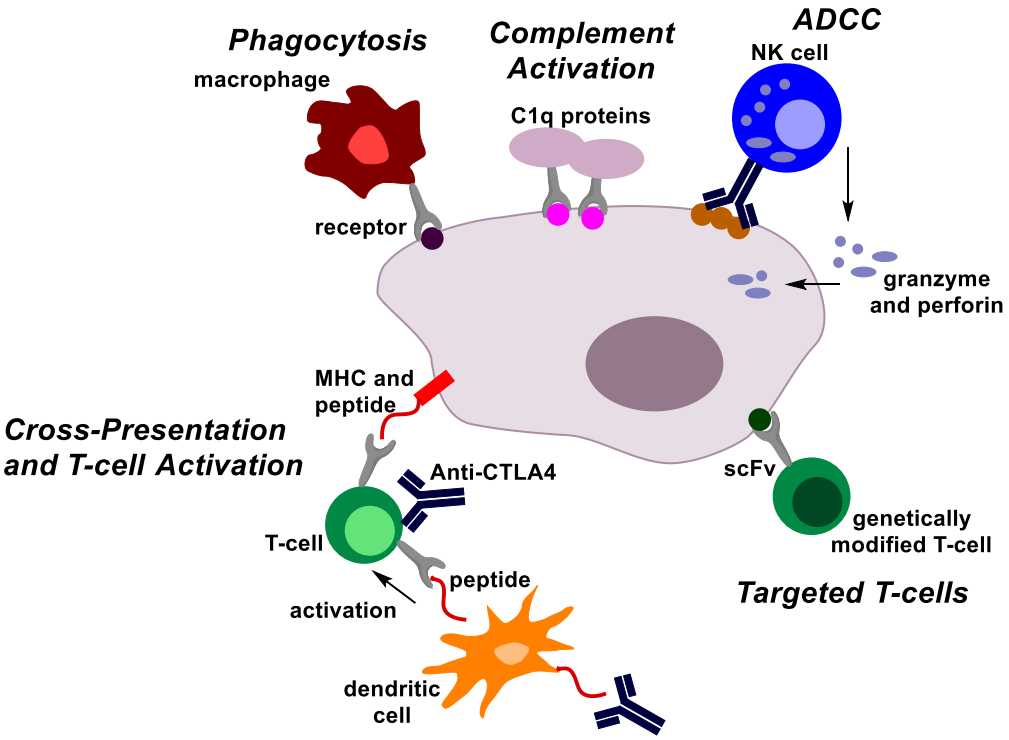

Figure 5.9 Mechanisms of immune-mediated cytotoxicity. The immune system can be activated for targeted cell death by induction of phagocytosis, activation of complement proteins, antibody-dependent cellular cytotoxicity (ADCC), genetically engineering T-cells to target diseased cells, T-cell activation by antibody mediated cross-presentation of an antigen to dendritic cells, and inhibition of cytotoxic T lymphocyte-associated antigen 4 (CTLA4) inhibitory receptors. This figure was adapted from *Nature Reviews Cancer* **2012,** *12,* 278.[42]

One approach to immune activation was recently reported by the Spiegel lab at Yale, and is referred to as antibody-recruiting small molecules (ARMs).[49] ARMs consist of an antibody recruiting small molecule attached through a linker to a cell-binding terminus (CBT). ARM reagents recognize and bind a disease relevant target, then endogenous anti-hapten antibodies bind to the antibody-binding terminus (ABT), followed by subsequent immune-mediated cytotoxicity.[49]

The Spiegel lab previously described the use of bifunctional antibody-recruiting small molecules to target prostate cancer cells (**Figure 5.10A**).[50] They employed a glutamate urea moiety to target prostate specific membrane antigen (PSMA), which is overexpressed in some prostate cancer cells (**Figure 5.10B**).[51] The antibody-binding terminus was equipped with a dinitrophenyl (DNP) group for endogenous antibody recognition. Although the source of endogenous anti-DNP antibodies is unclear (likely the result of ingestion of environmental DNP-containing molecules),[52,53] approximately 1% of immunoglobulins in the human body bind to DNP,[54] and DNP has been shown to elicit antibody-dependent cytotoxicity. The Spiegel lab demonstrated ADCC upon the

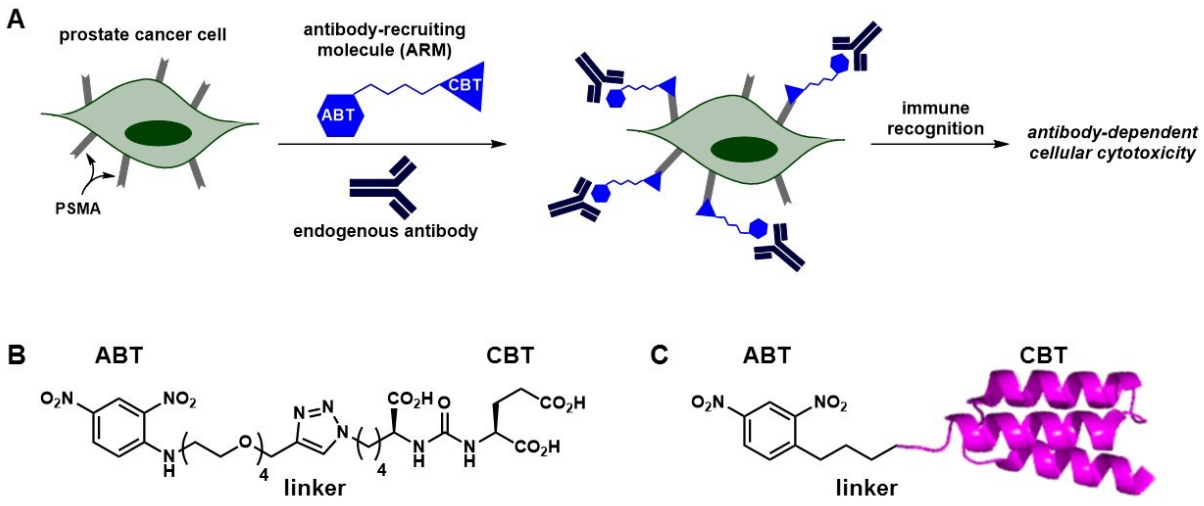

Figure 5.10 Antibody-recruiting molecules (ARMs) for immune-mediated cytotoxicity. LNCaP prostate cancer cells over-expressing prostate-specific membrane antigen (PSMA) are targeted by the cell binding terminus (CBT) of the ARM. The CBT is composed of a small molecule reagent, which bind PSMA. Endogenous antibodies are recruited to the prostate cancer cells by the antibody-binding terminus (ABT) of the ARM, which then induces antibody-dependent cellular cytotoxicity (ADCC) of the prostate cancer cells. B) Structure of bifunctional ARM used to target PSMA. C) Proposed ARM that employs proteins to act as the cell binding terminus.

addition of the bifunctional ARM, anti-DNP antibodies and peripheral blood mononuclear cells (PBMCs) to PSMA expressing LNCaP prostate cancer cells.[50] Therefore, confirming that antibody-recruiting small molecules can be used to activate and target the immune system to destroy cancer cells.

The fundamental limitation of ARM reagents, however, is the necessity for small molecule reagents that bind disease-relevant receptors on the surface of human cells. Chemical conjugation of the cell-binding molecule may present a challenge, depending on its chemical structure. Additionally, the majority of small molecule binding motifs that are used for ARM technology target well-studied ligand-receptor interactions. Therefore, if a diseased cell does not have a known small molecule receptor, one must be identified. As stated previously, this often requires laborious and expensive high-throughput small molecule screening.

An alternative approach to utilizing small molecule reagents to target cell surface macromolecules, is to employ proteins, such as affibodies and nanobodies, to target and bind a disease-relevant receptor (**Figure 5.10C**). Unlike small molecule reagents, protein-based affinity reagents can be evolved to bind almost any protein target with high affinity and selectivity through *in vitro* display technologies.[55,56] These methods allow for rapid identification of new binders, without the need for extensive knowledge of the target receptor. Affibodies and nanobodies are especially well suited affinity

reagents because of their high stability and ease of purification.[57,58] Moreover, nanobodies can be humanized to reduce adverse reactions that would be detrimental to treatment.[59]

5.10 Nanobodies and Affibodies that Target the HER2 Receptor on Breast Cancer Cells

Inspired by small molecule-reliant ARM reagents, and in an effort to expand this immunotherapeutic approach to proteinaceous reagents, we began a collaboration with the Spiegel lab. In considering protein components for use in antibody recruiting protein chimeras, we chose to focus on nanobody and affibody scaffolds. In contrast to full length antibodies and Fab fragments, nanobodies and affibodies can be easily expressed and purified from *E. coli*, but retain excellent target binding affinities and selectivity. Moreover, in contrast to small molecule discovery, these proteins can be matured to bind virtually any disease-relevant cell surface receptor, using macromolecular evolution or high-throughput screening methods.[57,58]

Nanobodies are single-domain proteins (~10-15 kDa) that consist of the antibody-binding fragment of camelid heavy chain only antibodies (**Figure 5.11**). Affibodies were developed from three-helical bundle structure of the B-domain of staphylococcal protein A and range in size from ~5-8 kDa.[58] These protein scaffolds are exceptionally

stable, resistant to chemical denaturation, and soluble at high concentrations, making them ideal affinity reagents.[57,58]

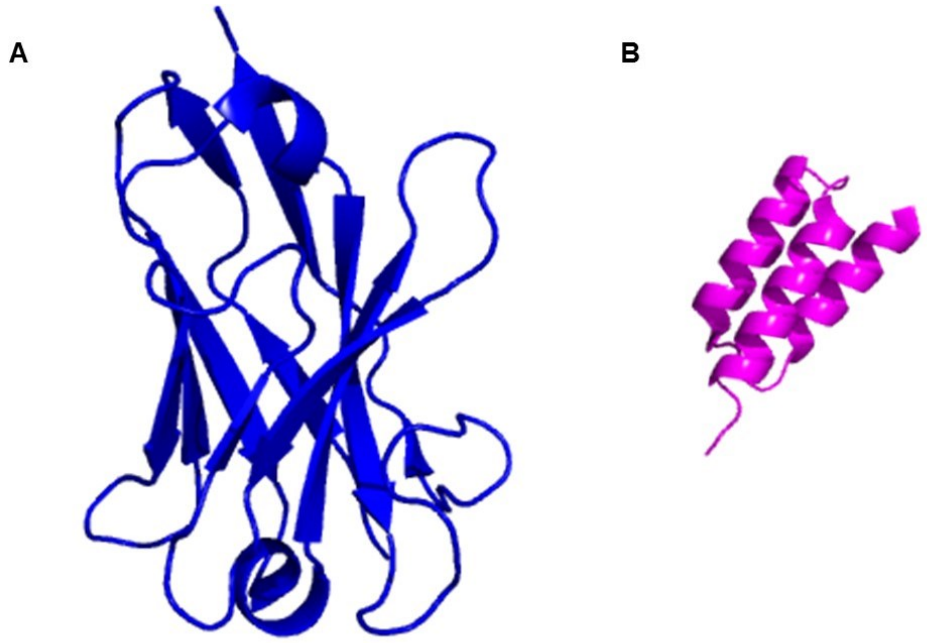

Figure 5.11 Representative examples of nanobody and affibody structures. A) Nanobody protein scaffold derived from the heavy chain region of camelid antibodies (PDB IU0Q).[57] B) ZHER2 affibody derived from the three-helix bundle of the B-domain of protein A (PDB 3MZW).[65]

In collaboration with the Spiegel lab at Yale, we were interested in targeting the human epidermal growth factor receptor 2 (HER2) on breast cancer cells. Researchers have observed that overexpression of HER2 has been associated with anywhere from ~10-30% of breast cancers.[60,61] Moreover, HER2 is expressed in relative low amounts in normal epithelial cells, thus it is a relevant cancer marker.[62] A number of nanobodies and affibodies have already been developed to selectively target and bind HER2 (**Figure**

5.12A); therefore, we chose to test two nanobodies (5F7 and 11A4)[63] and two affibodies (ZHER2 and 2891)[64,65] to act as affinity reagents for our antibody recruiting molecules.

We began by confirming that each protein was able to bind to breast cancer cells, SKBR-3 cells, expressing HER2. I constructed protein fusions with eGFP to visualize binding to the surface of SKBR-3 cells. As shown in **Figure 5.12B**, each of the protein fusions were able to bind to the surface of SKBR-3 cells at relatively low concentrations. NIH-3T3 cells, which do not express HER2, do not show appreciable GFP fluorescence.

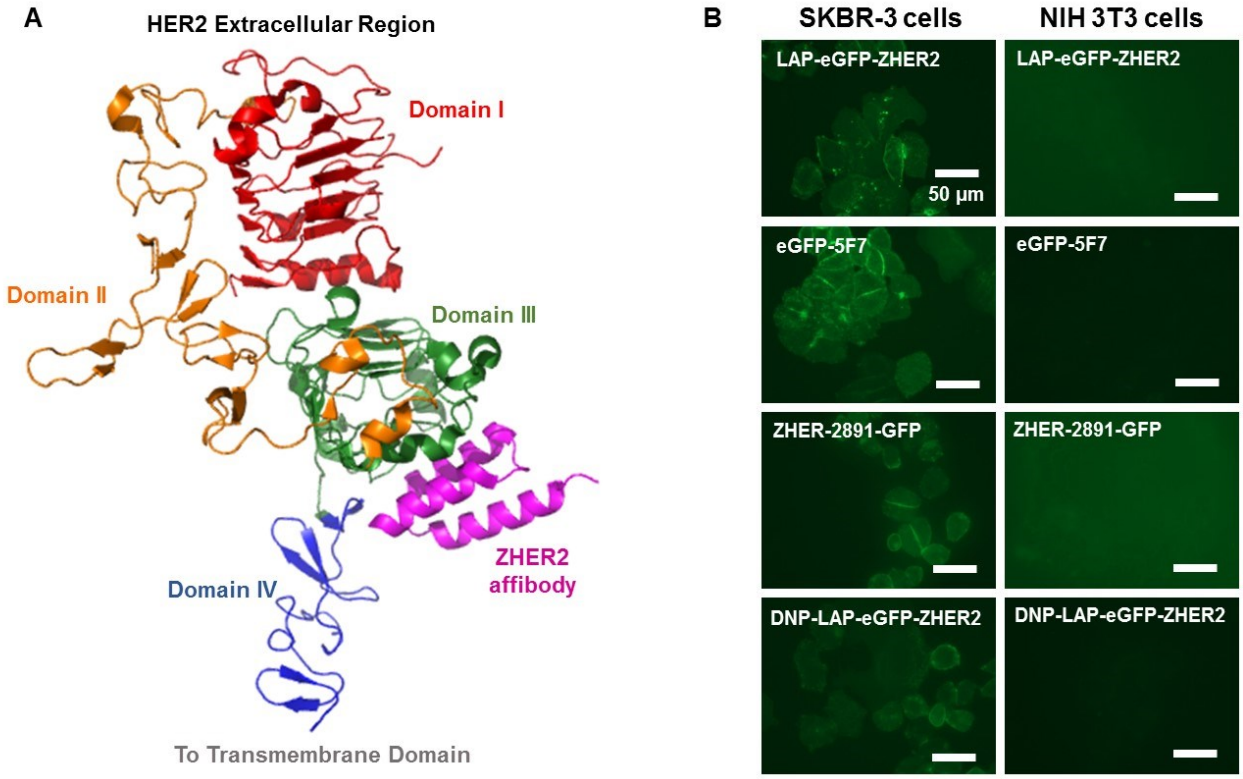

Figure 5.12 Evaluation of HER2 binding. A) ZHER2 affibody binding to domain III of the extracellular region of HER2 (PDB 3MZW). B) Fluorescence images of affibody and nanobody fusions to eGFP incubated with SKBR-3 cells (HER2 positive) and NIH-3T3 cells (HER2 negative) showing selective binding of HER2-expressing cells at 500 nM protein concentration. Images were acquired on EVOS fl fluorescence microscope with 80% lamp intensity, 500 msec exposure.

Therefore, we confirmed that these nanobodies and affibodies do bind to the surface of cells expressing HER2 and will be viable affinity reagents.

5.11 Dinitrophenyl Conjugation to Proteins with Lipoic Acid Ligase

Our next task was to attach our protein affinity reagents to the antibody recruiting reagent dinitrophenyl moiety. This can be easily achieved by chemical coupling to the free amines on the protein surfaces with an amine reactive *N*-hydroxysulfosuccinimide ester. However, this is a non-specific reaction that could potentially block protein binding to HER2. The DNP moiety must also be available for antibody binding so we needed to precisely control where the DNP was presented on the protein. Therefore, we chose to employ a site-specific conjugation technique to label the proteins with DNP.

Our aim was to site-specifically attach an orthogonal chemical moiety to the protein to be used as a reactive functional group for further conjugation with a DNP containing molecule. Biotinylation with BirA biotin ligase is one example of site-specifically conjugating a small molecule on a protein displaying a peptide tag.[66] This occurs by reaction of the carboxylic acid of biotin with a lysine on the biotin acceptor peptide. Unfortunately, this does not leave a reactive site for the addition of the DNP moiety. Alice Ting's lab at MIT has developed a set of diverse biotin derivatives that can

be ligated to proteins with a mutated BirA.[67] However, these substrates are relatively difficult to synthesize.

An alternative enzyme for selective small molecule conjugation is lipoic acid ligase (LplA). LplA catalyzes the ligation of lipoic acid onto a lysine residue on the 13 amino acid LplA acceptor peptide (LAP) tag. The Ting group was also able to expand the substrate scope of LplA to accept a wide range of substrates with reactive functionalities.[68–71] We utilized the aryl aldehyde reaction, which could then be conjugated to a commercially available dinitrophenyl hydrazine, to display DNP on our protein.[71]

I synthesized the aryl hydrazine by methods previously described (detailed in Experimental Methods). The 13 amino acid LplA acceptor peptide was then genetically encoded onto the N- or C-terminus of the nanobodies and affibodies to enable display away from the binding site. A $(GGS)_4$ linker was also encoded between the LAP tag and protein to position the DNP group away from the protein for optimal antibody binding. As shown in **Figure 5.13**, I first conjugated the aryl aldehyde onto the proteins with LplA, washed to remove any remaining aldehyde, and then performed an aniline-catalyzed bis-aryl hydrazone formation to conjugate the DNP-hydrazine to the protein. I evaluated ligation efficiency by mass spectrometry and found that all protein had been fully conjugated (**Table 5.1**). Additionally, I performed a western blot to confirm that

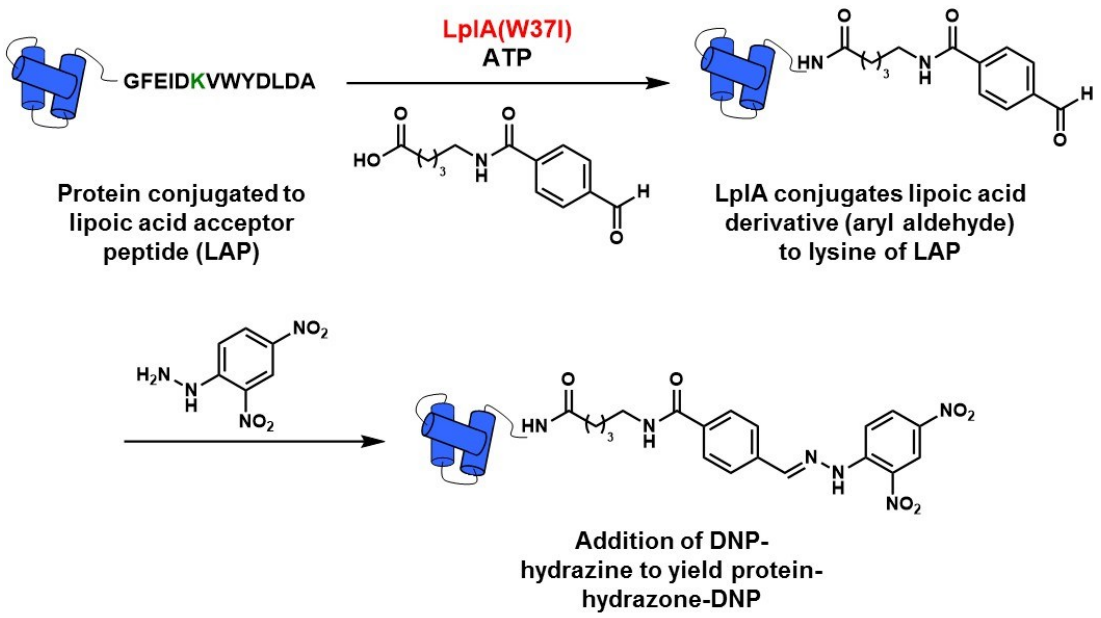

Figure 5.13 Conjugation of dinitrophenyl (DNP) onto protein affinity reagents with lipoic acid ligase (LplA). The proteins are genetically modified to encode a lipoic acid acceptor peptide (LAP) at the N- or C-terminus. LplA then couples the carboxylic acid of the lipoic acid derivative to the lysine of the LAP tag. After washing to remove excess aryl aldehyde, the protein is reacted with a DNP-hydrazine to form the final protein-hydrazone-DNP product.

DNP was displayed on nanobody 5F7 (**Figure 5.14**). Antibody-dependent cellular cytotoxicity is currently being tested by Melissa Gray, a talented undergraduate student in the McNaughton lab, and Ran Tao, a graduate student in the Spiegel lab.

5.12 Conclusions

In collaboration with the Spiegel lab, we are currently developing protein-based antibody-recruiting reagents for targeted cytotoxicity of breast cancer cells. We are utilizing affibodies or nanobodies to bind to the HER2 receptor expressed on the surface

Table 5.1 Mass spectrometry data

Protein fusion	predicted mass (Da)	observed mass (Da)
LAP-GFP-ZHER2	36877	36877.03
DNP-LAP-GFP-ZHER2	37288	37288.62
ZHER2-LAP	10144	10144.11
ZHER2-LAP-DNP	10555	10555.96
2891-LAP	9950	9950.36
2891-LAP-DNP	10361	10361.41
LAP-5F7	15997	15996.63
DNP-LAP-5F7	16408	16408.09

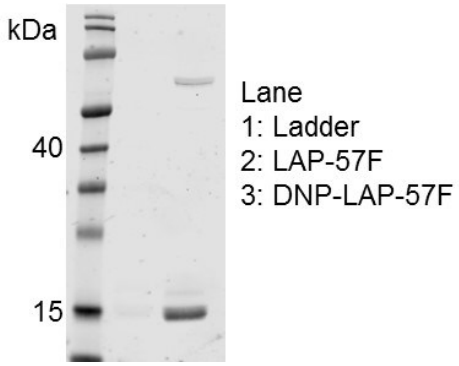

Figure 5.14 Western blot confirming DNP conjugation to nanobody 5F7. Affibody and nanobody reagents were conjugated to DNP following the previously described protocol, then washed and run on a 12% TGX PAGE gel. A western blot analysis was then performed on the proteins with an anti-DNP antibody (abcam).

of SKBR-3 breast cancer cells. The DNP antibody recruiting reagent was conjugated onto the proteins by using a lipoic acid ligase enzyme to ligate an aryl aldehyde, which can then be reacted with DNP-hydrazine. The reagents are currently being tested for antibody-dependent cellular cytotoxicity.

5.13 Experimental Methods

Materials

Phosphate buffered saline (PBS) – Hyclone/Thermo Scientific
0.25% Trypsin – Hyclone/Thermo Scientific
4-Formyl benzoic acid – Sigma Aldrich

Ethylcarbodiimide HCl – Sigma Aldrich
N-hydroxysuccinimide – Sigma Aldrich
Dinitrophenyl hydrazine – Sigma Aldrich
5-Aminovaleric acid – Sigma Aldrich
Imidazole – Sigma Aldrich
All organic solvents – Fisher Scientific
Fetal bovine serum (FBS) – PAA Laboratories
Dulbecco's modified Eagle medium (DMEM) – Hyclone/Thermo Scientific
Mammalian cell culture dishes – Fisher Scientific
BL21-DE3 competent *E. coli* – New England Biolabs
SHuffle T7 competent *E. coli* – New England Biolabs
BPER – Pierce/Thermo Scientific
Modified Lowry Protein Assay Kit – Pierce/Thermo Scientific

Instrumentation

Fluorescence microscopy images were taken on an EVOS fluorescence inverted microscope from the Advance Microscopy Group (AMG). Mass spectrometry data was obtained on an Agilent 6220 Time-of-Flight Mass Spectrometer.

Mammalian Cell Culture

Human breast cancer (SKBR-3) and NIH-3T3 cells were cultured in Dulbecco's modified Eagle's medium (DMEM) with 10% fetal bovine serum (FBS) at 37 °C, 5% CO_2.

Synthesis of Succinimidyl 4-formylbenzoate

Succinimidyl 4-formylbenzoate (S-4FB) was prepared as previously described.[72] 4-Formyl benzoic acid (0.5 g, 3.33 mmol, 1 equiv), ethylcarbodiimide HCl (0.57 g, 3.66 mmol, 1.1 equiv), and *N*-hydroxysuccinimide (0.42 g, 3.66 mmol, 1.1 equiv) were dissolved in 15 mL acetonitrile (CH_3CN). The solution was stirred overnight at room temperature. CH_3CN was removed in vacuo and the resultant white precipitant was

dissolved in 25 mL of DCM. The solution was washed three times with water, once with brine and dried over $MgSO_4$. The DCM was removed in vacuo to yield a white powder. Yield 80.3%. ^{1}H NMR (300 MHz, $CDCl_3$) δ 2.94 (s, 4H), 8.01 (d, *J*= 9 Hz, 2H), 8.30 (d, *J*= 9 Hz, 2H), 10.14 (s, 1H).

Synthesis of Aryl Aldehyde Lipoic Acid Derivative

5-Aminovaleric acid (100 mg, 0.854 mmol, 1.5 equiv) was dissolved in 20 mL dimethylformamide (DMF) and 0.127 mL of triethylamine was added. The solution was stirred for 10 minutes at room temperature, then succinimidyl 4-formylbenzoate (140 mg, 0.569 mmol, 1.0 equiv) was added. The solution was stirred overnight at room temperature. The next day, 20 mL of water was added to the solution and the pH was adjusted to pH=4.0 with 1 M HCl. The product was extracted three times with ethyl acetate, then washed with water. The mixture was then washed four times with a 10% LiCl solution, once with brine, and dried over sodium sulfate. Ethyl acetate was removed in vacuo to yield a white solid. Yield 49.58%. ^{1}H NMR (400 MHz, DMSO-d_6) δ 1.53 (quint, *J*= 4 Hz, 4H), 2.23 (t, *J*= 4 Hz, 2H), 3.26 (q, *J*= 4 Hz, 2H), 4.98 (dd, *J*= 12, 8 Hz, 4H), 8.66 (t, *J*= 4 Hz, 1H), 10.66 (s, 1H), 11.99 (s, 1H). $C_{13}H_{15}NO_4$ M_{calc} = 249.27, MH^+ = 250.11 (see spectrum in **Figure 5.15**).

Plasmid Construction

All constructs were cloned into pET plasmids. LAP fusions were encoded and assembled using oligonucleotide overlap gene construction and PCR.

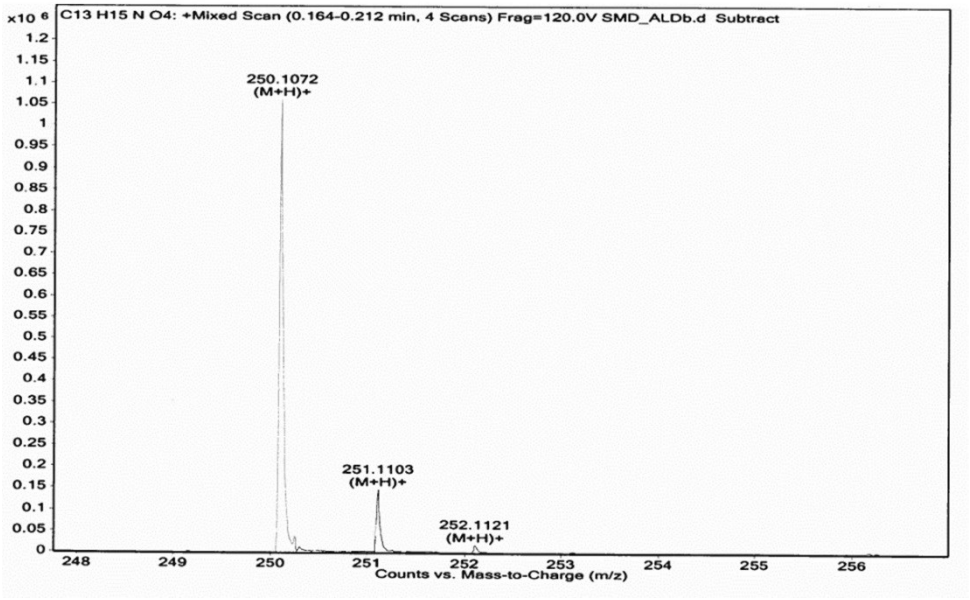

Figure 5.15 Mass spectrum of aryl aldehyde lipoic acid derivative.

Protein Purification

BL21-DE3 *E. coli* was used for the expression of all proteins except the nanobodies (5F7 and 11A4), which were expressed in SHuffle T7 *E. coli.* Cultures were grown to OD_{600} ~0.6 and induced with 1 mM IPTG at 25 °C overnight. Cells were then pelleted by centrifugation and lysed with 10 mL B-PER and sonication. Cell lysate was cleared by centrifugation at 9500 rpm, 30 minutes and supernatant was mixed with 1 mL Ni-NTA agarose resin for 1 hour at 4 °C. The resin was collected by centrifugation and washed with 40 mL of Tris wash buffer (25 mM Tris-HCl, 150 mM NaCl, 20 mM imidazole, pH 7.5). Protein was then eluted with 5 mL Tris elution buffer (25 mM Tris-HCl, 150 mM NaCl, 400 mM imidazole, pH 7.5). The eluted protein was dialyzed with 25 mM Tris-HCl, 150 mM NaCl, pH 7.5 and analyzed by SDS-PAGE followed by Coomassie Blue

(**Figure 5.16**). Protein concentrations were measured using a modified Lowry protein assay kit.

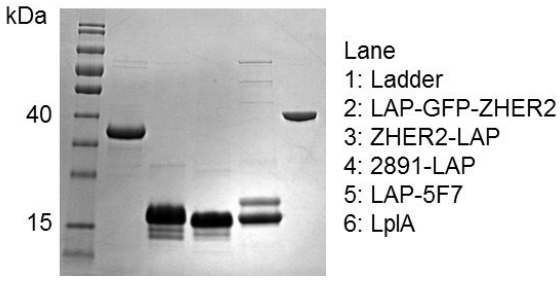

Figure 5.16 SDS-PAGE of proteins after purification.

DNP Coupling to LAP Fusion Proteins

LplA-W37I (1 μM), ATP (5 mM), Aryl Aldehyde (1 mM dissolved in DMSO), and LAP fusion protein (20 μM) was added to aldehyde ligation buffer (5 mM magnesium acetate, 25 mM Na_2HPO_4, pH 7.2) to a total volume of 5 mL. The solutions were rotated for 2 hours at room temperature. The mixture was then concentrated to ~0.5 mL and washed three times with PBS adjusted to pH 5.2 in an ultrafiltration concentration column MWCO of 3 kDa. The proteins were diluted to a total volume of 2.5 mL in PBS pH 5.2 and 2 mM DNP-hydrazine and 40 mM aniline was added to the solutions. The proteins were rotated with the mixture overnight at 4 °C. The solutions were then concentrated in ultrafiltration concentration columns and washed three times with PBS pH 7.2. The resultant DNP-conjugated proteins were analyzed by mass spectrometry and western blot for DNP conjugation. The concentration of the proteins was determined using a modified Lowry protein assay kit.

Western Blot of DNP Conjugated Proteins

Samples were run on 12% TGX precast gels (BioRad), and transferred to PVDF membrane with iBlot transfer stack (Invitrogen). The blot was initially blocked with milk for 45 minutes at room temperature. The membrane was then incubated with anti-DNP primary antibody for 15 minutes at room temperature, then incubated with goat-anti-rabbit IR Dye 800 CW secondary antibody for 15 minutes at room temperature. The western blot was imaged on the LI-COR Odyssey Imager.

Mass Spectrometry Sample Preparation

Approximately 100 μL of 50 μM purified proteins or DNP-fusion proteins was diluted to 5 mL with water. The samples were then concentrated in 3 kDa MWCO ultrafiltration concentration columns to approximately 50 μL. Mass spectra are shown below (**Figure 5.17**).

A

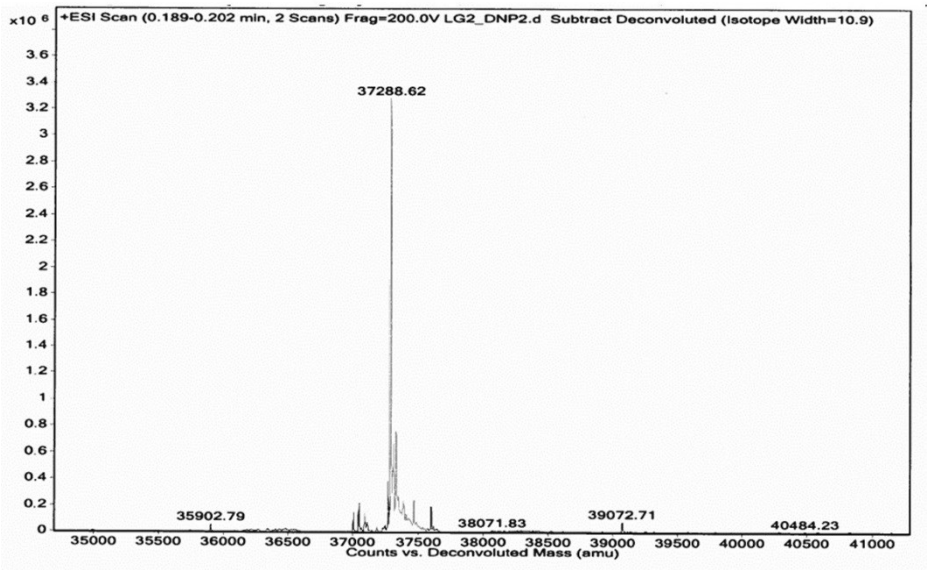

B

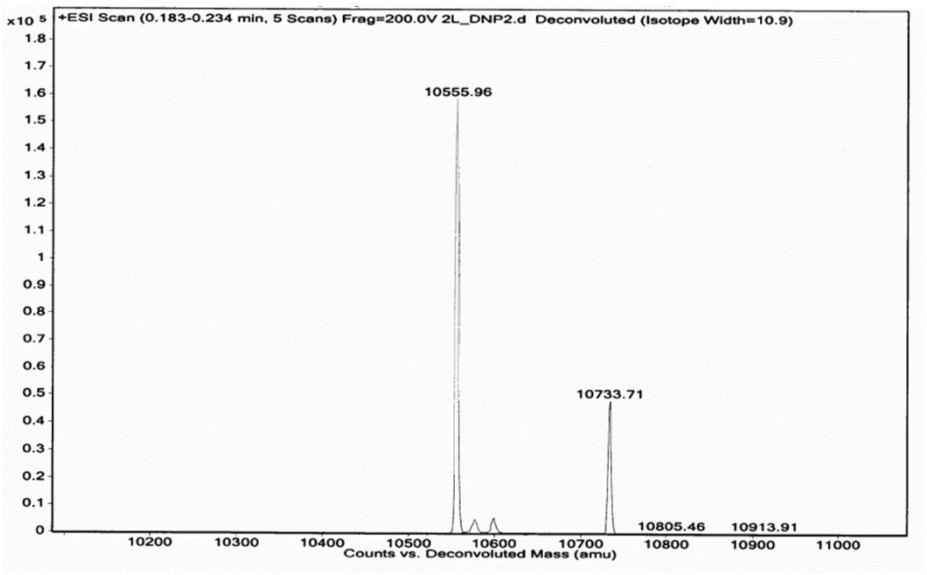
+ESI Scan (0.183-0.234 min, 5 Scans) Frag=200.0V 2L_DNP2.d Deconvoluted (Isotope Width=10.9)
x10 5
10555.96
10733.71
10805.46
10913.91
Counts vs. Deconvoluted Mass (amu)

C

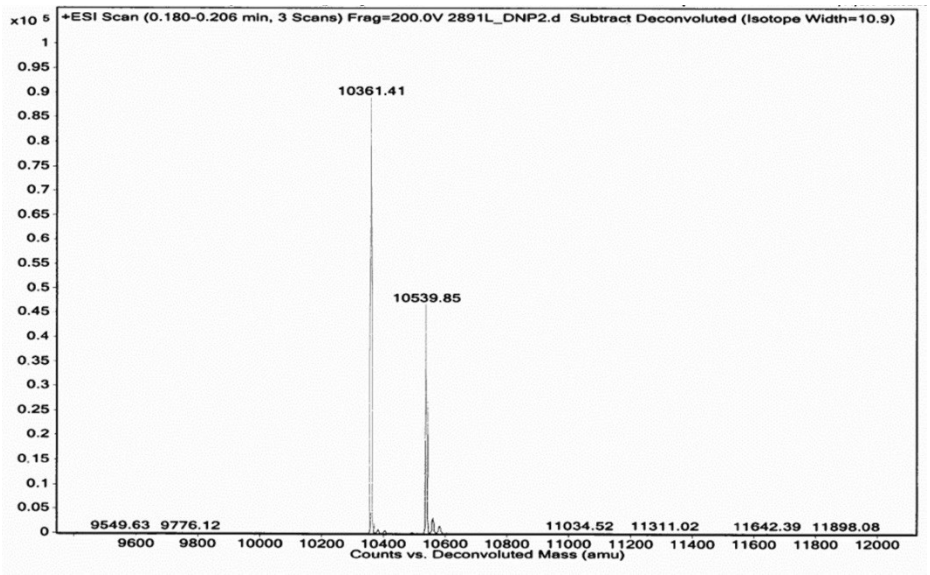
+ESI Scan (0.180-0.206 min, 3 Scans) Frag=200.0V 2891L_DNP2.d Subtract Deconvoluted (Isotope Width=10.9)
x10 5
10361.41
10539.85
9549.63
9776.12
11034.52
11311.02
11642.39
11898.08
Counts vs. Deconvoluted Mass (amu)

D

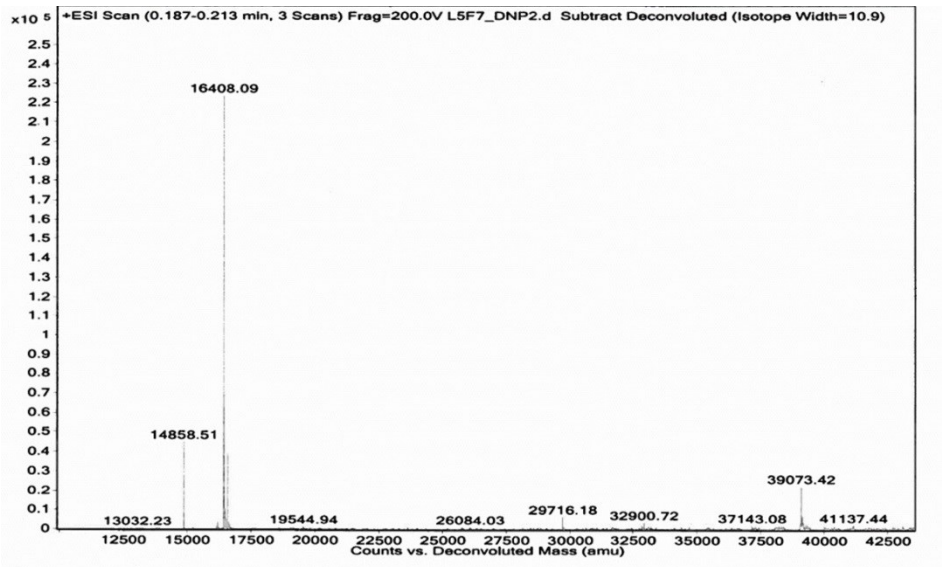

Figure 5.17 Mass spectra of DNP conjugated proteins. A) DNP-LAP-eGFP-ZHER2 B) ZHER2-LAP-DNP C) 2891-LAP-DNP D) DNP-LAP-5F7

Sequence Information

LplA W37I

KHHHHHHHMSTLRLLISDSYDPWFNLAVEECIFRQMPATQRVLFLIRNADTVVIGR
AQNPWKECNTRRMEEDNVRLARRSSGGGAVFHDLGNTCFTFMAGKPEYDKTISTSI
VLNALNALGVSAEASGRNDLVVKTVEGDRKVSGSAYRETKDRGFHHGTLLLNADLS
RLANYLNPDKKKLAAKGITSVRSRVTNLTELLPGITHEQVCEAITEAFFAHYGERVEA
EIISPNKTPDLPNFAETFARQSSWEWNFGQAPAFSHLLDERFTWGGVELHFDVEKGH
ITRAQVFTDSLNPAPLEALAGRLQGCLYRADMLQQECEALLVDFPEQEKELRELSAW
MAGAVR

ZHER2-LAP

GHHHHHHVDNKFNKEMRNAYWEIALLPNLNNQQKRAFIRSLYDDPSQSANLLAE
AKKLNDAQAPKGGSGGSGGSGGSGFEIDKVWYDLDAGGS

LAP-eGFP-ZHER2

GFEIDKVWYDLDAGGSMGHHHHHHGVSKGEELFTGVVPILVELDGDVNGHKFSVS
GEGEGDATYGKLTLKFICTTGKLPVPWPTLVTTLTYGVQCFSRYPDHMKQHDFFKSA
MPEGYVQERTIFFKDDGNYKTRAEVKFEGDTLVNRIELKGIDFKEDGNILGHKLEYN
YNSHNVYIMADKQKNGIKVNFKIRHNIEDGSVQLADHYQQNTPIGDGPVLLPDNH

YLSTQSALSKDPNEKRDHMVLLEFVTAAGITLGMDELYKGGSGSGSSVDNKFNKEM
RNAYWEIALLPNLNNQQKRAFIRSLYDDPSQSANLLAEAKKLNDAQAPK

2891-LAP

GHHHHHHAEAKYAKEMRNAYWEIALLPNLTNQQKRAFIRKLYDDPSQSSELLSEA
KKLNDSQAPKGGSGGSGGSGGSGFEIDKVWYDLDA

2891-eGFP

MGHHHHHHAEAKYAKEMRNAYWEIALLPNLTNQQKRAFIRKLYDDPSQSSELLSE
AKKLNDSQAPKGGSGGSGGVSKGEELFTGVVPILVELDGDVNGHKFSVSGEGEGDA
TYGKLTLKFICTTGKLPVPWPTLVTTLTYGVQCFSRYPDHMKQHDFFKSAMPEGYVQ
ERTIFFKDDGNYKTRAEVKFEGDTLVNRIELKGIDFKEDGNILGHKLEYNYNSHNVYI
MADKQKNGIKVNFKIRHNIEDGSVQLADHYQQNTPIGDGPVLLPDNHYLSTQSALS
KDPNEKRDHMVLLEFVTAAGITLGMDELYK

LAP-5F7

GFEIDKVWYDLDAGGSGGSGGSGGSEVQLVESGGGLVQAGGSLRLSCAASGITFSINT
MGWYRQAPGKQRELVALISSIGDTYYADSVKGRFTISRDNAKNTVYLQMNSLKPEDT
AVYYCKRFRTAAQGTDYWGQGTQVTVSSHHHHHH

eGFP-5F7

VSKGEELFTGVVPILVELDGDVNGHKFSVSGEGEGDATYGKLTLKFICTTGKLPVPWP
TLVTTLTYGVQCFSRYPDHMKQHDFFKSAMPEGYVQERTIFFKDDGNYKTRAEVKFE
GDTLVNRIELKGIDFKEDGNILGHKLEYNYNSHNVYIMADKQKNGIKVNFKIRHNIE
DGSVQLADHYQQNTPIGDGPVLLPDNHYLSTQSALSKDPNEKRDHMVLLEFVTAAG
ITLGMDELYKGGSGSGSTEVQLVESGGGLVQAGGSLRLSCAASGITFSINTMGWYRQ
APGKQRELVALISSIGDTYYADSVKGRFTISRDNAKNTVYLQMNSLKPEDTAVYYCK
RFRTAAQGTDYWGQGTQVTVSSHHHHHH

LAP-11A4

GFEIDKVWYDLDAGGSGGSGGSGGSEVQLVESGGGLVQAGGSLRLSCATSGITFMRY
ALGWYRQSPGKQREMVASINSGGTTNYADSVKGRFTISRDNAKNTVYLQMNSLKPE
DTAVYYCNARWVKPQFIDNNYWGQGTQVTVSSHHHHHH

eGFP-11A4

VSKGEELFTGVVPILVELDGDVNGHKFSVSGEGEGDATYGKLTLKFICTTGKLPVPWP
TLVTTLTYGVQCFSRYPDHMKQHDFFKSAMPEGYVQERTIFFKDDGNYKTRAEVKFE
GDTLVNRIELKGIDFKEDGNILGHKLEYNYNSHNVYIMADKQKNGIKVNFKIRHNIE
DGSVQLADHYQQNTPIGDGPVLLPDNHYLSTQSALSKDPNEKRDHMVLLEFVTAAG
ITLGMDELYKGGSGGSGGSEVQLVESGGGLVQAGGSLRLSCATSGITFMRYALGWYR
QSPGKQREMVASINSGGTTNYADSVKGRFTISRDNAKNTVYLQMNSLKPEDTAVYY
CNARWVKPQFIDNNYWGQGTQVTVSSHHHHHH

REFERENCES

(1) DePorter, S. M., Lui, I., and McNaughton, B. R. (2012) Programmed cell adhesion and growth on cell-imprinted polyacrylamide hydrogels. *Soft Matter 8*, 10403.

(2) DePorter, S. M., Hendricks, N. K., Gray, M. a., and McNaughton, B. R. (2012) A one-pot synthesis of micron-sized and nanoscale poly(N-acryloxysuccinimide-co-N-vinylpyrrolidone) particles. *Tetrahedron Lett. 53*, 6436–6438.

(3) Guillame-Gentil, O., Semenov, O., Roca, A. S., Groth, T., Zahn, R., Vörös, J., and Zenobi-Wong, M. (2010) Engineering the extracellular environment: Strategies for building 2D and 3D cellular structures. *Adv. Mater. 22*, 5443–62.

(4) Khademhosseini, A., Langer, R., Borenstein, J., and Vacanti, J. P. (2006) Microscale technologies for tissue engineering and biology. *Proc. Natl. Acad. Sci. U. S. A. 103*, 2480–7.

(5) Kim, D.-H., Lee, H., Lee, Y. K., Nam, J.-M., and Levchenko, A. (2010) Biomimetic nanopatterns as enabling tools for analysis and control of live cells. *Adv. Mater. 22*, 4551–66.

(6) Murthy, N., Campbell, J., Fausto, N., Hoffman, A. S., and Stayton, P. S. (2003) Bioinspired pH-responsive polymers for the intracellular delivery of biomolecular drugs. *Bioconjug. Chem. 14*, 412–9.

(7) Griffith, L. G., and Lopina, S. (1998) Microdistribution of substratum-bound ligands affects cell function: hepatocyte spreading on PEO-tethered galactose. *Biomaterials 19*, 979–986.

(8) Groves, J. T., Mahal, L. K., and Bertozzi, C. R. (2001) Control of Cell Adhesion and Growth with Micropatterned Supported Lipid Membranes. *Langmuir 17*, 5129–5133.

(9) Pierschbacher, M. D., and Ruoslahti, E. (1984) Variants of the cell recognition site of fibronectin that retain attachment-promoting activity. *Proc. Natl. Acad. Sci. 81*, 5985–5988.

(10) Orner, B. P., Derda, R., Lewis, R. L., Thomson, J. A., and Kiessling, L. L. (2004) Arrays for the combinatorial exploration of cell adhesion. *J. Am. Chem. Soc. 126*, 10808–9.

(11) Kruss, S., Wolfram, T., Martin, R., Neubauer, S., Kessler, H., and Spatz, J. P. (2010) Stimulation of cell adhesion at nanostructured teflon interfaces. *Adv. Mater. 22*, 5499–506.

(12) Meyers, S. R., Hamilton, P. T., Walsh, E. B., Kenan, D. J., and Grinstaff, M. W. (2007) Endothelialization of Titanium Surfaces. *Adv. Mater. 19*, 2492–2498.

(13) Vermesh, U., Vermesh, O., Wang, J., Kwong, G. A., Ma, C., Hwang, K., and Heath, J. R. (2011) High-density, multiplexed patterning of cells at single-cell resolution for tissue engineering and other applications. *Angew. Chem. Int. Ed. Engl. 50*, 7378–80.

(14) Chandra, R. A., Douglas, E. S., Mathies, R. A., Bertozzi, C. R., and Francis, M. B. (2006) Programmable cell adhesion encoded by DNA hybridization. *Angew. Chem. Int. Ed. Engl. 45*, 896–901.

(15) Hsiao, S. C., Crow, A. K., Lam, W. A., Bertozzi, C. R., Fletcher, D. A., and Francis, M. B. (2008) DNA-coated AFM cantilevers for the investigation of cell adhesion and the patterning of live cells. *Angew. Chem. Int. Ed. Engl. 47*, 8473–7.

(16) Selden, N. S., Todhunter, M. E., Jee, N. Y., Liu, J. S., Broaders, K. E., and Gartner, Z. J. (2012) Chemically programmed cell adhesion with membrane-anchored oligonucleotides. *J. Am. Chem. Soc. 134*, 765–8.

(17) Singhvi, R., Kumar, A., Lopez, G., Stephanopoulos, G., Wang, D., Whitesides, G., and Ingber, D. (1994) Engineering cell shape and function. *Science (80-.). 264*, 696–698.

(18) Veiseh, M., Wickes, B. T., Castner, D. G., and Zhang, M. (2004) Guided cell patterning on gold-silicon dioxide substrates by surface molecular engineering. *Biomaterials 25*, 3315–24.

(19) Eisenberg, J. L., Piper, J. L., and Mrksich, M. (2009) Using self-assembled monolayers to model cell adhesion to the 9th and 10th type III domains of fibronectin. *Langmuir 25*, 13942–51.

(20) St Pierre, C. A., Leonard, D., Corvera, S., Kurt-Jones, E. A., and Finberg, R. W. (2011) Antibodies to cell surface proteins redirect intracellular trafficking pathways. *Exp. Mol. Pathol. 91*, 723–32.

(21) Revzin, A., Tompkins, R. G., and Toner, M. (2003) Surface Engineering with Poly(ethylene glycol) Photolithography to Create High-Density Cell Arrays on Glass. *Langmuir 19*, 9855–9862.

(22) Qin, D., Xia, Y., and Whitesides, G. M. (2010) Soft lithography for micro- and nanoscale patterning. *Nat. Protoc. 5*, 491–502.

(23) Kane, R. (1999) Patterning proteins and cells using soft lithography. *Biomaterials 20*, 2363–2376.

(24) Ofir, Y., Moran, I. W., Subramani, C., Carter, K. R., and Rotello, V. M. (2010) Nanoimprint lithography for functional three-dimensional patterns. *Adv. Mater. 22*, 3608–14.

(25) Vaidya, R., Tender, L. M., Bradley, G., O'Brien, M. J., Cone, M., and López, G. P. Computer-controlled laser ablation: a convenient and versatile tool for micropatterning biofunctional synthetic surfaces for applications in biosensing and tissue engineering. *Biotechnol. Prog. 14*, 371–7.

(26) Park, A., and Griffith, L. G. (1998) Integration of surface modification and 3D fabrication techniques to prepare patterned poly(L-lactide) substrates allowing regionally selective cell adhesion. *J. Biomater. Sci. Polym. Ed. 9*, 89–110.

(27) Lee, J.-S., Kaibara, M., Iwaki, M., Sasabe, H., Suzuki, Y., and Kusakabe, M. (1993) Selective adhesion and proliferation of cells on ion-implanted polymer domains. *Biomaterials 14*, 958–960.

(28) Ayon, A. (2007) Molding of Deep Polydimethylsiloxane Microstructures for Microfluidics and Biological Applications. *J. Biomech. Eng. 121*, 28.

(29) Curtis, A., and Wilkinson, C. (1997) Topographical control of cells. *Biomaterials 18*, 1573–1583.

(30) Jiang, X., Takayama, S., Qian, X., Ostuni, E., Wu, H., Bowden, N., LeDuc, P., Ingber, D. E., and Whitesides, G. M. (2002) Controlling Mammalian Cell Spreading and Cytoskeletal Arrangement with Conveniently Fabricated Continuous Wavy Features on Poly(dimethylsiloxane). *Langmuir 18*, 3273–3280.

(31) Bettinger, C. J., Orrick, B., Misra, A., Langer, R., and Borenstein, J. T. (2006) Microfabrication of poly (glycerol-sebacate) for contact guidance applications. *Biomaterials 27*, 2558–65.

(32) Richert, L., Vetrone, F., Yi, J.-H., Zalzal, S. F., Wuest, J. D., Rosei, F., and Nanci, A. (2008) Surface Nanopatterning to Control Cell Growth. *Adv. Mater. 20*, 1488–1492.

(33) Bolisay, L. D., Culver, J. N., and Kofinas, P. (2006) Molecularly imprinted polymers for tobacco mosaic virus recognition. *Biomaterials 27*, 4165–8.

(34) Hayden, O., and Dickert, F. L. (2001) Selective Microorganism Detection with Cell Surface Imprinted Polymers. *Adv. Mater. 13*, 1480–1483.

(35) Hayden, O., Mann, K.-J., Krassnig, S., and Dickert, F. L. (2006) Biomimetic ABO blood-group typing. *Angew. Chem. Int. Ed. Engl. 45*, 2626–9.

(36) Peppas, N. A., Hilt, J. Z., Khademhosseini, A., and Langer, R. (2006) Hydrogels in Biology and Medicine: From Molecular Principles to Bionanotechnology. *Adv. Mater. 18*, 1345–1360.

(37) Lee, K. Y., and Mooney, D. J. (2001) Hydrogels for Tissue Engineering. *Chem. Rev. 101*, 1869–1880.

(38) Hahn, M. S., Miller, J. S., and West, J. L. (2006) Three-Dimensional Biochemical and Biomechanical Patterning of Hydrogels for Guiding Cell Behavior. *Adv. Mater. 18*, 2679–2684.

(39) Slaughter, B. V, Khurshid, S. S., Fisher, O. Z., Khademhosseini, A., and Peppas, N. A. (2009) Hydrogels in regenerative medicine. *Adv. Mater. 21*, 3307–29.

(40) Langer, R., and Vacanti, J. (1993) Tissue engineering. *Science (80-.). 260*, 920–926.

(41) Freed, L. E., Engelmayr, G. C., Borenstein, J. T., Moutos, F. T., and Guilak, F. (2009) Advanced material strategies for tissue engineering scaffolds. *Adv. Mater. 21*, 3410–8.

(42) Scott, A. M., Wolchok, J. D., and Old, L. J. (2012) Antibody therapy of cancer. *Nat. Rev. Cancer 12*, 278–87.

(43) Murphy, K. M. (2011) Janeway's Immunobiology, p 888. Garland Science.

(44) Nimmerjahn, F., and Ravetch, J. V. (2008) Fcgamma receptors as regulators of immune responses. *Nat. Rev. Immunol. 8*, 34–47.

(45) Dhodapkar, K. M., Krasovsky, J., Williamson, B., and Dhodapkar, M. V. (2002) Antitumor monoclonal antibodies enhance cross-presentation of cellular antigens and the generation of myeloma-specific killer T cells by dendritic cells. *J. Exp. Med. 195*, 125–33.

(46) Akiyama, K., Ebihara, S., Yada, A., Matsumura, K., Aiba, S., Nukiwa, T., and Takai, T. (2003) Targeting Apoptotic Tumor Cells to Fc R Provides Efficient and Versatile Vaccination Against Tumors by Dendritic Cells. *J. Immunol. 170*, 1641–1648.

(47) Cioca, D. P., Deak, E., Cioca, F., and Paunescu, V. (1997) Monoclonal antibodies targeted against melanoma and ovarian tumors enhance dendritic cell-mediated cross-presentation of tumor-associated antigens and efficiently cross-prime CD8+ T cells. *J. Immunother. 29*, 41–52.

(48) Murillo, O., Dubrot, J., Palazón, A., Arina, A., Azpilikueta, A., Alfaro, C., Solano, S., Ochoa, M. C., Berasain, C., Gabari, I., Pérez-Gracia, J. L., Berraondo, P., Hervás-Stubbs, S., and Melero, I. (2009) In vivo depletion of DC impairs the anti-tumor effect of agonistic anti-CD137 mAb. *Eur. J. Immunol. 39*, 2424–36.

(49) McEnaney, P. J., Parker, C. G., Zhang, A. X., and Spiegel, D. A. (2012) Antibody-recruiting molecules: an emerging paradigm for engaging immune function in treating human disease. *ACS Chem. Biol. 7*, 1139–51.

(50) Murelli, R. P., Zhang, A. X., Michel, J., Jorgensen, W. L., and Spiegel, D. A. (2009) Chemical control over immune recognition: a class of antibody-recruiting small molecules that target prostate cancer. *J. Am. Chem. Soc. 131*, 17090–2.

(51) Holmes, E. H., Greene, T. G., Tino, W. T., Boynton, A. L., Aldape, H. C., Misrock, S. L., and Murphy, G. P. (1996) Analysis of glycosylation of prostate-specific membrane antigen derived from LNCaP cells, prostatic carcinoma tumors, and serum from prostate cancer patients. *Prostate. Suppl. 7*, 25–9.

(52) Ju, K.-S., and Parales, R. E. (2010) Nitroaromatic compounds, from synthesis to biodegradation. *Microbiol. Mol. Biol. Rev. 74*, 250–72.

(53) Lauer, K. (1990) Environmental nitrophenols and autoimmunity. *Mol. Immunol. 27*, 697–8.

(54) Ortega, E., Kostovetzky, M., and Larralde, C. (1984) Natural DNP-binding immunoglobulins and antibody multispecificity. *Mol. Immunol. 21*, 883–888.

(55) Rothe, A., Hosse, R. J., and Power, B. E. (2006) In vitro display technologies reveal novel biopharmaceutics. *FASEB J. 20*, 1599–610.

(56) Nord, K., Nilsson, J., Nilsson, B., Uhlén, M., and Nygren, P. A. (1995) A combinatorial library of an alpha-helical bacterial receptor domain. *Protein Eng. 8*, 601–8.

(57) Kolkman, J. A., and Law, D. A. (2010) Nanobodies - from llamas to therapeutic proteins. *Drug Discov. Today. Technol. 7*, e95–e146.

(58) Löfblom, J., Feldwisch, J., Tolmachev, V., Carlsson, J., Ståhl, S., and Frejd, F. Y. (2010) Affibody molecules: engineered proteins for therapeutic, diagnostic and biotechnological applications. *FEBS Lett. 584*, 2670–80.

(59) Vincke, C., Loris, R., Saerens, D., Martinez-Rodriguez, S., Muyldermans, S., and Conrath, K. (2009) General strategy to humanize a camelid single-domain antibody and identification of a universal humanized nanobody scaffold. *J. Biol. Chem. 284*, 3273–84.

(60) Ross, J. S., and Fletcher, J. A. (1998) The HER-2/neu oncogene in breast cancer: prognostic factor, predictive factor, and target for therapy. *Stem Cells 16*, 413–28.

(61) Slamon, D., Clark, G., Wong, S., Levin, W., Ullrich, A., and McGuire, W. (1987) Human breast cancer: correlation of relapse and survival with amplification of the HER-2/neu oncogene. *Science 235*, 177–182.

(62) Capala, J., and Bouchelouche, K. (2010) Molecular imaging of HER2-positive breast cancer: a step toward an individualized "image and treat" strategy. *Curr. Opin. Oncol. 22*, 559–66.

(63) Kijanka, M., Warnders, F.-J., El Khattabi, M., Lub-de Hooge, M., van Dam, G. M., Ntziachristos, V., de Vries, L., Oliveira, S., and van Bergen En Henegouwen, P. M. P. (2013) Rapid optical imaging of human breast tumour xenografts using anti-HER2 VHHs site-directly conjugated to IRDye 800CW for image-guided surgery. *Eur. J. Nucl. Med. Mol. Imaging 40*, 1718–29.

(64) Feldwisch, J., Tolmachev, V., Lendel, C., Herne, N., Sjöberg, A., Larsson, B., Rosik, D., Lindqvist, E., Fant, G., Höidén-Guthenberg, I., Galli, J., Jonasson, P., and Abrahmsén, L. (2010) Design of an optimized scaffold for affibody molecules. *J. Mol. Biol. 398*, 232–47.

(65) Eigenbrot, C., Ultsch, M., Dubnovitsky, A., Abrahmsén, L., and Härd, T. (2010) Structural basis for high-affinity HER2 receptor binding by an engineered protein. *Proc. Natl. Acad. Sci. U. S. A. 107*, 15039–44.

(66) Beckett, D., Kovaleva, E., and Schatz, P. J. (1999) A minimal peptide substrate in biotin holoenzyme synthetase-catalyzed biotinylation. *Protein Sci. 8*, 921–9.

(67) Slavoff, S. A., Chen, I., Choi, Y.-A., and Ting, A. Y. (2008) Expanding the substrate tolerance of biotin ligase through exploration of enzymes from diverse species. *J. Am. Chem. Soc. 130*, 1160–2.

(68) Baruah, H., Puthenveetil, S., Choi, Y.-A., Shah, S., and Ting, A. Y. (2008) An Engineered Aryl Azide Ligase for Site-Specific Mapping of Protein-Protein Interactions through Photo-Cross-Linking. *Angew. Chemie 120*, 7126–7129.

(69) Uttamapinant, C., White, K. A., Baruah, H., Thompson, S., Fernández-Suárez, M., Puthenveetil, S., and Ting, A. Y. (2010) A fluorophore ligase for site-specific protein labeling inside living cells. *Proc. Natl. Acad. Sci. U. S. A. 107*, 10914–9.

(70) Liu, D. S., Tangpeerachaikul, A., Selvaraj, R., Taylor, M. T., Fox, J. M., and Ting, A. Y. (2012) Diels-Alder cycloaddition for fluorophore targeting to specific proteins inside living cells. *J. Am. Chem. Soc. 134*, 792–5.

(71) Cohen, J. D., Zou, P., and Ting, A. Y. (2012) Site-specific protein modification using lipoic acid ligase and bis-aryl hydrazone formation. *Chembiochem 13*, 888–94.

(72) Phillips, J. A., Morgan, E. L., Dong, Y., Cole, G. T., McMahan, C., Hung, C.-Y., and Sanderson, S. D. (2009) Single-step conjugation of bioactive peptides to proteins via a self-contained succinimidyl bis-arylhydrazone. *Bioconjug. Chem. 20*, 1950–7.